INTERFERENCE SUPPRESSION BY USING SPACE-TIME ADAPTIVE
PROCESSING FOR AIRBORNE RADAR

A THESIS SUBMITTED TO
THE GRADUATE SCHOOL OF NATURAL AND APPLIED SCIENCES
OF
MIDDLE EAST TECHNICAL UNIVERSITY

BY

ÖZGÜR ERYİĞİT

IN PARTIAL FULLFILLMENT OF THE REQUIREMENTS
FOR
THE DEGREE OF MASTER OF SCIENCE
IN
ELECTRICAL AND ELECTRONICS ENGINEERING

MAY 2008

Approval of the thesis:

INTERFERENCE SUPPRESSION BY USING SPACE-TIME ADAPTIVE
PROCESSING FOR AIRBORNE RADAR

submitted by **ÖZGÜR ERYİĞİT** in partial fulfillment of the requirements for the
degree of **Master of Science in Electrical and Electronics Engineering
Department, Middle East Technical University** by,

Prof. Dr. Canan Özgen

Dean, Graduate School of **Natural and Applied Sciences**

Prof. Dr. İsmet Erkmen

Head of Department, **Electrical and Electronics Engineering**

Assist. Prof. Dr. Ali Özgür Yılmaz

Supervisor, **Electrical and Electronics Engineering Dept., METU**

Examining Committee Members:

Prof. Dr. Yalçın Tanık

Electrical and Electronics Engineering Dept., METU

Assoc. Prof. Dr. Sencer Koç

Electrical and Electronics Engineering Dept., METU

Assist. Prof. Dr. Ali Özgür Yılmaz

Electrical and Electronics Engineering Dept., METU

Assist. Prof. Dr. Çağatay Candan
Electrical and Electronics Engineering Dept., METU

M. Sc. Bülent Şen

REHİS-TTD, ASELSAN

Date:

I hereby declare that all information in this document has been obtained and presented in accordance with academic rules and ethical conduct. I also declare that, as required by these rules and conduct, I have fully cited and referenced all material and results that are not original to this work.

Name, Last name : Özgür Eryiğit

Signature :

ABSTRACT

INTERFERENCE SUPPRESSION BY SPACE-TIME ADAPTIVE PROCESSING FOR AIRBORNE RADAR

Eryiğit, Özgür

M. Sc., Department of Electrical and Electronics Engineering
Supervisor: Assist. Prof. Dr. Ali Özgür Yılmaz

May 2008, 118 pages

Space-Time Adaptive Processing (STAP) is an effective method in Ground Moving Target Indicator (GMTI) operation of airborne radars. Clutter suppression is the key to successful MTI operation. Airborne radars are different than the ground based ones in regard to clutter due to the displacement of the platform during operation. When STAP methods are to be investigated, one needs to have accurate signal models while evaluating performance. In this thesis, a comprehensive received signal model is developed first for an airborne antenna array. The impacts of the aircraft motion and irregularities in it, aircraft displacement during reception, intrinsic clutter motion and radar parameters have been accounted in the model and incorporated into a simulator environment. To verify the correctness of the signal simulator, the classical DPCA approach and optimum STAP methods are inspected.

Keywords: Radar, Space-Time Adaptive Processing, GMTI, Clutter Suppression

ÖZ

HAVA ARAÇLARINDAKİ RADARLAR İÇİN UZAY-ZAMAN UYARLAMALI İŞLEME TEKNİĞİ KULLANILARAK GİRİŞİM BASTIRILMASI

Eryiğit, Özgür

Yüksek Lisans, Elektrik Elektronik Mühendisliği Bölümü
Tez Yöneticisi: Yrd. Doç. Dr. Ali Özgür Yılmaz

Uzay-Zaman Uyarlamalı İşleme (STAP), hava radarlarında kullanılan etkili bir Yerde Hareketli Hedef Belirtisi (GMTI) yöntemidir. Kargaşanın bastırılması, başarılı bir MTI operasyonu için anahtardır. Operasyon sırasında hava aracının yer değiştirmesine bağlı olarak hava radarları, yerde konuşlu radarlara göre kargaşa açısından farklıdır. STAP yöntemleri araştırıldığında, performans değerlendirmesi yapabilmek için doğru sinyal modellerine ihtiyaç duyulmaktadır. Bu tez kapsamında, hava radarında konuşlu bir anten dizisi için kapsamlı bir alınan sinyal modeli geliştirilmiştir. Hava aracının hareketi ve bu hareketteki düzensizlikler, alma esnasında hava aracının yer değiştirmesi, kargaşanın özünde olan hareket ve radar parametrelerinin modelde göz önüne alınmış ve simülasyon ortamına aktarılmıştır. Sinyal simülatörünü doğrulamak için, klasik DPCA yaklaşımı ve optimal STAP yöntemleri incelenmiştir.

Anahtar Kelimeler: Radar, Uzay-Zaman Uyarlamalı İşleme, GMTI, Kargaşa Bastırılması

To My Family …

ACKNOWLEDGEMENTS

I would like to express my deepest gratitude to my supervisor Assist. Prof. Dr. Ali Özgür Yılmaz for his encouragements, guidance, advice, criticism and insight throughout the research.

I would like to thank ASELSAN Inc. for support provided for the completion of this thesis.

I would like to forward my appreciation to all my friends and colleagues who contributed to my thesis with their continuous encouragement.

I would also like to express my profound appreciation to my family and fiancée for their continuous support.

TABLE OF CONTENTS

LIST OF TABLES

TABLES

LIST OF FIGURES

LIST OF ABBREVIATIONS

Abbreviation	Explanation
AMTI	Airborne Moving Target Indicator
CPI	Coherent Processing Interval
CNR	Clutter to Noise Power Ratio
DPCA	Displaced Phased Center Antenna
GMTI	Ground Moving Target Indicator
ICM	Intrinsic Clutter Motion
JNR	Jammer to Noise Power Ratio
MTI	Moving Target Indicator
PRI	Pulse Repetition Interval
PRF	Pulse Repetition Frequency
RCS	Radar Cross Section
SAR	Synthetic Aperture Radar
SINR	Signal to Interference-Noise Power Ratio
SNR	Signal to Noise Power Ratio
STAP	Space-Time Adaptive Processing
ULA	Uniform Linear Array

CHAPTER 1

INTRODUCTION

Airborne aircrafts employ different kinds of radar and algorithms to detect targets on the ground. In addition to the target back-scattered signal, the received signal includes unintended interferences such as reflection of ground clutter or jammer signals sent by hostile agents.

As ground based radars are considered, the radar is stationary so that the clutter reflections are almost stationary so that moving targets can easily be detected by using the Doppler information. However, airborne radars are in continuous motion so that even though clutter is almost stationary clutter appears to have a relative motion. This relative motion spreads the clutter reflections in Doppler domain degrading the radar performance to detect targets. Especially, slow moving targets are buried in clutter spread.

Thus, some extra effort shall be spent to mitigate the interference and detect the target. In literature, the classical method called "Displaced Phased Center Antenna (DPCA)" has been proposed for aircraft motion compensation [1, 6]. The environment is sampled by two consecutive phase centers which replaces position in a single pulse repetition interval (PRI). DPCA simply subtracts these two samples to cancel out the clutter which assumed to have the same Doppler shift during the PRI time. This kind of processing is based on the basic two pulse MTI process in which the radar is stationary and the target is in motion as opposed to

airborne radar case. DPCA is a successful method to compensate the Doppler spread of clutter due to the aircraft motion by using two consecutive samples. However, DPCA brings some extra requirements that are hard to satisfy and is not adaptive to changing environment.

In order to improve the target detection performance of radar, interference should be suppressed by processing over all possible domains. Although SAR (Synthetic Aperture Radar) processing works very well on airborne radar with single antenna for imaging stationary environments and objects, the same does not hold true for the moving objects. It is known that the use of multiple antennas enhances the detection capability of moving objects in airborne radar.

In early 1970s, joint domain signal processing approach called Space-Time Adaptive Processing (STAP) was proposed. By employing multiple antennas, spatial and temporal samples are collected by receiving the echos of multiple pulses for each individual antenna. STAP is a multidimensional signal processing technique which employs processing of spatial and temporal samples. Unfortunately, due to the lack of signal processing power, this method was not found feasible to implement and studies in this subject did not flourish until 1990s. After 1990s, with the help of the rapid improvements in signal processing and computation, STAP enjoyed a renewed interest.

An airborne radar with an N element antenna array is utilized in order to feed the STAP processor. Each antenna array element is assumed to be identical and has its own receiver. The output of each of the N channels is M time samples taken every PRI (pulse repetition interval) time during the CPI (coherent processing interval) period. All these time samples are collected from array elements by the signal processor for integration to make a decision on the target existence. The derivations of optimum processors, their efficient implementations, approximate processors are the main research topics in STAP literature [1, 2, 3, 6, 7].

The starting point of this thesis study was to investigate the STAP algorithms proposed in literature and make a performance comparison of these algorithms under different kinds of conditions arising from the aircraft motion and other environmental impacts. An extensive study on various STAP algorithms has been performed. After the literature survey, the need for data to be used as input signal for the test of algorithms has surfaced. Many research centers use real data collected during flights or use emulated signals collected in similar flight scenarios [11]. Some other studies generate data by signal simulators. However, none of these data are open to public. As a consequence, it is decided to develop a signal simulator to produce as accurately as possible the signals to be received in airborne radar. The basic signal model given in the literature is improved to include the effects of aircraft motion, environmental impacts, etc.

It has been realized that when more and more effects are included, developing an accurate signal simulator is an involved task. In addition, developing a simulator to cover many of the aircraft and environmental issues gives an insight to understand airborne radar problem. Consequently, the thesis study mostly shifted towards investigation of received signals and development of a received signal simulator.

In the first stage of development, the basic model proposed in literature is implemented. Throughout the simulator development, it has been noticed that the basic model proposed in literature has to be improved in order to include defects to be seen in airborne radar. Thus, after developing the basic signal simulator, additional capabilities are added to simulate the received signal much closer to reality.

In almost all of the papers, the aircraft motion is assumed to be along the x-axis which is the axis of antenna array and aircraft velocity is assumed to be constant during the time interval of data collection and processing (CPI). This model is

3

improved to have aircraft motion in any direction and have some velocity irregularities in any direction at each PRI. The reason of this irregularity is that aircraft moves in air which makes it prone to sudden velocity changes. The effect of this issue on the produced data has been examined.

The basic model also takes the aircraft stable at the place where the first sample is collected during the CPI period, but the aircraft slowly changes location at each PRI. Aircraft motion causes the displacement of the antenna array elements from the initial location. The location change which is discarded in literature due to short CPI interval is expected to alter the spatial sampling characteristics. This effect is modeled over the basic signal model and change on spatial sampling is verified.

There also some other issues influencing the received signal other than the aircraft motion. For the environmental modeling, clutter model is improved to include the intrinsic clutter motion simulating the change of clutter signal in time. This issue is supposed to cause clutter reflections to be spread in time domain. The results are discussed with the output of the simulator.

As a final step of this study, optimum STAP and DPCA are compared. The results obtained through performance evaluation of these methods match what is available in the literature. This is an indication of the accuracy of the signal model and simulator developed in the thesis.

CHAPTER 2

AIRBORNE RADAR CONCEPTS

AND

SIGNAL MODELING

2.1 General Information

Moving Target Indicator (MTI) and pulsed Doppler radars use the Doppler effect as a tool to suppress the clutter existing in the received signal and detect moving targets. In many ground radar systems, clutter is supposed to be stationary or slowly moving so that its center frequency is zero. On the contrary, moving targets have nonzero Doppler frequency. Unlike ground based radars, non-stationary radars employing MTI, such as the Airborne Moving Target Indicator-AMTI and Ground Moving Target Indicator-GMTI, suffer from the Doppler spread effect of the clutter due the continuous aircraft motion. In the other words, clutter will not be seemed as stationary any more. Especially, GMTI radars will suffer a complex clutter modeling problem because ground clutter consist of many parameters like terrain, intrinsic clutter motion, surface reflections etc. [1]. Clutter spread covers a wider region in the Doppler spectrum that slowly moving targets (which is the main concern of GMTI) may be buried under the clutter with high reflection power. As a

consequence, some additional processing should be done to eliminate the clutter effect besides the conventional one dimensional MTI Doppler processing.

Space-Time Adaptive Processing (STAP) is a multidimensional adaptive filtering technique proposed to suppress the unintended interference (clutter and jammer if present) that exists in the received signal. Especially, STAP deals with the clutter Doppler spread induced by the aircraft motion. STAP employs the joint domain filtering in both spatial and temporal domains that the processing is coherently performed on the echo signals pertained to the M transmitted pulses received by N individual antenna element.

STAP is similar to the basic way of aircraft motion compensator called Displaced Phase Center Antenna (DPCA). DPCA employs two phase centers that one replaces the other one in a pulse repetition interval so that the environment seems to be stationary. Multiple antennas are utilized in STAP where the signals corresponding to each antenna are individually observed and jointly processed later. In this respect, STAP is a generalized and advanced form of DPCA.

2.2 Airborne Radar System Description

In this section, parameters and receive characteristics of the airborne radar that will be considered in the scope of this thesis will be introduced. Airborne radars utilize different kinds and orientations of radar antennas and radiation characteristics related to mission objectives.

The aircraft is flying at a fixed altitude of h with a constant velocity v over the x-plane. The aircraft maneuvers and ascends/descends will not be taken into account in this section which is another problem to be studied under title "motion compensation".

The antenna array is usually aligned in the same direction of the velocity vector. There can also be cases that the velocity vector and the antenna array may be misaligned where this misalignment causes some problems.

The radar receiver consists of N independent receive antenna array elements which are usually uniformly distributed in space. This kind of radar antenna arrays is called as Uniform Linear Array (ULA). ULA is installed on the aircraft in a sidelooking orientation. The antenna elements are supposed to be identical and independent. Each of the antenna elements has its own receiver part behind it which brings the capability of processing of the signals received by each element. Throughout the thesis, the baseband signals after the A/D will be considered. Array elements are spaced by a distance d which is usually selected as $\lambda/2$, half of the wavelength. The first element is selected as the reference element so that the nth element is located on the x plane at a distance $(n-1)d$.

The flight direction of the aircraft is denoted by the x-axis. A 90 degree sidelooking orientation corresponds to the y-axis, whereas the z-axis stands for the altitude of the flight with respect to a region of interest possibly on the ground. The radar antenna orientation is shown on Figure 2-1.

Radar transmits M pulses with a constant PRI, Tr and reflections from the scene related to these pulses are collected by N receive elements to be processed coherently. PRI selection is another important issue that should be made carefully because there is a tradeoff between the range and Doppler ambiguities depending on the PRI value [4]. Low PRF transmission is safe from range ambiguities whereas high PRF transmission is beneficial with regard to Doppler ambiguities.

a.

b.
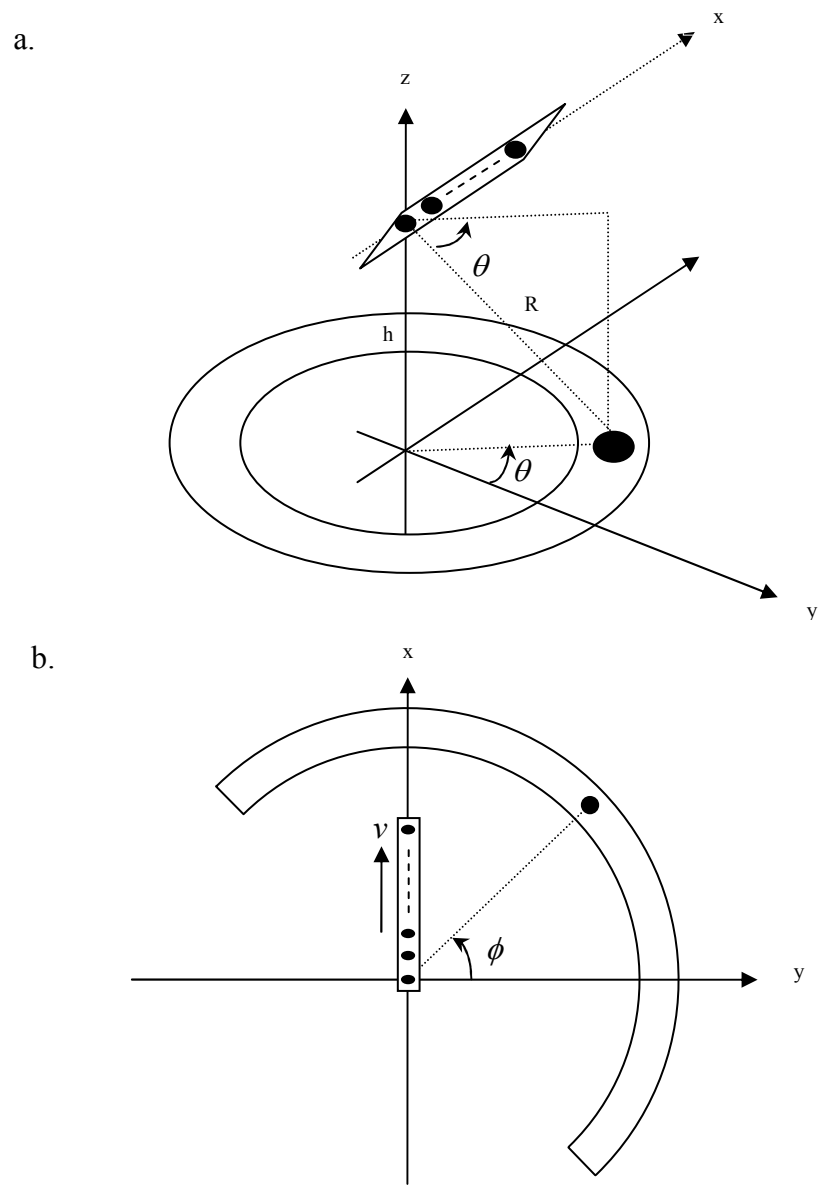
Figure 2-1 Radar antenna orientation with a single point scatterer a. 3D view b. 2D view.

Each transmitted pulse has a pulse width Tp. Pulse width, which is related to the resolution in range, plays an important role on forming iso-range rings. Specially, scatterers which are at the same distance from an antenna lie in the same iso-ring. The ring width is defined as $\Delta R \cong c/2B$ where B is the instantaneous bandwidth (related to the pulse width) and c is the speed of light. Modern radars employ pulse compression techniques to increase the range resolution. Pulse compression is achieved by using chips whose time duration is relatively small as compared with the original pulse width. Pulse is formed by using these chips. Then, the range resolution is just defined by the chip duration not with pulse duration [10].

Some of the radar system parameters of interest here are summarized in Table 2-1.

Table 2-1 Radar system parameters [2].

Parameter Symbol	Definition
N	Number of antenna array elements
M	Number of pulses integrated in a CPI
L	Number of range samples per PRI
w=2πf	Radar operating frequency
λ	Radar operating wavelength
d	Spacing between antenna array elements
T_r	Pulse repetition interval (PRI)
f_r	Pulse repetition frequency (PRF)
T_p	Pulse width
P_t	Peak transmitted power
B	Instantaneous bandwidth
$G_t(\theta,\phi)$	Transmit power gain
$g(\theta,\phi)$	Element pattern (power)
L_t	System losses on transmit
L_r	System losses on receive
N_0	Receiver noise power spectral density
h	Aircraft altitude
v	Aircraft velocity

Consequently, the scene reflections are sampled by each of N elements which corresponds to sampling in space dimension. Moreover, the scene is also sampled by using M pulses. The latter sampling is referred to as sampling in time, alternately

called slow-time sampling. Each element samples the scene reflections in range which is called fast time sampling, that is, radar take L samples from the interested range in a single PRI.

The total time interval spent to collect M pulses (MT_r) is called the Coherent Processing Interval (CPI). The Datacube shown in Figure 2-2 is defined as an LxMxN complex matrix of LMN complex samples collected during a single CPI.
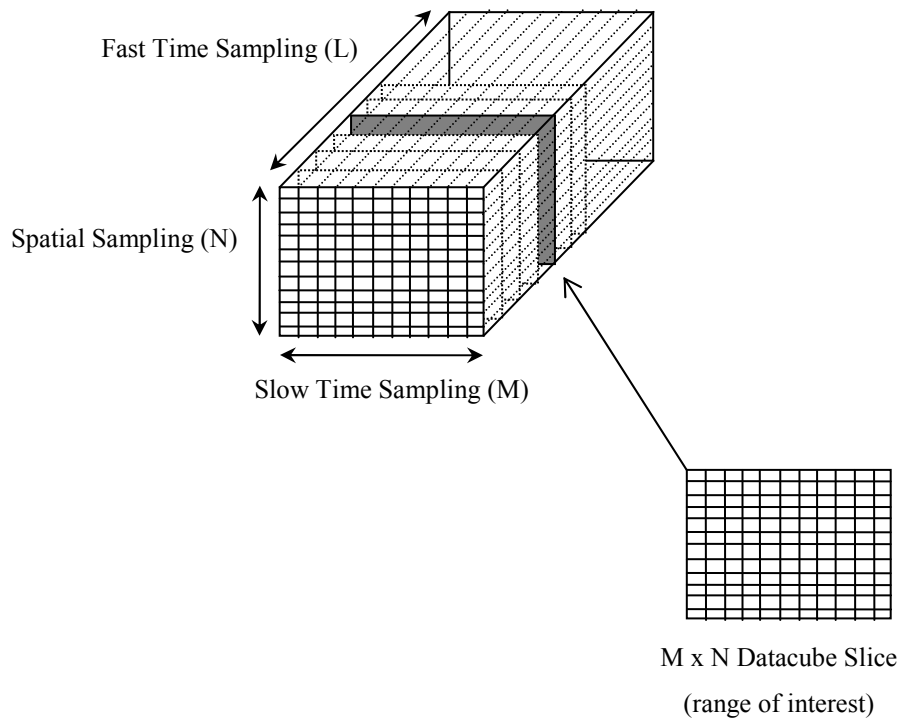
Figure 2-2 LxMxN dimensional datacube received in a single CPI and the space-time snapshot of range of interest.

2.3 Signal Sampling (One Dimensional)

2.3.1 Spatial Sampling (Beamforming)

Radars consisting of many antenna elements receive the reflection signal of a scatterer with different phases on antenna element due to the array orientation. The direction information of the scatterer can be obtained by using the phase difference between the antenna elements. Throughout this section, the signal processing of the signal received by an N-element ULA will be discussed. The study will be based on the baseband data.

This subsection on a one dimensional processing is sometimes called the Spatial Sampling. Figure 2-3 shows the physical illustration of the signal reception. The elements are spaced from each other with a distance d which is usually selected as the half of the wavelength of the signal, λ. The first element is the reference element from which a phase difference will be calculated. Suppose that the signal impinges on each array element with an angle θ with the array normal.
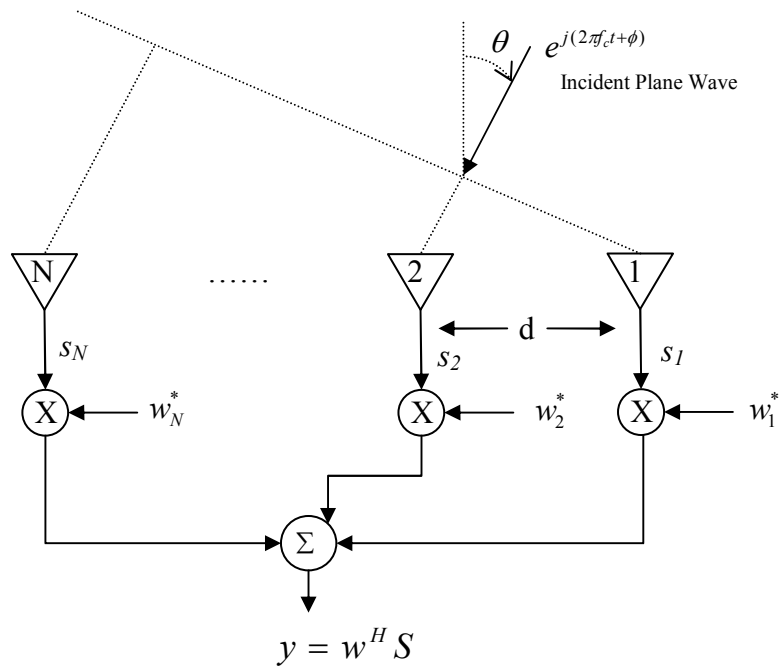
Figure 2-3 Signal reception and processing by N element antenna array.

The spatial frequency is derived from the phase difference between antenna array elements as defined in [3]. The phase shift of the nth element due to the time delay between reception of the signal by the reference element and the nth element is defined as

$$\gamma_n = \tau_n \omega \qquad (2\text{-}1)$$

where τ_n is time delay of the signal on the nth element which is equal to $(n-1)d\sin(\theta)/c$ and ω is the radian frequency.

Then the complex envelope of the received signal on the nth element is equal to

$$s_n = e^{j2\pi(n-1)\frac{d}{\lambda}\sin(\theta)}, \qquad (2\text{-}2)$$

where the spatial frequency is defined as [1, 2, 3]

$$f_{sp} = \frac{d}{\lambda}\sin(\theta).$$
(2-3)

The received signal can be passed through a weight vector to optimize the response in some sense for a specific angle. This operation is referred to as beamforming. The output can be written as

$$y = \sum_{0}^{N-1} w_n^* s_n = w^H S_s .$$
(2-4)

where * is the complex conjugate operator, a^H denotes the Hermitian of a and S_S is the N-dimensional complex signal vector coming from a specific angle θ:

$$S_S = \begin{bmatrix} s_0 \\ s_1 \\ \vdots \\ s_{N-1} \end{bmatrix} = \begin{bmatrix} e^{j0} \\ e^{j2\pi\frac{d}{\lambda}\sin(\theta)} \\ \vdots \\ e^{j2\pi(N-1)\frac{d}{\lambda}\sin(\theta)} \end{bmatrix}.$$
(2-5)

The first element is chosen as the reference of the array. This vector is also called the spatial steering vector. The vector w contains the weights related to each element which makes the actual beamforming

$$w = \begin{bmatrix} w_0 \\ w_1 \\ \vdots \\ w_{N-1} \end{bmatrix}.$$
(2-6)

The main goal of the beamformer is often to maximize the signal response of the receiver in the direction of received signal in respect to signal-to-noise power ratio (SNR). In order to achieve this goal, the optimum weight vector shall be gathered to maximize SNR at the output.

13

$$\max_{\mathbf{w}} |y|^2 = \max_{\mathbf{w}} |w^H S|^2 .\tag{2-7}$$

This is a widely-used optimization problem which can be solved by using the condition to meet the upper bound of Schwarz's inequality ($|w'S|^2 \leq ||w||^2||S||^2$). Upper bound or the equality holds if the vectors are collinear, i.e, $w = \kappa S$ where κ is a scalar used for normalization.

The obtained weight vector contains weights for each channel which are correcting the phase shifts occurring due to the time delay of the signal between array elements. If the output is considered, it can be easily seen that each channel output is coherently integrated. Thus, the output is steered to the angle of interest θ for maximum gain at that direction.

As a remark, beamformer response (main beam width) depends on the length of the antenna and the number of array elements, N. In the other words, if the number of antenna elements is increased while the inter-element spacing is kept fixed, the beamformer response becomes finer because the spatial sampling rate is increased.

2.3.2 Temporal Processing (Doppler Processing)

Operational radars, radars have to deal also with the echos of the natural environment such as land, sea and weather all of which are called the clutter [4]. Clutter signals having large echo power in comparison to targets of interest may degrade the performance of the radar so that targets in range cells around clutter affected cells are undetectable. For detection of targets buried in heavy clutter, most of the modern radars make use of the frequency change of the signals due to the relative velocity between the radar and the reflectors. This frequency change is due to the Doppler Effect. Doppler Effect enables radars to distinguish the received echos from each other according to their frequencies to reflect relative velocities with respect to radar. Clutter is usually taken to be stationary. However, non-

stationary clutter is also present in reality. This situation will be discussed later under Intrinsic Clutter Motion (ICM).

Suppose that a single element airborne radar is transmitting N pulses with wavelength λ and PRI T_r. The received pulses with PRI intervals are processed in scope of their Doppler frequency shifts. This is a one dimensional processing and sometimes called as "Temporal Sampling". Figure 2-4 shows the physical illustration of the signal processing scheme. Each T_r block denotes a time delay of PRI so that N pulses are integrated coherently. The M-tap delay line canceller is an example to this operation [4]. Signal is sampled in time at every PRI seconds. This process is analogous to the spatial sampling that phase progression in time due to Doppler effect is similar to the phase progression between the elements of the antenna array elements [1].
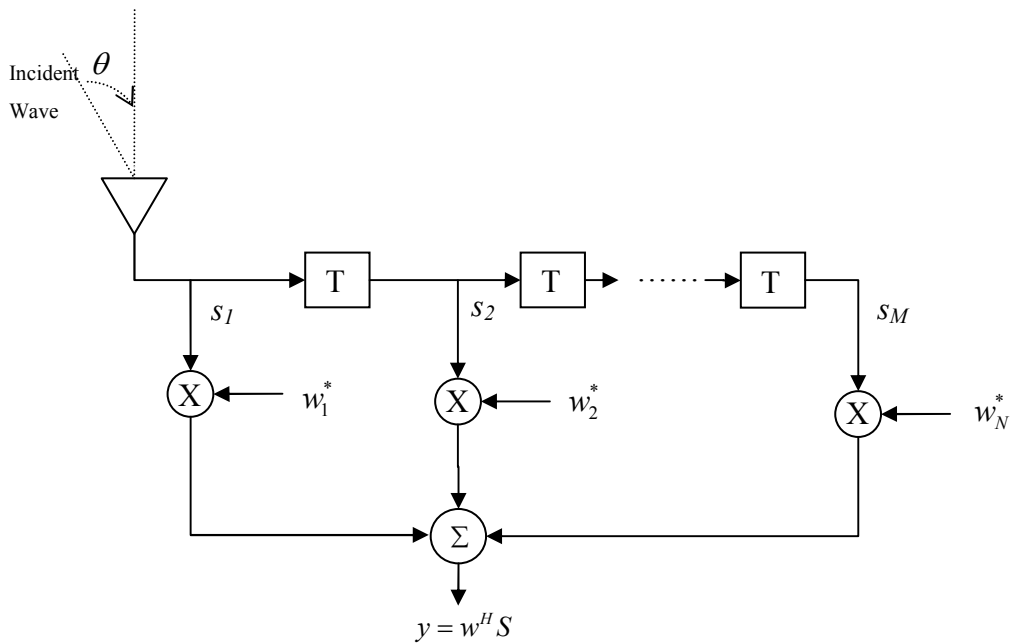
Figure 2-4 Tapped delay line illustration for signal processing of single antenna array element

Let's take a single scatterer at an initial distance of R_0. The phase shift due to the two way propagation delay for the mth pulse is

$$\phi_m = \tau_n \omega,$$ (2-8)

where τ_m is time delay for the mth pulse which is equal to $\dfrac{\text{distance}}{c} = \dfrac{2R_0 + m2\Delta R}{c}$, ω is the radian frequency and ΔR is the pulse-to-pulse change in range.

The Doppler frequency f$_d$ is found by taking the derivative of the phase

$$\frac{1}{2\pi} \frac{d\phi_m}{dt} = f_d = \frac{2v_r}{\lambda},$$ (2-9)

where $v_r = v \sin(\theta)$ is the relative velocity between the radar and the scatterer and θ is the angle between the scatterer and the array normal.

The normalized Doppler frequency is defined as [1, 2, 3]

$$\tilde{f}_d = f_d T = \frac{2vT}{\lambda} \sin(\theta),$$ (2-10)

which results in the complex envelope of the received signal corresponding to the mth pulse:

$$s_m = e^{j2\pi(m-1)\frac{2vT}{\lambda}\sin(\theta)}.$$ (2-11)

The received signal can be passed through a weight vector to maximize the signal response for a Doppler frequency. The output can be written in the same way as in spatial processing

$$y = \sum_0^{M-1} w_m{}^* s_m = \mathbf{w}^H S_t,$$ (2-12)

where S_t is the M-dimensional complex signal vector coming from a specific angle θ, in the other words, Doppler frequency:

$$S_t = \begin{bmatrix} s_0 \\ s_1 \\ \vdots \\ s_{M-1} \end{bmatrix} = \begin{bmatrix} e^{j0} \\ e^{j2\pi\frac{2vT}{\lambda}\sin(\theta)} \\ \vdots \\ e^{j2\pi(M-1)\frac{2vT}{\lambda}\sin(\theta)} \end{bmatrix}. \qquad (2\text{-}13)$$

The first received echo is chosen as the reference of the array. This vector is also called the temporal steering vector.

The vector w contains the weights related to each pulse

$$w = \begin{bmatrix} w_0 \\ w_1 \\ \vdots \\ w_{N-1} \end{bmatrix}. \qquad (2\text{-}14)$$

If airborne radar is considered, for most of the cases there is always a non-zero relative velocity between the airborne radar and the scatterers because of the aircraft's motion.

2.4 Two Dimensional Received Signal Modeling

Transmitted pulses are reflected back by the scatterers (clutter and target if present) on the ground. In addition to these reflected signals, the received signal may contain hostile jammer signals that are trying to blind the radar. Another signal component is the receiver noise added to the signal at the receiver.

The signal vector reaching to the processor after the receiver operations (down conversion, matched filtering, A/D) can be written as

17

$$X = X_t + X_i + X_n \qquad\qquad (2\text{-}15)$$

where X_t, X_i and X_n are the target, interference and noise signal vectors, respectively. The signal term X_i is composed of two vectors that are X_c and X_j which are the clutter and jammer vectors, respectively.

All the processing work will be performed on a slice of data cube taken from the fast time (range of interest). The slice shown on Figure 2-2 is an N x M matrix composed of the N spatial samples related to all M transmitted pulses for a range of interest. This slice is called the space-time snapshot.

A space-time snapshot is converted into an MN x 1 vector to be used in the rest of the thesis. Thus, the received signal from a single range can be written as [2]

$$X = \begin{bmatrix} X_0 \\ X_1 \\ \vdots \\ X_{M-1} \end{bmatrix} = \begin{bmatrix} x_{00} \\ x_{10} \\ \vdots \\ x_{(N-1)0} \\ \vdots \\ \vdots \\ x_{0(M-1)} \\ x_{1(M-1)} \\ \vdots \\ x_{(N-1)(M-1)} \end{bmatrix}, \qquad\qquad (2\text{-}16)$$

where X_k is the N-dimensional array output for the k$^\text{th}$ pulse.

The processor shall check the range of interest for the existence of any target. Thus, there are two hypotheses for the received data to make a decision of target existence:

$$
\begin{aligned}
X &= X_i + X_n; && H_0 : \text{No target is present} \\
X &= X_t + X_i + X_n; && H_1 : \text{Target is present.}
\end{aligned}
\qquad (2\text{-}17)
$$

Clutter, jammer and noise are mutually independent. These unknowns are the main problem of the radar to be compensated to enhance the detection capability of radar.

STAP algorithms take the space-time snapshot vector X_{MNx1} as the input and coherently process the samples to give an output for a threshold comparison. Threshold comparison is a way of making a decision between the two hypotheses

$$X \xrightarrow{STAP} y \underset{\underset{H_1}{>}}{\overset{\overset{H_0}{<}}{}} \text{Threshold} . \qquad (2\text{-}18)$$

The signal components described above will be modeled in the following sections to understand the signal characteristics better.

2.4.1 Single Point Scatterer

In this section, a single point scatterer's echo contribution to the received signal will be derived to use while modeling clutter and target echos. Consider an antenna array and single point scatterer as shown in Figure 2-1. The scatterer on the ground is located at a position having an azimuth angle ϕ and elevation angle θ. The relative velocity between the radar and the scatterer is defined as v_s.

The normalized Doppler frequency is defined as [1-6]

$$f_d = \frac{2vT}{\lambda} \cos(\theta) \sin(\phi) . \qquad (2\text{-}19)$$

For a fixed PRF the normalized Doppler frequency is in the range $-0.5 \leq f_d \leq 0.5$ [1]. The spatial frequency is defined as [1-6]

$$f_s = \frac{d}{\lambda} \cos(\theta) \sin(\phi) . \qquad (2\text{-}20)$$

19

Having defined the related frequencies, the signal corresponding to space-time snapshot vector elements can be written as

$$x_{nm} = \alpha \ e^{j2\pi m f_d} e^{j2\pi n f_{sp}} , \qquad (2\text{-}21)$$

where α is the complex amplitude of the scatterer's signal reaching to the receiver element, n=0,…,N-1 and m=0,...,M-1. α is found by using the radar equation that includes the two way propagation and system losses, scatterer reflection characteristics, look angle, and antenna gains. For a space-time snapshot, α is assumed to be constant for each of the space-time samples since the look angle from the antenna to the scatterer do not significantly change in a CPI. A slowly but randomly varying α will be considered in subsequent sections.

Thus, the received data vector can be written by using the steering vectors in space and time dimensions as follows

$$X = \alpha S , \qquad (2\text{-}22)$$

where S is the MN x 1 dimensional space time steering vector:

$$S = S_t \otimes S_s = \begin{bmatrix} S_{t_0} S_{s_0} \\ S_{t_0} S_{s_1} \\ \vdots \\ S_{t_0} S_{s_{N-1}} \\ \vdots \\ S_{t_{M-1}} S_{s_0} \\ S_{t_{M-1}} S_{s_1} \\ \vdots \\ S_{t_{M-1}} S_{s_{N-1}} \end{bmatrix} = \begin{bmatrix} S_s S_{t_0} \\ S_s S_{t_1} \\ \vdots \\ S_s S_{t_{M-1}} \end{bmatrix} . \qquad (2\text{-}23)$$

S_t and S_s are the spatial and the temporal steering vectors defined in space and time dimensions, respectively. (Section 2.3.1 and 2.3.2) Steering vectors are

multiplied in a special manner which is called the Kronecker product denoted by the symbol $\otimes$. (Appendix A-2)

$$S_s = \begin{bmatrix} s_{s_0} \\ s_{s_1} \\ \vdots \\ s_{s_{N-1}} \end{bmatrix} = \begin{bmatrix} e^{j0} \\ e^{j2\pi\frac{d}{\lambda}\cos(\theta)\sin(\phi)} \\ \vdots \\ e^{j2\pi(N-1)\frac{d}{\lambda}\cos(\theta)\sin(\phi)} \end{bmatrix} \tag{2-24}$$

$$S_t = \begin{bmatrix} s_{t_0} \\ s_{t_1} \\ \vdots \\ s_{t_{M-1}} \end{bmatrix} = \begin{bmatrix} e^{j0} \\ e^{j2\pi\frac{2vT}{\lambda}\cos(\theta)\sin(\phi)} \\ \vdots \\ e^{j2\pi(M-1)\frac{2vT}{\lambda}\cos(\theta)\sin(\phi)} \end{bmatrix} \tag{2-25}$$

The spatial steering vector is similar to the Vandermonde form that there is a geometric progression between elements of vector. This is because of the uniform structure of the array and that elements of the arrays are identical.

The temporal steering vector also has a Vandermonde form. This is due to the facts that pulses are transmitted with constant PRI and the relative velocity is supposed to be constant in a CPI.

The model proposed above is the ideal model which is not applicable for some real life conditions. There can be some mismatch between the antenna elements. In real life, antenna array elements may have different patterns and characteristics so that the assumption of identical array elements may not hold. Also the elements may not be placed with exactly the same spacing. These situations make the phase progression between the elements to differ.

There can be also instabilities at the transmitter of the radar that pulses may not be separated exactly by PRI. Also the velocity changes of the aircraft between pulses will result in degradation due to change of Doppler frequencies.

The problems listed above will change the ideal space-time steering vector given above such that Vandermonde form is no more satisfied. The receiver processor may attempt to compensate these errors. For the sake of easiness of modeling, these effects are discarded but in real life these should be taken into account.

2.4.2 Target Signal Model

In this section, the contribution of moving target echo to the received signal will be covered. The location of ground target on the x-y plane is given by the distance R_t to radar and angles in the azimuth ϕ_t and elevation θ_t (Figure 2-1). The target has a velocity of v_t relative to the radar. The target will have an echo signal similar to the single point scatterer case. (Section 2.4.1) The relative velocity component does not depend on only the aircraft velocity since the target is supposed to move on ground. Thus, the components of the target signal vector X_t can be written as

$$X_t = \alpha_t S_t(f_s, f_d) \tag{2-26}$$

$$
\begin{aligned}
x_{t_{nm}} &= \alpha_t e^{j2\pi m f_s} e^{j2\pi m f_d} \\
&= \alpha_t e^{j2\pi m \frac{d}{\lambda}\cos(\theta_t)\sin(\phi_t)} e^{j2\pi m \frac{2v_t Tr}{\lambda}\cos(\theta_t)\sin(\phi_t)}
\end{aligned}
\tag{2-27}
$$

where α_t is the amplitude of the signal. α_t can be found by single pulse Signal to Noise Ratio (SNR) at a single array element [2]. SNR can be written by using the radar equation

$$SNR = \frac{P_t T_p G_t(\theta_t, \phi_t) g(\theta_t, \phi_t) \lambda^2 \sigma_t}{(4\pi)^3 N_0 L_s R_t^4}, \tag{2-28}$$

$$\alpha_t = \sqrt{SNR\sigma^2}, \tag{2-29}$$

where σ_t is the radar cross section of the target and $\sigma^2 = N_0 B$ is thermal noise power per array element.

2.4.3 Receiver Noise Model

The antenna array elements own individual receivers. Mutual coupling and similar derogatory effects are not taken into account in this work. The noise samples generated by different array elements are mutually independent. In addition, the noise samples generated by a single element are temporally uncorrelated [2] when sampled carefully. Thus, receiver noise has neither spatial nor temporal correlation. Therefore, the noise in the receiver is taken to be white both in space and time.

The noise model satisfies the condition

$$E\left\{x_{n_{n_1 m}} x_{n_{n_2 m}}^*\right\} = \sigma^2 \delta_{n_1 - n_2} , \qquad (2\text{-}30)$$

$$E\left\{x_{n_{nm_1}} x_{n_{nm_2}}^*\right\} = \sigma^2 \delta_{m_1 - m_2} , \qquad (2\text{-}31)$$

or equivalently

$$E\left\{x_{n_{m_1 m_1}} x_{n_{n_2 m_2}}^*\right\} = \sigma^2 \delta_{n_1 - n_2} \delta_{m_1 - m_2} , \qquad (2\text{-}32)$$

where δ_{a-b} is equal to 1 for $a = b$ and 0 for $a \neq b$, σ^2 is thermal noise power per array element equal to $N_0 B$ which is taken as 1 throughout this script in order to consider SNR as the signal level.

When I_{MN} is the MN x MN identity matrix, the covariance matrix of noise is

$$R_n = E\left\{X_n X_n^H\right\} = \sigma^2 I_{MN} \qquad (2\text{-}33)$$

In real life, sky noise also exists in the environment which brings spatially correlated noise components to the signal model [2].

2.4.4 Jammer Signal Model

While airborne radars fly over the hostile regions, there may be jammers which transmit signals to the radar to degrade its performance. There are different kinds of jammers applying various jamming techniques. In the scope of the thesis, jammers applying noise jamming technique will be considered. Ward [2] stated that the signal samples received from a jammer are temporally uncorrelated from pulse to pulse that looks like thermal noise stated in Section 2.4.3. However, samples are spatially correlated from element to element like a point target described in Section 2.4.2.

Consider single jammer at a distance to radar, R_j and angles in the azimuth ϕ_j and elevation θ_j with an effective radiating power P_j.

Then, jammer space-time snapshot vector can be written as

$$X_j = \alpha \otimes J = \begin{bmatrix} \alpha_0 J \\ \alpha_1 J \\ \vdots \\ \alpha_{M-1} J \end{bmatrix} \tag{2-34}$$

where α is M x 1 dimensional amplitude vector of the jammer related to each of M pulses and J is the N x 1 dimensional spatial steering vector.

The temporally uncorrelated signal satisfies the following

$$E\left\{\alpha_{m_1} \alpha_{m_2}^*\right\} = \frac{JNR}{\sigma^2} \delta_{m_1 - m_2}, \tag{2-35}$$

where σ^2 is thermal noise power per array element and JNR is the jammer to noise power ratio. JNR is defined in [2] as

$$JNR = \frac{P_j g(\theta_j, \phi_j)\lambda^2}{(4\pi)^2 N_0 L_r R_j{}^2}$$

(2-36)

Then, the covariance matrix of single jammer is

$$R_n = E\left\{X_j X_j{}^H\right\} = \sigma^2 JNR\, I_M \otimes (JJ^H).$$

(2-37)

2.4.5 Clutter Signal Model

Clutter is defined as the unintended scatterer echos coming back to the radar. It doesn't have any tactical information, besides it degrades the radar performance. The main source of the clutter for airborne radar is the echos coming from the ground. In real life, the clutter is hard to model because it is very heterogeneous in many aspects such as angle, range, Doppler spread, clutter type, ground model [2].

The clutter interference will be the main type of signal a STAP algorithm has to suppress. This section will cover received clutter signal model that is present in the received samples. The model will consider the space-time snapshot vector as the other sources (target, jammer and noise) in contributing to the received signal samples. Also the covariance matrix of clutter will be investigated. Finally, the issues that change the clutter model will be described.

2.4.5.1 Signal Model

Ground clutter echo can be modeled as the sum of clutter patches whose echos resembles the echo of a single point scatterer defined Section 2.4.1. Clutter patches are supposed to be inherently stationary. Consequently, the relative velocity

between any clutter patch and the radar depends only on the velocity of the aircraft and orientation between them.

The ground clutter echo is supposed to be reflected back from the whole region in field of view of the radar. In other words, there is no clutter contribution for longer distance than the radar horizon. Radar horizon is defined in [2] as

$$R_h = \sqrt{2a_e h + h^2} \approx \sqrt{2a_e h} \,,$$
(2-38)

where $a_e \approx 4/3*6.378 \, \text{km}$ is the effective earth radius.

A radar's unambiguous range is defined as $R_u = cT_r/2$. If PRI is selected such that the unambiguous range is greater than the radar horizon, clutter contribution to the received signal is said to be unambiguous in range. This means, the received signal will be related to just one pulse. Otherwise, the signal will have an ambiguity so that the received signal may contain echo due to the recent pulse from close-by regions along with echo due to the previous pulses from far away regions. For the second situation, the radar is not able to distinguish whether the received signal is from the nearer regions or from further regions.

In real life, R_h is supposed to be so far that ambiguity in range will always exist. Ward [2] states that clutter signal vector will have contributions from all ambiguous ranges found by superposition of the echos. Actually, what differs between the range cells is the elevation angle.

Suppose there are N_r range ambiguities. Each ambiguous range also consists of N_c independent clutter patches. For the ik^{th} patch, i denotes the range R_i or the elevation angle θ_i and k denotes the azimuth angle ϕ_k. The normalized Doppler frequency and spatial frequencies defined as

$$f_{d_{ik}} = \frac{2vT}{\lambda} \cos(\theta_i) \sin(\phi_k) \,,$$
(2-39)

26

$$f_{sp_{ik}} = \frac{d}{\lambda}\cos(\theta_i)\sin(\phi_k).$$

(2-40)

Then, the space-time snapshot vector of clutter described by the model in [2] is

$$X_c = \sum_{i=1}^{N_r}\sum_{k=1}^{N_c}\alpha_{ik}S_{ik}$$

(2-41)

where $S_i = S(f_{d_{ik}}, f_{sp_{ik}}) = S(\varphi_k, \theta_i)$ is the space-time steering vector the same as that of the single point scatterer in Section2.4.1 defined for $f_{d_{ik}}, f_{sp_{ik}}$ and α_{ik} is the random clutter amplitude of ik[th] clutter patch.

The average power in α_{ik} directly depends on the effective area of the clutter patch. For a single iso-ring, the azimuth angle width is defined by the number of the clutter patches N_c as $\Delta\phi = 2\pi / N_c$ and the range ring width is the range resolution find by $\Delta R \cong c / B$.

Each clutter patch has its own radar cross section (RCS)

$$\sigma_{ik} = \sigma_0(\phi_k, \theta_i) \text{ x Patch area} = \sigma_0(\phi_k, \theta_i) \, R_i\Delta R\Delta\phi\sec\psi_i$$

(2-42)

where ψ_i is the angle between the range vector of the ith range and the surface tangent and $\sigma_0(\theta_i, \phi_k)$ is the area reflectivity of the ground which depends on the location (angle and range) of the ith clutter patch [2].

The clutter patch amplitude satisfies the conditions

$$E\{\alpha_{ik}\alpha_{ik}*\} = \sigma^2 CNR_{ik}$$

(2-43)

where σ^2 is thermal noise power and Clutter to Noise Ratio (CNR) is defined for each of the clutter patch according to the angle and range [2]:

$$CNR_{ik} = \frac{P_t T_p G_t(\phi_k, \theta_i) g(\phi_k, \theta_i) \lambda^2 \sigma_{ik}}{(4\pi)^3 N_0 L_s R_i^4}.$$
(2-44)

The clutter patches are also assumed to be uncorrelated so that

$$E\{\alpha_{ik}\alpha_{jl}*\} = \sigma^2 CNR_{ik}\delta_{i-j}\delta_{k-l}$$
(2-45)

Finally, the covariance matrix which shows the characteristics of the clutter can be written as

$$R_c = \sigma^2 \sum_{i=1}^{N_r} \sum_{k=1}^{N_c} CNR_{ik} S_{ik} S_{ik}^H.$$
(2-46)

2.4.5.2 Special Cases

Ideal conditions have been assumed so far in developing the signal models. However, there are some effects which significantly alter these models and can potentially degrade the receiver performance [1, 2, 6]. An important one of these effects is the decorrelation that may occur in spatial and/or temporal domain.

2.4.5.2.1 Clutter Ridge

The normalized Doppler and spatial frequencies of a single clutter patch shows a special relationship. That is, the normalized Doppler frequency can be written in terms of spatial frequency multiplied with a coefficient as in

$$f_d = \frac{2vT}{d}\left(\frac{d}{\lambda}\cos(\theta)\sin(\phi)\right) = \frac{2vT}{d}f_{sp} = \beta f_{sp},$$
(2-47)

where

$$\beta = \frac{2vT}{d}.$$
(2-48)

The parameter β defines the slope between the normalized Doppler and spatial frequencies. It represents how many half interelement spacing is traveled by aircraft during a single PRI. In the other words, this parameter reveals the ratio of the spatial Nyquist frequency to the operational spatial frequency. Consider interelement spacing is the half of the wavelength. Then, $\beta = 4vT/\lambda$ defines the amount of the clutter spectrum aliasing into unambiguous Doppler range [2].

For the airborne radar, there is a possibility that clutter echo may reflect back to the radar from any angle. Thus, the existence of clutter on the angle-Doppler space can be drawn to see how much of the angle-Doppler space is occupied by clutter. This area is called the clutter ridge.

The clutter ridge directly depends on β so that it defines how many times the Doppler space is spanned. It can be seen that it depends directly on the aircraft velocity and the PRI. For the cases $\beta \leq 1$, it can be said that the clutter is unambiguous in Doppler. Unambiguous in Doppler means that for a given Doppler frequency there may be at most one angle that may have coincidence with target which degrades the target detection. However when $\beta > 1$ then the clutter is ambiguous that clutter may be observed in more than one spatial angle for a single Doppler frequency. The observable space is assigned by the value of the PRF and if β value exceeds 1 than the clutter spectrum extends over the observable space, i.e. aliasing occurs. Consequently, as β gets larger, the clutter occupancy on the angle-Doppler space increases with ambiguity degrading the radar performance on target detection. In the latter cases, clutter suppression becomes harder.

Clutter ridge is summarized on the angle-Doppler graphs for different values of β by changing velocity, PRF and interelement spacing variables. Figure 2-5 denotes the ideal case ($\beta = 1$) where the clutter ridge occupies all the diagonal of angle-Doppler space.
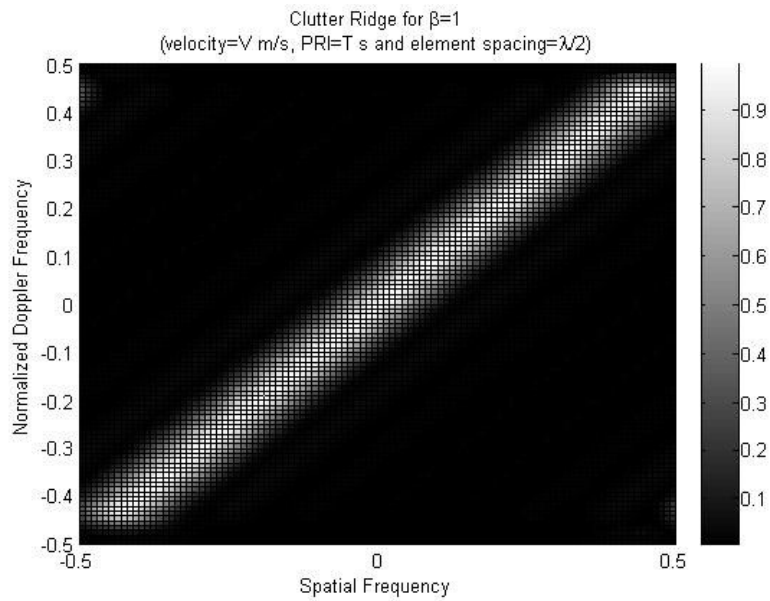
Figure 2-5 Clutter Ridge for $\beta = 1$

Figure 2-6 and Figure 2-7 shows the location of the clutter patches in case of PRF and interelement spacing is kept constant and the velocity is varied. In Figure 2-6, the velocity is reduced to half of it initial value that the Doppler frequencies are also reduced. It is ambiguous in Doppler as shown in Figure 2-7. That is, the aircraft moves so fast that the sampling frequency in time domain is not enough which causes aliasing in Doppler domain. The clutter seems to occupy wide area in the angle-Doppler space.
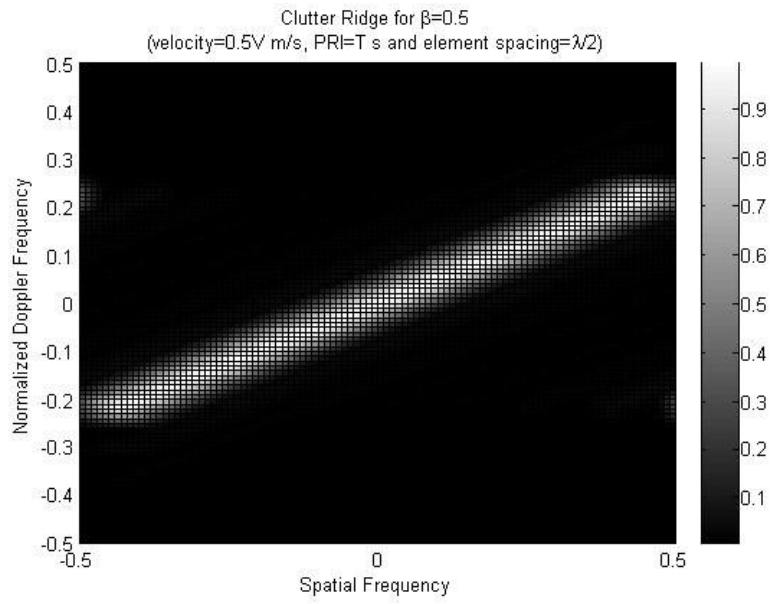
Figure 2-6 Clutter Ridge for $\beta = 0.5$
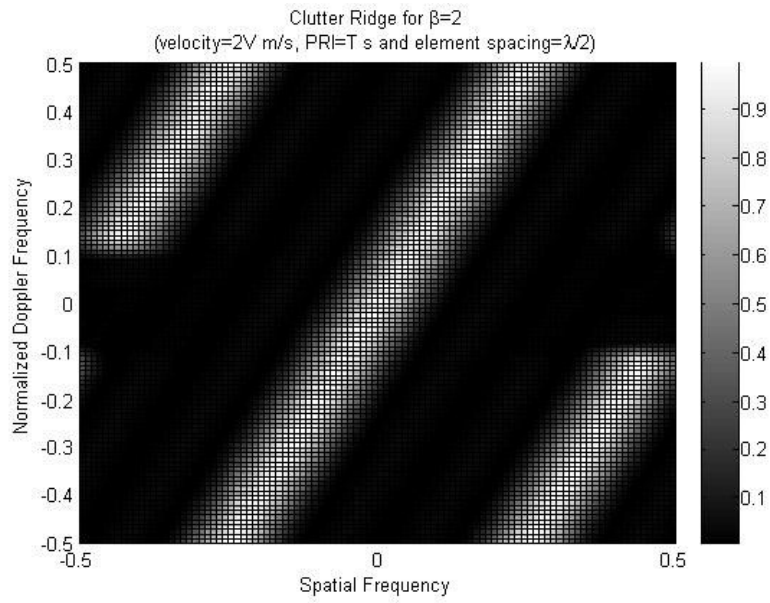
Figure 2-7 Clutter Ridge for $\beta = 2$

31

As an alternative, Figure 2-8 and Figure 2-9 shows the location of the clutter patches in case of the velocity and interelement spacing are kept constant and the PRF is varied. In Figure 2-8, the PRF is increased to double of it initial value that the normalized Doppler frequencies are reduced. It is ambiguous in Doppler as observed in Figure 2-9. That is, the PRF is not enough to sample fast that aliasing in Doppler space occurs. The clutter seems to occupy wide area in the angle-Doppler space.
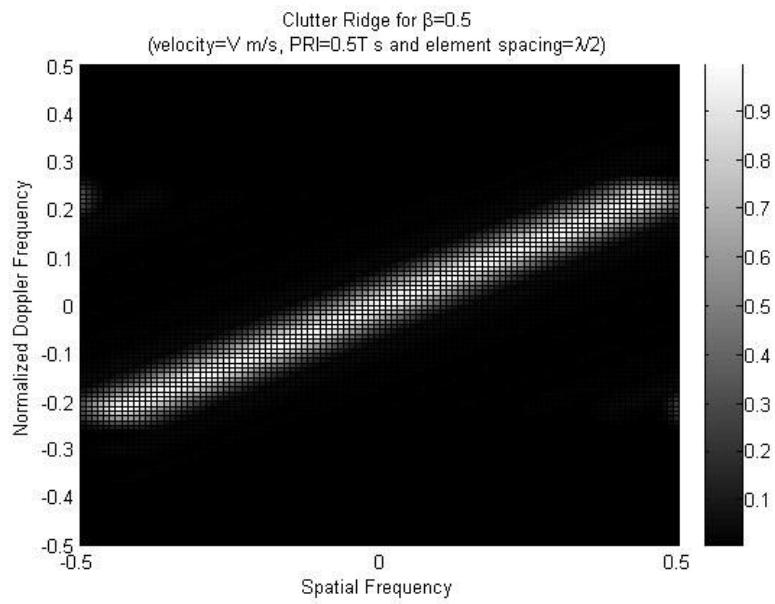
Figure 2-8 Clutter Ridge for $\beta = 0.5$
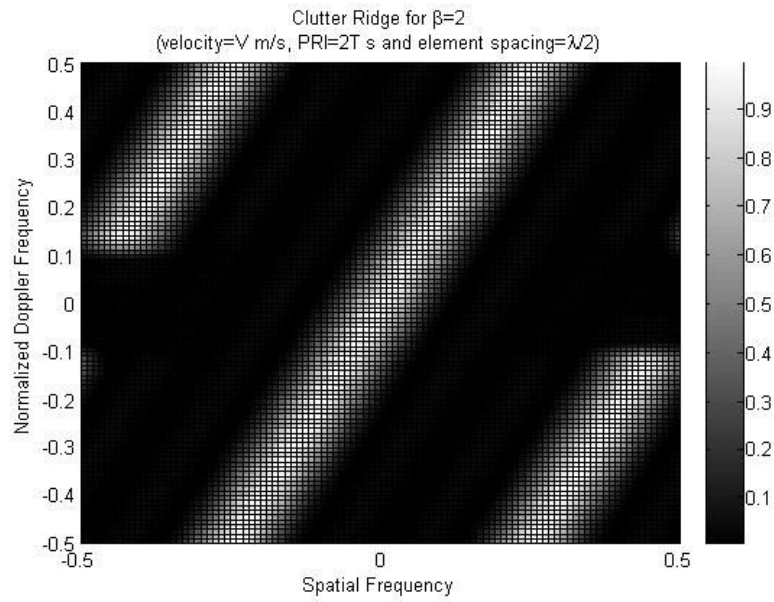
Figure 2-9 Clutter Ridge for $\beta = 2$

As a last observation, Figure 2-10 and Figure 2-11 shows the location of the clutter patches in case of the velocity and PRF is kept constant and the interelement spacing is changed. It is spatially ambiguous as seen in Figure 2-10. That is, the interelement spacing is so wide that spatial sampling is insufficient and aliasing occurs. The clutter seems to occupy a wide area in the angle-Doppler space. In Figure 2-11, the interelement spacing is reduced to half of it initial value that the spatial frequencies are also reduced.
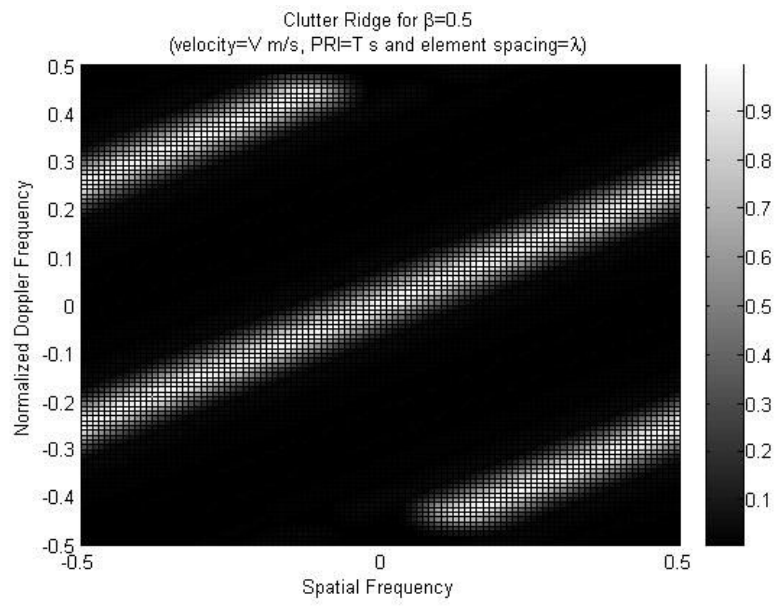
Figure 2-10 Clutter Ridge for $\beta = 0.5$
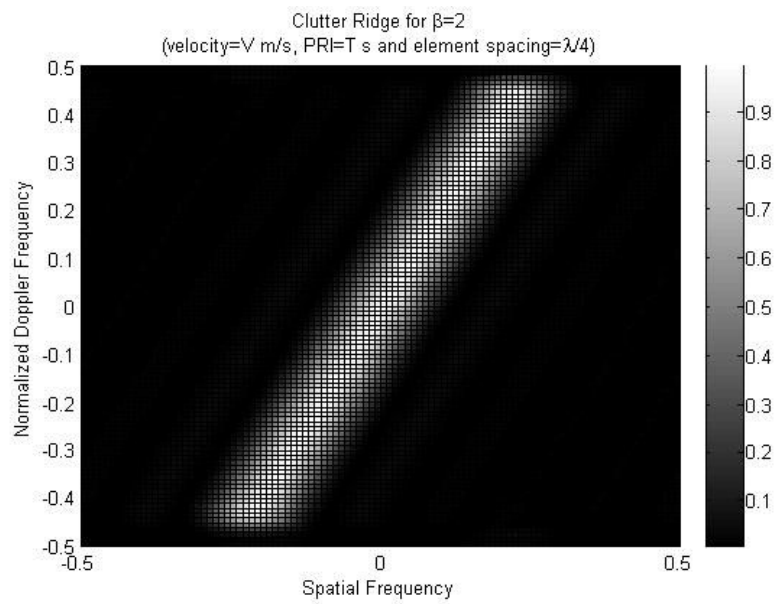
Figure 2-11 Clutter Ridge for $\beta = 2$

34

As it can be seen from Figure 2-6 to Figure 2-11, if the aircraft velocity, PRF and interelement spacing are not selected properly, clutter spread widens in the angle-Doppler space.

Rank of clutter covariance matrix is important since it determines the clutter spread. The covariance matrix of clutter can be written with eigenvalue decomposition:

$$R_c = E_c \Lambda_c E_c^{H} .$$
(2-49)

Brennan and Staudaher [2, 5] has showed that the rank of the clutter covariance matrix can be written approximately as a function of β

$$rank(R_c) = \left\lfloor N + (M-1)\beta \right\rfloor$$
(2-50)

Brennan rule tells the number of eigenvalues which exceeds zero. The rank is determined by the number of independent observations. For the case $\beta = 1$, the aircraft moves just one interelement spacing in a PRI time. Thus, the observation of two consecutive elements in one PRI time coincide that the second observation of the latter element is same as the first observation of the preceding element. As a consequence of equation (2-48), it can be observed that low PRF radars have higher rank of covariance matrix. Also as the aircraft moves faster, the rank is also increased. Because of the linear relation of the rank with β value, rank also determines the amount of Doppler ambiguity.

This rule does not take into account the case of any back-lobe reception, velocity misalignment of the ULA due to crabbing of aircraft, element mismatches of ULA and intrinsic clutter motion. These situations increase the rank of the clutter covariance matrix and are ignored while deriving the Brennan rule. Ward [2] showed for the noninteger values of β that Brennan rule underestimates the rank.

2.4.5.2.2 Aircraft Velocity Vector Misalignment with ULA

When the aircraft is flying there may be some drift due to the crabbing. Crabbing corresponds to the case that the air speed of the aircraft is not the same as the speed on ground. The velocity vector is misaligned with the antenna array which is in the direction of aircraft heading. The offset due to the crabbing is shown on Figure 2-12.

Figure 2-12 Aircraft crabbing
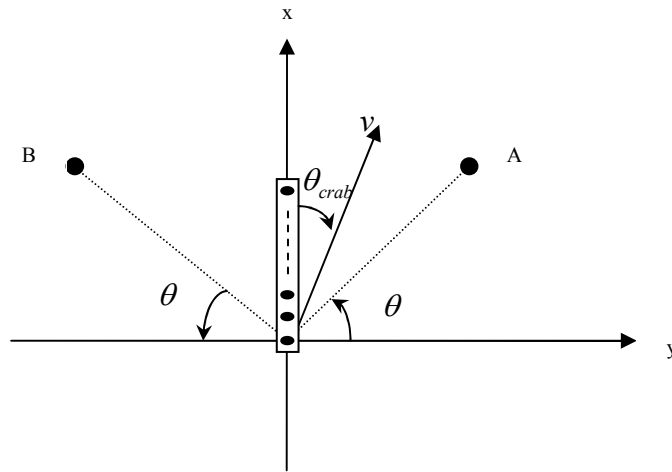
The clutter ridge dependence on the crabbing angle is summarized from Figure 2-13 to Figure 2-16.
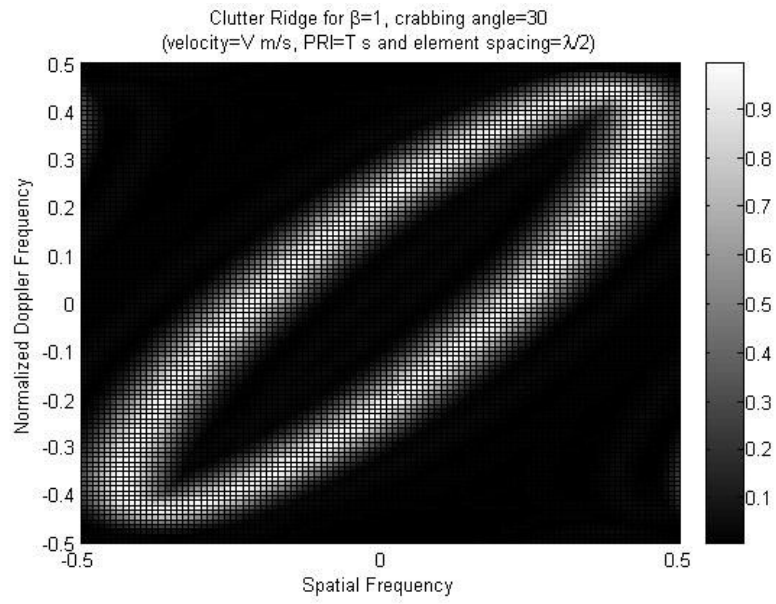
Figure 2-13 Clutter Ridge for $\beta = 1$ and crabbing angle is $30°$
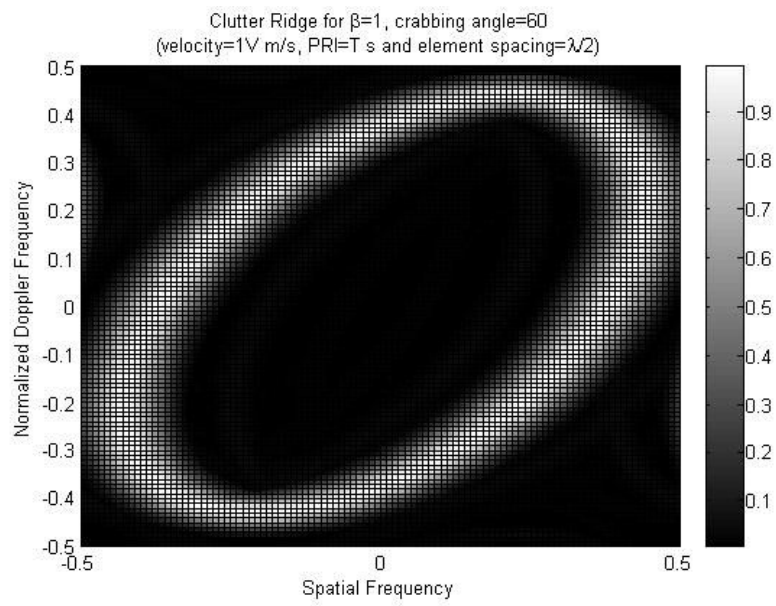
Figure 2-14 Clutter Ridge for $\beta = 1$ and crabbing angle is $60°$
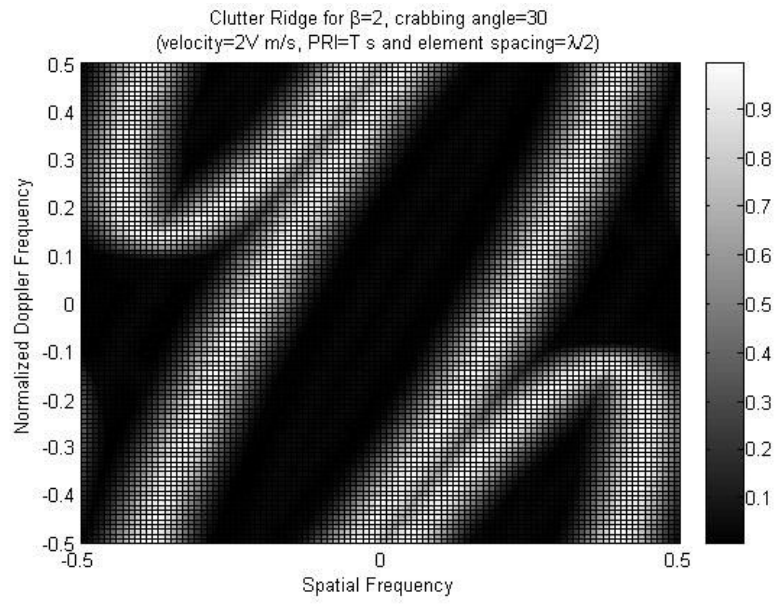
Figure 2-15 Clutter Ridge for $\beta = 2$ and crabbing angle is $30°$
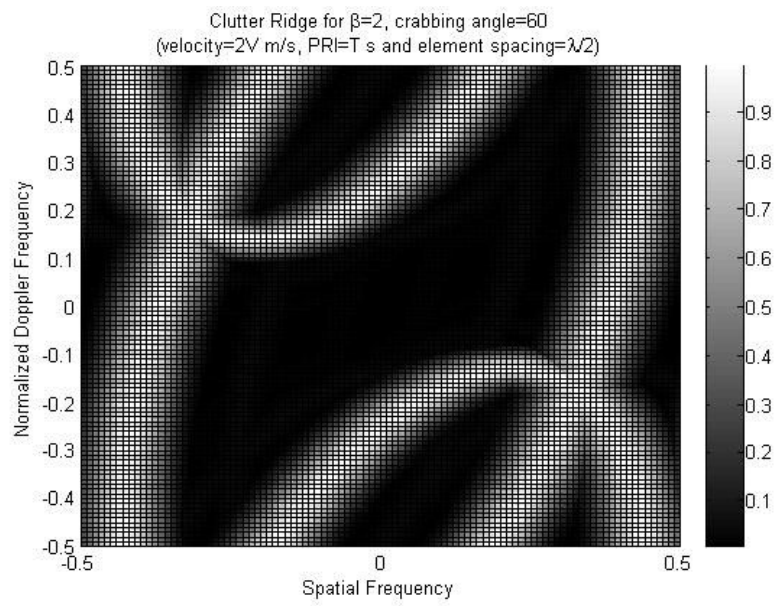
Figure 2-16 Clutter Ridge for $\beta = 2$ and crabbing angle is $60°$

It is assumed that the aircraft crabbing is only on the azimuth. So, there is a misalignment angle, ϕ_{crab} between the velocity vector and the antenna array axis. If there isn't any misalignment, the scattered signals from point A and B shown on Figure 2-12 at angles ϕ and $180 - \phi$ has the same Doppler frequencies. However if there is a slight crabbing, the Doppler frequencies start to differ. This is mainly the problem due to the back-lobe reception that clutter occupies much region in Doppler space degrading the radar performance of target detection. The upper side of the clutter ridge (upper side of diagonal) shown in the figures from Figure 2-13 to Figure 2-16 represents the front-lobe reception and the below side represents the back-lobe reception. It is clear that back-lobe suppression prevents the radar to be sensitive to the effect of velocity misalignment.

As the crabbing angle gets larger, clutter ridge occupies a larger area on the Doppler space so that the possibility of a target to be collocated with clutter in angle-Doppler is increased. Actually it is doubled since the place of the front-lobe and back-lobe clutter start to be different on the angle-Doppler space. The need for degree of freedom is then increased. Instead of being a straight line, the clutter ridge becomes elliptic which turns to be a circle as the crabbing angle increased to 90 degrees (forward looking case).

Crabbing affects only the normalized Doppler frequency [2]

$$f_d = \frac{2vT_p}{\lambda} \cos(\theta) \sin(\phi - \phi_{crab}) , \qquad (2\text{-}51)$$

whereas the spatial frequency is still the same

$$f_{sp} = \frac{d}{\lambda} \cos(\theta) \sin(\phi) . \qquad (2\text{-}52)$$

To conclude, as the crabbing angle increases, clutter interference region becomes larger and the rank of the clutter covariance matrix increases so that the Brennan

rule loses the validity. The velocity misalignment brings the need for a higher degree of freedom for suppression purposes.

2.4.5.2.3 Intrinsic Clutter Motion (ICM)

For the sake of simplicity, the clutter has been so far assumed to be stationary during one CPI, i.e., the echo signal from a patch is constant and the space-time snapshot matrix is modeled by using the temporal and spatial steering vectors. However, in reality the clutter echoes fluctuate from pulse to pulse due to decorrelation of clutter so that the model has to be modified. The reason for the fluctuation of the received echo may also be the instabilities of the radar receiver.

No matter what the reasons are, these fluctuations are studied under the general title of Intrinsic Clutter Motion (ICM) [2]. ICM can also be handled by using wider clutter notch filters and an increased degree of freedom.

ICM can also be modeled by multiplying the temporal steering vector with coefficients related to ICM [2]. Consider a single clutter patch

$$X_c = (\alpha \bullet S_t) \otimes S_{sp} \tag{2-53}$$

where α is the random amplitude vector.

The strength of ICM determines in the rank of clutter covariance matrix. In particular, higher ICM increases the rank. As the rank increases, the need for larger degrees of freedom increases because the clutter occupies wider region in the angle-Doppler space.

2.4.5.2.4 Range Walk

There is a time delay of T_r between receptions of reflections from consecutive range rings. During this time delay the aircraft moves a little in the x direction causing the

latter range ring also moving the same distance in the x direction. Thus, in a single PRI, movement of range ring of interest causes a decorrelation of the signals received in consecutive PRI's. For the sake of simplicity, the clutter and platform is supposed to be stationary so that no range walk effect is encountered. Thus, this effect is not included in the model.

2.5 Received Signal Processing

In this section, the STAP technique will be discussed as a multidimensional signal processing (joint domain processing) approach for the received signal. The optimum solution for STAP will be derived to be used as the basis of the performance comparison with the DPCA technique.

2.5.1 Displaced Phase Center Antenna (DPCA)

It is introduced in the introduction that DPCA is a traditional method used in many airborne radar applications to compansate the aircraft motion effect. It aims to mitigate the interference and detect the target. The ground is sampled by two consecutive phase centers. The rear phase center replaces the position of the other in a single PRI. Simple subtraction of these two samples cancels out the clutter which is assumed to be stationary. However the target has a velocity creating an additional Doppler frequency other than the one created by aircraft velocity. This process is analogous to the basic two pulse MTI process in which the radar is stationary and the target is in motion as opposed to the airborne radar case. DPCA seems theoretically very successful to compensate the Doppler spread of clutter due to the aircraft motion. However, it brings some extra requirements that are hard to satisfy like the aircraft shall replace the phase center's location in exactly one PRI time. Aircraft velocity is prone to change in magnitude and direction very easily in air that this requirement may not be met. Additionally, the plain DPCA does not propose an adaptive solution to give an optimum result in changing environments.

The DPCA weight vector is derived for an antenna array with multiple pulse receptions in [1]. The weight vector is calculated by using the NM x 1 dimensional desired signal vector S as

$$w = \Omega^H \Omega S, \tag{2-54}$$

where

$$\Omega = \begin{bmatrix} w_1' & w_2' & 0' & \cdots & 0' \\ 0' & w_1' & w_2' & \cdots & 0' \\ \vdots & & \ddots & & \vdots \\ 0' & 0' & \cdots & w_1' & w_2' \end{bmatrix}, \tag{2-55}$$

$$w_1 = \begin{bmatrix} 0 \\ 1 \\ \vdots \\ 1 \end{bmatrix}, \quad w_2 = \begin{bmatrix} -1 \\ \vdots \\ -1 \\ 0 \end{bmatrix}. \tag{2-56}$$

Note that Ω is a sort of a transformation applied on the desired signal vector. It includes N-dimensional weight vectors w_1 and w_2 which are used for the DPCA operation. They clear the first and last spatial samples respectively. Another point is that only two successive pulses are included so that there is no M pulse coherent processing.

2.5.2 Space-Time Adaptive Processing (STAP)

As it is discussed in Section 2.1, STAP tries to reach an optimum solution for the detection of a target at a specific range and angle. STAP is fed by a MNx1 space-time snapshot vector of the range of interest. This sample input is multiplied by a MNx1 weight vector and integrated coherently. By the way, each space-time sample is multiplied by its own weight. (See Figure 2-17) The main goal of STAP is to find an optimum weight to null the unwanted components (interference) in the

received signal and maximize the gain for the target. STAP works on both dimensions coherently that the beamforming and the Doppler filtering is done at the same time. This section will first discuss the fully adaptive STAP with optimum weights. This algorithm is supposed to possess the interference correlation matrixes as a priori information to compute the weights. In real life, interference correlation matrices are unknown and thus have to be estimated to compute the weights.

The general scheme of the STAP processor system is drawn in the Figure 2-17.
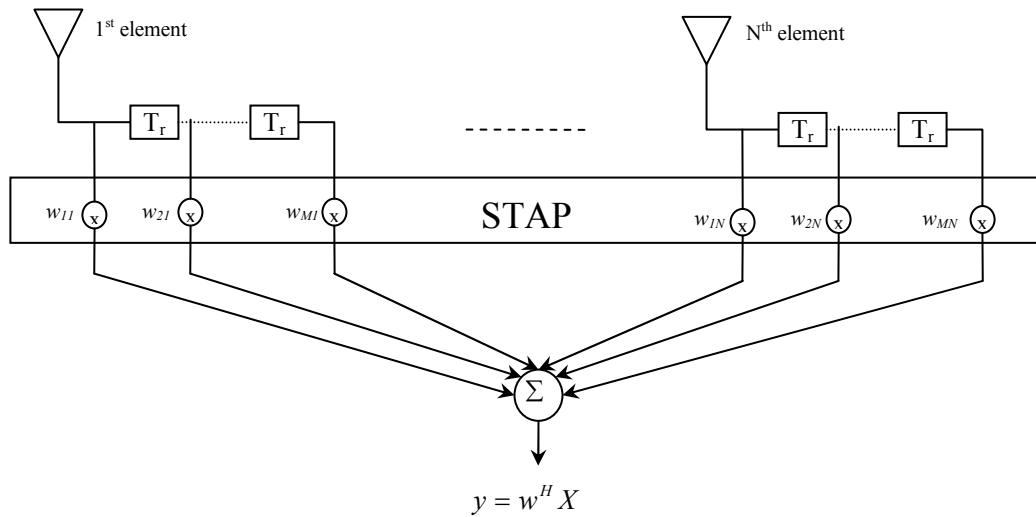
Figure 2-17 STAP architecture, each element of the space-time snapshot is multiplied by its own weight.

STAP processor is fed by the datacube and space-time samples are weighted to cover all the ranges, angles and Doppler frequencies. The space-time sample vector which is gathered for a single range is multiplied by the MNx1 dimensional weight vector w:

$$y = w^H X,$$

<div align="right">(2-57)</div>

where X is the NM x 1 dimensional input vector and y is the scalar output.

The output of the STAP is a scalar value to be compared with a threshold to make the target existence decision in the range ring for a specific angle and Doppler pair.

STAP searches angle and Doppler regions that are suspected to have target presence. Weights are computed according to the interference and target angle and Doppler information. Weight calculation is a computationally extensive process that linear system equations have to be solved to suppress the interference while maximizing the gain for target. For all the range rings available in the CPI and in the interested area individual weight vectors shall be computed.

The interference (clutter and jammer) autocorrelation matrices are unknowns for the processor so that the datacube is used for estimation of the interference present in the range of interest. The other space-time snapshots belonging to the range rings other than the interested one (other slices of the datacube) are used as training data or secondary data. Especially, the closer range rings to the interested range ring are used since their interference characteristics are similar to the range ring of interest. Training data shall be sufficient to have a good estimate of the autocorrelation.

Since the datacube is updated every CPI, weights shall be updated even. Also there can be unstationary conditions that change the environment. There shall be also a check mechanism to notice the unstationary and change the weight vector accordingly. Number of the available data depends on the number of the range rings which changes with pulse repetition interval and pulse width.

2.5.2.1 Optimum STAP Algorithm

Analogous to the one dimensional processing, the optimum solution for the weight to null the interference and maximize target signal is found by maximizing the signal to interference plus noise ratio (SINR).

Let's consider an input signal

$$X = X_t + X_c + X_j + X_n. \tag{2-58}$$

The signal components other than that of the target are random so that target just shifts the mean value of the signal. The NM x NM dimensional covariance matrix is obtained then

$$R = R_c + R_j + R_n. \tag{2-59}$$

The optimum weight vector w tries to maximize the SINR at the output of the STAP processor. By applying the Schwarz inequality, the upper bound for the SINR can be found.

$$\begin{aligned} \max_{w} \frac{|w^H S_t|^2}{w^H R w} &= \max_{w} \frac{|w^H R^{1/2} R^{-1/2} S_t|^2}{w^H R w} \\ &\leq \frac{(w^H R w)(S_t^H R^{-1} S_t)}{w^H R w} = S_t^H R^{-1} S_t \end{aligned} \tag{2-60}$$

The equality holds if the $R^{1/2} w$ and $R^{-1/2} S_t$ are collinear. Then, the optimum weight vector is found as

$$w = \kappa R^{-1} S_t, \tag{2-61}$$

where κ is some arbitrary constant.

45

The weight vector contains both the autocorrelation information of the interference and the hypothesized position of the target angle and Doppler. A bank of weights is used to check the existence of target in various angle-Doppler pairs.

Another difficulty while obtaining the weight vector is the estimation of the interference covariance matrix. There may be some errors occurring due to the ideal system modeling like velocity misalignment of the array with the aircraft velocity vector, antenna mismatches etc. As it is stated in the beginning of Section 2.5.2, weight vectors shall be updated for each received datacube which may change every CPI according to change in the orientation in space and also the changing environment. The change of the environment between range rings can be also handled by obtaining weight vectors for range rings individually.

The performance between different STAP algorithms is compared in accordance to the SINR loss, minimum detectable velocity, SINR improvement factor and sample support requirement [1, 2, 6].

SINR loss is the ratio of the SINR at the STAP algorithm output with the interference-free SNR. Similarly, SINR improvement factor is the ratio of the SINR at the STAP algorithm output with single element-single pulse SINR. Minimum detectable velocity is another criterion of performance comparison that it is the velocity closest to main lobe clutter with acceptable SINR loss. Sample support requirement corresponds to the number of data samples for a sufficiently good estimation of the covariance matrix of the interference to be used in the weight calculation.

The covariance matrix of the interference can be estimated from the near-by range rings of the range ring of interest because it is assumed that the interference in these range rings exhibit similar behavior with the interference of the inspected range ring. Then the estimate of R is

$$\hat{R} = \frac{1}{L}\sum_{i=1}^{L} X_i X_i^H,\qquad (2\text{-}62)$$

where L is the number of the range rings used for estimation and X_i is the space-time snapshot vector of the ith range ring.

CHAPTER 3

RECEIVED SIGNAL SIMULATION

FOR AIRBORNE RADAR

3.1 Introduction

The main purpose of this thesis is to model the received signal as close to reality as possible. In CHAPTER 2, airborne radar system parameters are introduced and modeling of the received signal in GMTI radars has been discussed.

The received signal model can vary according to many aspects. In this chapter, the detail of the implementation of received signal simulator is explained. The simulation provides a signal both in space and time dimensions composed of ground clutter, target and the receiver noise. Jammer signal model is not included in the simulator.

Firstly, the simulation study starts with the basic model proposed in literature [1, 2, 3, 6, 7]. The basic model generates clutter, target and the receiver noise signals separately and then superposes them into a single received signal. Ground clutter is modeled as a composition of small clutter patches to form a grid structure on the ground, i.e. x-y plane. These patches are assumed to scatter independent signals from each other in time. Each of the patches is defined with the elevation and azimuth angles found from the x-y coordinates of the patch. The areas of the

patches assumed to be equal and comparably small with the range resolution. After the formation of patches, the ones, which are in the iso-ring of interest, are selected to be used in the simulation. Iso-ring is found by using the range resolution of the radar on ground. In the other words, iso-ring for a range of interest contains clutter patches whose back-scattered signals are received in single pulse width duration.

The basic spatial and temporal steering vectors are obtained to form the space-time steering vector which defines the location of clutter patches on the angle-Doppler space. This vector strictly depends on the elevation and the azimuth angle of the clutter patch to the antenna array. As a next step, the power of the clutter patches are calculated including the radar system parameters like antenna beam pattern. Then, the final space-time snapshot for each of the clutter patches is found and the total clutter space-time snapshot vector is found by superposition of these vectors.

Target resembles a single clutter patch on ground. Hence, the same model of clutter patch is used for calculation of the space-time steering snapshot of the target. Besides the aircraft velocity creating the Doppler frequency of target, the target is assumed to have its own velocity opposed to the stationary clutter patch assumption. Thus, the space-time steering vector of the target is modified by re-calculation of the relative speed between the target and the antenna array.

Noise is modeled to have spatial and temporal components uncorrelated in time and space. Finally, the total received signal is obtained by superposition of clutter, target and receiver noise signals.

Following the development of the basic model, new features are added to the simulator to make it capable of simulating the effects of aircraft motion, velocity irregularities of the aircraft and also the clutter characteristics on the produced signal. These additional capabilities give insight to understand how the received signal behaves under these aspects. The space-time steering vectors of clutter patches and target are modified in this manner so that the basic model is improved.

To sum up, in this chapter, a simulation study will be introduced to be used as a medium input for testing the performance of some algorithms. The simulation provides a multi-antenna signal composed of received signal back-scattered from clutter, a single target, and also the receiver noise. CHAPTER 4 provides the output of the simulator under different system parameters and aspects added over the basic model.

3.2 Received Signal Simulation (Clutter, Target and Noise)

This section will describe the signal models of the clutter and target model to be used as an input for the evaluation of STAP algorithms. The simulation comprised of two phases; signal modeling and implementation of simulation.

In the 3-dimensional view, the "x-y" plane is assumed to be the ground to be observed. The scatterer sources on the ground include a single target and clutter. The clutter signal model is taken from [2] with slight modifications by the concepts provided in Section 2.2.

3.2.1 Assumptions

In consideration of airborne radar signal reception, there exist many aspects that affect the characteristics of the received signal if one desires to correctly model the received signal on an actual aircraft. Therefore, the real data collected by airborne radar includes many aspects which are hard to implement on the simulator. Consequently, main aspects that are thought to have much influence on the signal model are taken into consideration in the simulator. These aspects are the aircraft and scatterer (both clutter and target) orientations, aircraft flight characteristic, radar parameters, and also the scatterer characteristics. Actually, the rest of the aspects other than these aspects are discarded in this thesis study. The following assumptions are made during the signal modeling for simulator.

Airborne radars are exposed to different weather and other atmospheric conditions so that the received signal characteristics from scatterers differ from the expected case. Since this subject is under the scope of electromagnetic wave propagation, it is neglected for the purposes of this work.

Among various kind of clutter, the ground clutter which has the main influence on the signal is considered in the simulator. Ground clutter variation during each PRI is modeled according to intrinsic clutter motion (ICM) which is always available in nature.

Despite the fact that the earth's surface is rough and has hills and cavities in reality, the ground is assumed to be flat all over the region of interest so that all the scatterers are at zero altitude in simulations. The actual airborne case makes the problem hard to simulate the reception of signals since time of arrival of the signal coming from a clutter patch over the hills is earlier than a clutter patch inside the cavities. Thus, these two clutter patches may not fall into the same iso-ring of interest as opposed to the case of flat ground modeling.

During the flight of the airborne radar, the observed scene which is composed of the areas located on the iso-ring appears to move relative to radar. Consider a single iso-ring. The motion of the aircraft causes the effect of decorrelation since back-scattered samples from the expected iso-ring start to come from different clutter patches belonging to the adjacent iso-rings. This issue has been discussed in Section 2.4.5.2.4 under the topic of "range walk". In received signal simulation, the effect corresponding to this issue is discarded and not modeled since the CPI is taken short enough not to have the influence of range walk.

As discussed in Section 2.4.5.1, it is a fact that there is no clutter contribution into the received signal beyond the radar horizon due to the earth's round shape. The region of interest is selected such that clutter patches do not fall beyond the radar

horizon. Hence, the simulated signal does not have any contribution that is unavailable in reality.

Another check has been performed in the selection process of the iso-ring so that iso-ring does not have any clutter patch falling beyond the radar unambiguous range. If it was so, radar will have samples from different iso-rings at the same time as they were in the same range resolution cell. Remember the iso-ring definition is done for the clutter patches included in the same range resolution cell. This situation would make the target detection hard because the detector cannot decide easily in which iso-ring the target is exists.

Antenna array elements have some antenna beam patterns that cover the entire azimuth with different gains. As it is discussed in Section 2.4.5.2, back-lobe reception of antenna array elements may differ from the front-lobe reception in some cases such as velocity vector misalignment. For the sake of simplicity, back-lobe reception is assumed to be so weak that it is not included in the simulation. Thus, the clutter patches from only one side of the aircraft (+ y axis) are modeled.

3.2.2 Simulation of Clutter

3.2.2.1 Generation of Clutter Patches

Airborne radars are prone to receive back-scattered signals from a wide area on the ground, i.e. ground clutter. Reflection characteristics of the clutter differ according to elevation (also the range) and azimuth angle. In simulation, ground is divided into small areas corresponding to clutter patches that scatter back to the radar. Hence, a grid structure is formed. (Figure 3-1) The areas of clutter patches are taken to be equal. Clutter is defined as the superposition of scatterers lying on the ground in a specific area that corresponds to the region of interest (i.e. range to be sampled).
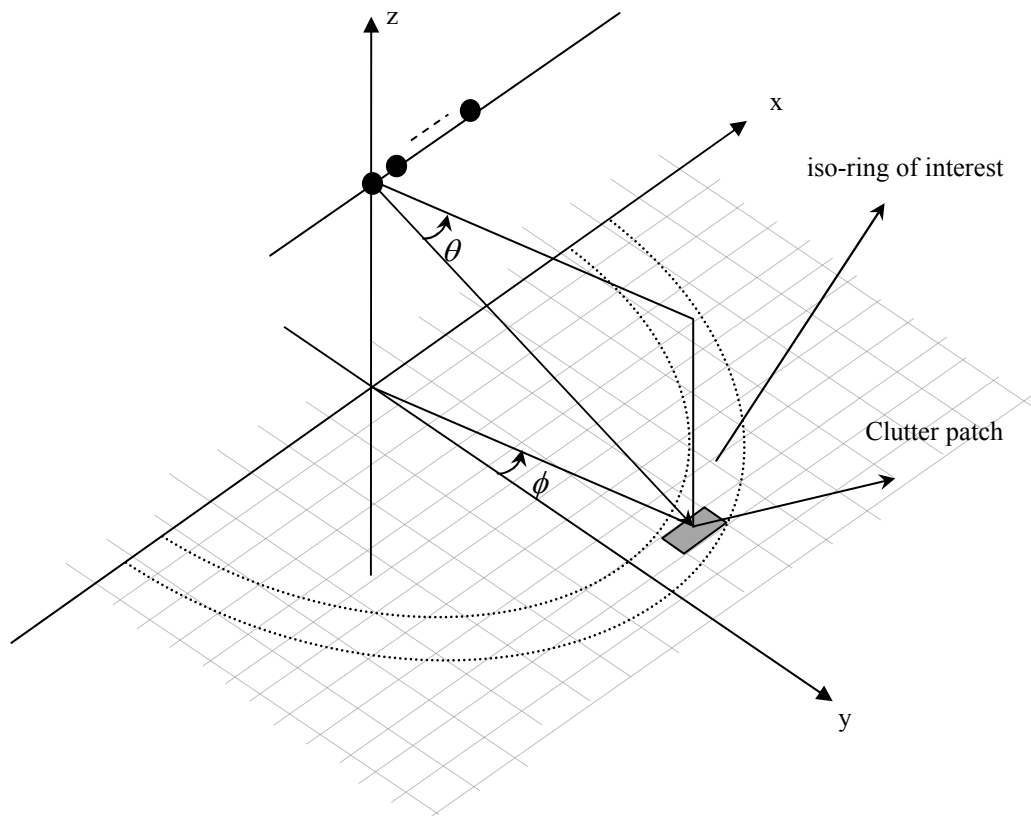
Figure 3-1 Clutter patches and the iso-ring illustration.

Range walk is ignored so that the simulator calculates the received signal with the clutter patches that are selected at time of the first sample. Thus, the clutter patches used for signal calculation do not change during the CPI interval. These patches stay in the iso-ring of interest, i.e. none of them go outside the iso-ring and also no other patches enter the iso-ring.

The range resolution of the airborne radar slightly differs from the basic radar case according to the angular view of the ground. For the basic radar, the range resolution is simply defined by half of the round trip delay of signal during the pulse width of the transmitted signal

$$\Delta R = \frac{cT_p}{2}.$$

(3-1)

If the pulse width increases, the range resolution increases. Roughly stated, two targets located in an area defined by half of the pulse width times the speed of light cannot be distinguishable. The received signals from multiple targets arrive the radar receiver in a pulse width time and radar declares a target existence but radar cannot decide on the possible presence of multiple targets.
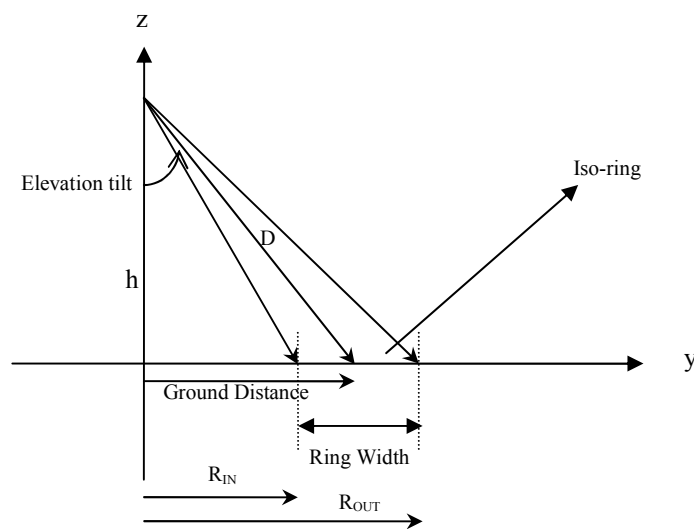
Figure 3-2 Range ring Formation.

Range rings are defined as ring areas from where back-scattered signal arrive at the receiver within single pulse duration. The clutter patches belonging to the same range ring are referred as an iso-ring. The simulation program selects one slice of the datacube that is the iso-ring of interest found by using a given elevation angle. Elevation angles of all generated clutter patches are compared with an elevation

angle interval and others that fall in this interval are taken to generate back-scattered echos.

The range resolution formulation for airborne radars is the same but the observed area is making an angle with the line of sight of the radar causing a slight difference. The range resolution (range rings) is changing with the elevation angle. This is shown in Figure 3-2.

The back-scattered signals from any of the scatterers in the iso-ring reach the antenna in one pulse-width time. The line of sight from the radar makes an angle with the iso-rings that is the iso-ring width is also proportional with the elevation angle. As a consequence the range resolution or equivalently the iso-ring width is calculated by taking this angle into account. In simulation, the width of the interested iso-ring shown on Figure 3-2 is found as follows

$$\text{Distance to array} = D = \frac{h}{\sin(elevation\_tilt)} \, , \qquad (3\text{-}2)$$

$$\text{Ground distance} = R = D * \cos(elevation\_tilt) \, , \qquad (3\text{-}3)$$

$$\Delta R \cong \sqrt{(D + \frac{cT_p}{2})^2 - h^2} - \sqrt{D^2 - h^2} \, , \qquad (3\text{-}4)$$

where ΔR is the width of the iso-ring of interests, D is the distance of iso-ring (from the middle) to the antenna array and R is the ground distance from the iso-ring of interest to the array projection on ground. Different than this, Ward [2] takes the range rings to have the same width, $\Delta R \approx c / B$. The two approaches give equivalent results under some conditions.

The inner and outer boundaries of the iso-ring of interest are found as follows

$$R_{IN} = D - \frac{\Delta R}{2} \, , \qquad (3\text{-}5)$$

$$R_{OUT} = D + \frac{\Delta R}{2}.$$
(3-6)

For each generated patch, the x and y coordinates are found as the center of the clutter patches. In other words, each clutter is assumed as a single point scatterer with an area of patch at x, y coordinates. Ground distances for each of the clutter patches are also calculated and compared with the boundaries R_{IN} and R_{OUT} to check whether the clutter patch falls in the iso-ring or not. For a single slice of datacube corresponding to fast time sampling, only signal contributions from clutter patches which fall into the iso-ring of interest are taken into account. Consider the kth clutter patch at coordinates, x_k and y_k. First, the ground distance of each available clutter patch is found for the clutter patch selection process as follows

$$\text{Ground distance of k'th clutter patch} = R_k = \sqrt{x_k^2 + y_k^2}.$$
(3-7)

This distance is the distance calculated from the center of the clutter patch to the position of array projection on ground. Then, it is checked whether the kth clutter patch falls inside the iso-ring or not by

$$R_{IN} \leq R_k \leq R_{OUT}.$$
(3-8)

Subsequent calculations are made with only these selected patches. Since the back-lobe reception of the antenna array is discarded, only half of the iso-ring in the positive y region is included. Thus, azimuth angles of clutter patches range from -90 to 90 degrees.

When a clutter patch is considered, it is mentioned with the elevation angle (gives the range to the radar) θ and the azimuth angle ϕ. Steering vector of clutter patches strongly depends on these angles. So, for each clutter patch, the azimuth and elevation angles are calculated from the center of the patch to the reference element of the array. For each of the clutter patches found to be in the iso-ring of interest,

azimuth and elevation angles are calculated to be used in derivation of the back-scattered signal by

$$\phi_k = \arctan(\frac{x_k}{y_k}),$$ (3-9)

$$\theta_k = \arcsin(\frac{h}{R_k}).$$ (3-10)

Range rings correspond to range samples of the datacube that a space-time snapshot vector for each range ring is formed. Thus, the sampling rate of the radar in fast time is just equal to the pulse width, T_p. Space-time snapshot vectors are formed every T_p seconds.

The ambiguous range is calculated and it is checked that the considered iso-ring is not located beyond the ambiguous range R_u:

$$R_{OUT} < R_u.$$ (3-11)

PRI is selected carefully so that range ambiguity arising from the small PRI does not appear. It is hence assumed that the observed area is also limited in distance that no range ambiguity appears.

In addition to ambiguity check in range, it is checked that the iso-ring of interest is not located beyond the radar horizon, R_h. Thus, in the resultant signal, the ambiguous range contribution utilized in the clutter model of Ward [2] is not included:

$$R_{OUT} < R_h.$$ (3-12)

After clutter patch selection and calculation of azimuth and elevation angles of these patches, the received signal from the clutter can be modeled using this information.

3.2.2.2 Velocity of Aircraft

In literature, during the CPI time the aircraft is assumed to fly with a constant speed along the x-axis on which the antenna array is lying. In this situation, clutter ridge is located over the diagonal of the angle-Doppler space. If there is a velocity vector misalignment with the antenna array axis, the clutter ridge location on the angle-Doppler space changes. The detail of this issue is explained in Section 2.4.5.2.2.

To cover this issue in the simulation of the received signal, flight scenario is improved to have some deflection of the aircraft flight direction in any axis. In actual flight scenario, the speed of the aircraft in each direction is also prone to change in each PRI time that in addition to deflection model this aspect is modeled by adding some irregularities to the velocity.

Initially, at the time of the first pulse reception, the speed of the aircraft is taken as V_{ac} and aircraft is flying in the direction of θ_{ac} in elevation and ϕ_{ac} in azimuth. Also for velocity irregularity modeling, the speed is modeled to have some random changes at PRI instants. This random change is modeled as a Gaussian random variable with zero mean and variance V_{dev} to be added to the initial velocity. The aircraft velocity is supposed to be constant during a single PRI that random change is added instantly at the time of PRI instants. The velocity of the aircraft and its components along each axis at multiple PRI time instants is then written as

$$\hat{V} = V_x \hat{a}_x + V_y \hat{a}_y + V_z \hat{a}_z, \qquad (3\text{-}13)$$

where $\hat{a}_i$ is the unit norm vector in axis i. The velocity vector components in each axis (V_x, V_y and V_z) are obtained by adding the irregularities to the initial velocity vector components as shown in the following expressions;

$$V_x = \begin{bmatrix} V_{x1} \\ \vdots \\ V_{xM} \end{bmatrix} = V_{ac} \sin(\phi_{ac}) \cos(\theta_{ac}) + \begin{bmatrix} 0 \\ v_{x1} \\ v_{x1} + v_{x2} \\ \vdots \\ v_{x1} + \cdots + v_{xM-1} \end{bmatrix}, \qquad (3\text{-}14)$$

$$V_y = \begin{bmatrix} V_{y1} \\ \vdots \\ V_{yM} \end{bmatrix} = V_{ac} \cos(\phi_{ac}) \cos(\theta_{ac}) + \begin{bmatrix} 0 \\ v_{y1} \\ v_{y1} + v_{y2} \\ \vdots \\ v_{y1} + \cdots + v_{yM-1} \end{bmatrix}, \qquad (3\text{-}15)$$

$$V_z = \begin{bmatrix} V_{z1} \\ \vdots \\ V_{zM} \end{bmatrix} = V_{ac} \sin(\theta_{ac}) + \begin{bmatrix} 0 \\ v_{z1} \\ v_{z1} + v_{z2} \\ \vdots \\ v_{z1} + \cdots + v_{zM-1} \end{bmatrix}. \qquad (3\text{-}16)$$

The last additional vectors in the formula of each velocity vector components include the velocity irregularities. At each PRI instant, the additional velocity component is added to the preceding velocity so that velocity vector components at PRI instants include previous velocity irregularities. That is at M^{th} PRI time velocity vector includes the sum of all the velocity irregularities added to initial velocity.

This new velocity vector model plays an important role in the calculation of the space-time steering vector. At a first glance, it is clear that the Doppler velocity which is assumed to be constant in literature changes at each PRI instant. Therefore, Doppler frequency used in temporal steering vector calculation is no more taken as multiples of a single frequency. In addition to this effect, if the aircraft position change during the CPI time is included, the position change of antenna array elements includes some randomness to affect the spatial steering vector.

3.2.2.3 Aircraft Motion and Spatial Steering Vector

It is clear that the aircraft motion results in a change of antenna array element positions generating a phase difference along antenna array elements as compared with the initial positions. In literature this kind of motion is discarded [1, 2, 3, 6, 7] so that the phase difference between antenna array elements is assumed to be multiples of spatial frequency f_{sp} and the spatial steering vector is found in this manner.

It is shown in Section 2.3.1 that the position of an antenna array element referenced to the origin (or the reference element) generates a phase difference in the spatial domain giving the clue that position change of antenna array elements contributes a spatial phase difference. As opposed to the spatial domain, the location change of antenna array elements does not change the Doppler frequency so that there is no phase change contribution to the temporal domain. Actually, the Doppler frequency is assumed to remain unchanged since the elevation and azimuth angles of clutter patches, which change the relative velocity between aircraft and clutter patches, are assumed be same as it is in the initial position of the aircraft.

The initial position of the array is assumed to be along the x axis with antenna array elements separated from each other with a distance d. The distance of the kth clutter patch relative to the nth array element, which causes the time delay used to calculate the phase change in each PRI time [3], is found as follows;

$$\text{Distance} = \hat{D}_n \bullet \hat{k}, \qquad (3\text{-}17)$$

where $\hat{D}_n$ and $\hat{k}$ are the pointing vectors of the nth array element and the kth clutter patch respectively and Distance is found by the inner product of these vectors. These pointing vectors can be written as

$$\hat{k} = \sin(\phi_k)\cos(\theta_k)\hat{a}_x + \cos(\phi_k)\cos(\theta_k)\hat{a}_y + \sin(\theta_k)\hat{a}_z, \qquad (3\text{-}18)$$

60

$$\hat{D}_n = nd\hat{a}_x + \hat{D}_{nx} + \hat{D}_{ny} + \hat{D}_{nz}$$

$$= (nd + \begin{bmatrix} 0 \\ V_{x1} \\ V_{x1} + V_{x2} \\ \vdots \\ V_{x1} + \cdots + V_{xM-1} \end{bmatrix} T_r)\hat{a}_x$$

$$+ \begin{bmatrix} 0 \\ V_{y1} \\ V_{y1} + V_{y2} \\ \vdots \\ V_{y1} + \cdots + V_{yM-1} \end{bmatrix} T_r\hat{a}_y + \begin{bmatrix} 0 \\ V_{z1} \\ V_{z1} + V_{z2} \\ \vdots \\ V_{z1} + \cdots + V_{zM-1} \end{bmatrix} T_r\hat{a}_z \quad , \qquad (3\text{-}19)$$

where d is the interelement spacing between the antenna array elements and T_r is the PRI time.

As opposed to the assumption of stationary aircraft in a CPI time, the aircraft is supposed to move in the simulation. This motion is added by the vectors $\hat{D}_{nx}$, $\hat{D}_{ny}$ and $\hat{D}_{nz}$ so that the location of the nth array element is re-calculated at each PRI instant. Note that velocity irregularities at each PRI instant are also included in V_x, V_y and V_z vectors. Hence, the location change is not strictly at the multiples of velocity.

In the new case, the spatial frequency, f_{sp} changes at each time instant. This means that the spatial phase difference of antenna array elements with respect to the origin changes at every PRI instant in some amount according to the new positions of array elements. The model proposed in literature [1, 2, 3, 6, 7] takes the spatial frequency constant in time due to the stationary aircraft assumption. Therefore, there is an additional frequency, $F_{sp,motion}$ (Mx1 dimensional) to be included as a model of the phase difference in time due to the antenna array elements' position

changes. Then, the new spatial frequency at the mth PRI time for the nth array element is written as follows

$$
\begin{aligned}
\tilde{f}_{sp} = n f_{sp}(k) + F_{sp,motion}(m,k) &= \frac{\hat{D}_n \bullet \hat{k}}{\lambda} \\
&= \frac{nd\sin(\phi_k)\cos(\theta_k)}{\lambda} \\
&+ \frac{\hat{D}_{nx}(m)\sin(\phi_k)\cos(\theta_k) + \hat{D}_{ny}(m)\cos(\phi_k)\cos(\theta_k) + \hat{D}_{nz}(m)\sin(\theta_k)}{\lambda},
\end{aligned}
\tag{3-20}
$$

where

$$
f_{sp}(k) = \frac{d\sin(\phi_k)\cos(\theta_k)}{\lambda}, \tag{3-21}
$$

$$
F_{sp,motion}(k) = \frac{\hat{D}_{nx}\sin(\phi_k)\cos(\theta_k) + \hat{D}_{ny}\cos(\phi_k)\cos(\theta_k) + \hat{D}_{nz}\sin(\theta_k)}{\lambda}. \tag{3-22}
$$

As it can be seen from the formula, spatial frequency of any antenna array element is no more constant during a CPI time. It is modeled to be changing at each PRI instant because the locations of array elements are changing.

In literature [1, 2, 3, 6, 7], the spatial steering vector is modeled to be N-dimensional and constant at each PRI instant but if the motion of aircraft is included the new spatial steering vector varies in time. Thus, the spatial steering vector has to be modified to have spatial phase differences changing in time. As a consequence, the NMx1 dimensional spatial part of space-time steering vector can be written as follows;

$$\widetilde{S}_s(k) = S_{motion} \otimes S_s(k) = \begin{bmatrix} e^{j0} e^{j2\pi F_{sp,motion}(1,k)} \\ e^{j2\pi \frac{d}{\lambda}\sin(\phi_k)*\cos(\theta_k)} e^{j2\pi F_{sp,motion}(1,k)} \\ \vdots \\ e^{j2\pi \frac{(N-1)d}{\lambda}\sin(\phi_k)\cos(\theta_k)} e^{j2\pi F_{sp,motion}(1,k)} \\ \vdots \\ e^{j0} e^{j2\pi F_{sp,motion}(M,k)} \\ e^{j2\pi \frac{d}{\lambda}\sin(\phi_k)\cos(\theta_k)} e^{j2\pi F_{sp,motion}(M,k)} \\ \vdots \\ e^{j2\pi \frac{(N-1)d}{\lambda}\sin(\phi_k)\cos(\theta_k)} e^{j2\pi F_{sp,motion}(M,k)} \end{bmatrix}, \quad (3\text{-}23)$$

where

$$S_s(k) = \begin{bmatrix} e^{j0} \\ e^{j2\pi \frac{d}{\lambda}\sin(\phi_k)\cos(\theta_k)} \\ \vdots \\ e^{j2\pi(N-1)\frac{d}{\lambda}\sin(\phi_k)\cos(\theta_k)} \end{bmatrix}, \quad (3\text{-}24)$$

$$S_{motion}(k) = e^{j2\pi F_{sp,motion}(k)} = \begin{bmatrix} e^{j2\pi F_{sp,motion}(1,k)} \\ e^{j2\pi F_{sp,motion}(2,k)} \\ \vdots \\ e^{j2\pi F_{sp,motion}(M,k)} \end{bmatrix}. \quad (3\text{-}25)$$

S_s is the same basic spatial steering vector defined in the model in Section 2.4.1. As a modification of this basic model, S_{motion} which is the motion steering vector giving a phase difference to spatial steering vector at each PRI instant with a frequency $F_{sp,motion}$ is included. Thus, the new spatial steering vector is composed of spatial samples that are changing in time. As a note, S_{motion} includes $\hat{D}_{nx}$, $\hat{D}_{ny}$ and $\hat{D}_{nz}$ displacement components in each axis which also include the displacement changes in time due to the velocity irregularities.

3.2.2.4 Temporal Steering Vector

In literature the irregularities of velocity is discarded so that that velocity is taken as constant during CPI [1, 2, 3, 6, 7]. Thus, phase difference between samples received at each PRI instant is assumed to be multiples of temporal frequency f_d and the temporal steering vector is found in this manner.

However, as it is discussed in the spatial domain, the change in velocity during each PRI time also affects the normalized Doppler frequency since the Doppler frequency is directly proportional to velocity. Therefore, temporal steering vector of the clutter has to be also modified in order to include the velocity irregularities.

The calculation is done analogously to the one performed in spatial domain. The relative velocity between the aircraft and the kth clutter patch including the velocity irregularities is found as

$$
\begin{aligned}
\hat{V}_{rel} &= \hat{V} \bullet \hat{k} \\
&= V_x \sin(\phi_k)\cos(\theta_k) + V_y \cos(\phi_k)\cos(\theta_k) + V_z \sin(\theta_k)
\end{aligned}
\tag{3-26}
$$

where $\hat{V}$ and $\hat{k}$ are the velocity vector of the aircraft and the pointing vector of the kth clutter patch respectively. Note that the relative velocity, $\hat{V}_{rel}$ found by the inner product of these point vectors is the relative velocity between the aircraft and k^{th} clutter patch which is directly proportional to the velocity vector of aircraft and the location of the clutter patch on ground.

After calculating the velocity vector with components in each direction and with irregularities, the new temporal steering vector can be written as

$$S_t(k) = \begin{bmatrix} 1 \\ e^{j2\pi\frac{2T_p}{\lambda}\hat{V}_{rel}(1)} \\ e^{j2\pi\frac{2T_p}{\lambda}(\hat{V}_{rel}(1)+\hat{V}_{rel}(2))} \\ \vdots \\ e^{j2\pi\frac{2T_p}{\lambda}(\hat{V}_{rel}(1)+\cdots+\hat{V}_{rel}(M-1))} \end{bmatrix}. \tag{3-27}$$

The temporal frequency defined in the basic model of Section 2.4.1 is written to be constant in time due to the constant velocity. Different than the basic temporal steering vector, the modified temporal steering vector is formed of time samples having a temporal frequency varying in time because of the change of relative velocity.

3.2.2.5 Power Calculation

After the calculation of the steering vectors, the next step is to calculate the power of each clutter patch in the iso-ring of interest. If the back-scattered power from a single clutter patch is considered, it is related to the area covered by the clutter patch, the elevation angle and also the reflection coefficient changing with angle. The area of the kth clutter patch is equal to an area A_k with sufficient size found during the formation clutter patches (Section 3.2.2.1). Hence, all of the clutter patches are assumed to have equal areas. However, the antenna array elements do not have a direct vision of this clutter patch area because of the elevation angle. Consequently, effective area of the kth clutter patch is found by projecting the area to the line of sight of the array as

$$A_k = A\sin(\theta_k). \tag{3-28}$$

It can be easily seen that the incident area observed by the array is only proportional to the elevation angle. Since the clutter patches belonging to the same iso-ring have

very close elevation angles, effective areas of clutter patches of interest appear to be close to each other.

The area reflectivity ($\sigma_0(\phi_k, \theta_i)$) of all clutter patches are assumed to be the same and constant differently than the Ward [2] model in which reflectivity is assumed to change with the elevation and azimuth angles of clutter patches. Hence, the radar cross section of the kth clutter patch is defined as

$$\sigma_k = A_k \sigma_0 . \tag{3-29}$$

Another important point of the power calculation is the antenna beam pattern which directly affects the received power from the clutter patch. The beam pattern calculation is composed of two antenna patterns which are transmit and receive antenna patterns. In spite of using antenna patterns, antenna gain can be used since both of them tell how the power changes due to antenna characteristics. The transmit antenna is assumed to be a single antenna which is supposed to be omni-directional. Thus, the antenna gain at transmit G_t is assumed to be constant for all directions different from the proposed one [2] which changes both in elevation and azimuth angles.

As opposed to the transmit case, receiver antenna array elements have beam patterns to be included in the signal modeling. In simulation, the antenna beam patterns of array elements are assumed to be the same with the one of the reference element at origin. Therefore, antenna beam pattern, which is modeled to have directivity coefficient of reception changing both in azimuth and elevation angles [6], is taken in this study as given below

$$\begin{aligned} G_{az}(\phi) &= 0.5(1 + \cos 2(\phi - \phi_0)) \\ G_{el}(\theta) &= 0.5(1 + \cos 2(\theta - \theta_0)) \end{aligned} . \tag{3-30}$$

Then, the overall antenna beam pattern of array at reception of back-scattered signal is

$$G_r(\phi_k, \theta_k) = G_{az}(\phi_k)G_{el}(\theta_k),$$
(3-31)

where θ_0 and ϕ_0 are the angles where the directivity coefficient is maximum. Since the array is taken as sidelooking in this study, ϕ_0 is taken as 0 degrees. Since the back-lobe reception is ignored, ϕ is changing in between -90 and 90 degrees. In order to have maximum gain in the angle of the iso-ring, θ_0 is taken as the elevation tilt angle shown in Figure 3-2. The clutter patches have nearly the same elevation angle as the elevation tilt angle so that G_{el} is almost 1.

Then, the clutter-to-noise power ratio (CNR) of the kth clutter patch is found by using the formula given in Section 2.4.5.1

$$CNR_k = \frac{P_t T_p G_t G_r(\phi_k, \theta_k)\lambda^2 \sigma_k}{(4\pi)^3 N_0 L_s R_k^4}.$$
(3-32)

Finally, the reflected power from the kth clutter patch is found by multiplication of noise power with CNR as in the formula defined in [2]

$$P_k = \sigma^2 CNR_k,$$
(3-33)

where σ^2 is the noise power.

Although the antenna array elements are separated from each other and also the change of locations in each PRI time, the power receptions of the array elements are assumed to be almost the same since the movements within a CPI are small in comparison to the distance. Thus, the calculated power is the same for all elements at any time instant in a CPI. This means, the indices of the calculated space-time steering vector will have the same power for a single clutter patch.

3.2.2.6 Intrinsic Clutter Motion Modeling

The nature of the clutter tends to vary in time due to the Intrinsic Clutter Motion (ICM). The detail on ICM is given in Section 2.4.5.2.3. Consider each pulse back-scattered from a single clutter patch. Time samples of a single antenna change in each PRI time according to the ICM. ICM is also modeled in the simulation that temporal steering vector has the covariance matrix of ICM.

Consider a single clutter patch located in the iso-ring of interest. M pulse samples are received from this clutter patch at the reference element of the antenna array. It is supposed to have a decorrelation among all of the M pulses. The nature of this issue is modeled with an M x M covariance matrix given below

$$R_{ICM}(i,j) = \rho^{|i-j|^k}, \tag{3-34}$$

$$R_{ICM} = \begin{bmatrix} 1 & \rho^{1^k} & \rho^{2^k} & \cdots & \rho^{(M-1)^k} \\ \rho^{1^k} & 1 & \cdots & \cdots & \vdots \\ \rho^{2^k} & \cdots & 1 & \cdots & \vdots \\ \vdots & \cdots & \cdots & \ddots & \vdots \\ \rho^{(M-1)^k} & \cdots & \cdots & \cdots & 1 \end{bmatrix}, \tag{3-35}$$

where ρ is the correlation coefficient determining the decorrelation between different received pulses and $0 \leq \rho \leq 1$. Higher ρ means higher correlation between pulses received at different instants of time (multiples of PRI, T_r). The exponent k also affects the decorrelation time.

Note that antenna array elements have the same ICM effect in time since the entire antenna array elements are sampling in time coherently. Accordingly, the temporal steering vectors corresponding to each spatial sample have the same covariance matrix. In the simulation, it is also assumed that the clutter patches belonging to the

iso-ring of interest have the same covariance matrix because the clutter patches of the iso-ring are supposed to have similar reflection characteristics in time.

3.2.2.7 Generation of Space-Time Snapshot

Up to this section, the received signal vector for each clutter patch is derived by taking into account the back-scattered power, temporal and spatial vectors, randomness in clutter patches, and correlation between pulses. As a final stage of the clutter simulation, the obtained information will be merged to achieve the space-time snapshot vector of the total clutter present in the iso-ring interest.

Randomness due to ICM for a single clutter patch during each PRI interval is also added by multiplying the temporal steering vector with an Mx1 dimensional complex random vector, r. Finally the new temporal snapshot of kth clutter patch is obtained

$$\widetilde{S}_t(k) = (R_{ICM}{}^{1/2} r_{Mx1}) \circ S_t(k),$$ (3-36)

where $\circ$ is the Hadamard product given in Appendix A-1 and. The random vector r can be written as

$$r = \begin{bmatrix} r_1 \\ \vdots \\ r_M \end{bmatrix},$$ (3-37)

where r_i's are independent Gaussian complex random variables with zero mean and variance of 1. The modified temporal steering vector includes the velocity irregularities, effect of ICM and randomness of clutter patches as opposed to the basic temporal steering vector defined in Section 2.4.1.

In order to find the space-time steering vector of the kth clutter patch, the modified temporal steering vector of the reference antenna array element is multiplied by the

modified space steering vector found in Section 3.2.2.3. Then, the calculated power for the kth clutter patch is also multiplied with this recent space-time steering vector to achieve the MN x 1 dimensional space-time snapshot. This can be shown mathematically as

$$X_c(k)_{MNx1} = \sigma^2 CNR_k(\widetilde{S}_t(k) \otimes \widetilde{S}_s(k))$$

$$= \sigma^2 CNR_k \left[(((R_{ICM}^{1/2} r_{Mx1}) \circ S_t(k)) \otimes \begin{bmatrix} 1 \\ \vdots \\ N \end{bmatrix}) \circ (S_{motion} \otimes S_s(k)) \right], (3\text{-}38)$$

where $\widetilde{S}_s(k)$ and $\widetilde{S}_t(k)$ are the modified spatial and temporal steering vectors defined in Sections 3.2.2.3 and 3.2.2.4. $X_c(k)$ is the space-time snapshot specific to kth clutter patch parameters. The space-time snapshot of any patch differs from the others since the elevation and azimuth angle of the each patch is different.

The whole procedure defined above is performed only for a single clutter patch so it shall be repeated for each of the clutter patches located in the iso-ring of interest to find the total reflection coming at a time. After the calculation of the space-time snapshot vectors for each patch, the total clutter reflection from the iso-ring of interest is found by the superposition of individual vectors;

$$X_c = \sum_{k=1}^{K} X_c(k). \qquad (3\text{-}39)$$

where K is the number of clutter patches found in the iso-ring of interest and X_c is MN x 1 dimensional space-time snapshot of the clutter in the iso-ring of interest.

The target space-time snapshot vector and receiver noise will also be calculated and added to the clutter simulation to gather the overall received signal.

As it is stated in the introduction to CHAPTER 3, range walk is not included in the simulation. But the simulation can be configured to include range walk by selecting

the clutter patches falling inside the iso-ring of interest in each PRI time. The current simulator assumes that the iso-ring does not move so that clutter patches are selected to be the same during the whole CPI. Range walk brings the iso-ring to move so that it may include different clutter patches in each PRI time. In the other words, angles of clutter patches do not change but the clutter patches corresponding to those angles may change.

3.2.3 Simulation of Target

In the operational scenario of airborne radar, there can be many targets on ground to be detected. In the received signal simulation, single target is assumed to exist in the iso-ring of interest. The target is simulated to have some motion to be distinguishable from the clutter. If the characteristic of the signal back-scattered from the target is considered, target behaves very similar to a single clutter patch. Thus, as it is done in clutter signal simulation, target is assumed to be a single point scatterer with an area of A_t at a distinct elevation angle θ_t and azimuth angle ϕ_t. The mobile target is assumed to move on the ground (x-y plane) with a constant speed v_t with an azimuth angle of ϕ_{v_t}. Different from the clutter case, the Doppler frequency of the target will depend on the relative motion induced by both the aircraft and target velocity vectors.

3.2.3.1 Aircraft Motion and Spatial Steering Vector

Analogous to calculation of spatial steering vector of clutter patches including the aircraft motion at each PRI time, spatial steering vector can be found for the target. That is, the target is assumed to be like a clutter patch at a specific elevation and azimuth angle but having a velocity different form the stationary clutter patches. The distance of target relative to the nth array element is found as follows

$$\text{Distance} = \hat{D}_n \bullet \hat{t} , \qquad (3\text{-}40)$$

71

where $\hat{t}$ is the pointing vector of target

$$\hat{t} = \sin(\phi_t)\cos(\theta_t)\hat{a}_x + \cos(\phi_t)\cos(\theta_t)\hat{a}_y + \sin(\theta_t)\hat{a}_z. \qquad (3\text{-}41)$$

The new spatial frequency at m^{th} PRI time for n^{th} array element is written as

$$
\begin{aligned}
\tilde{f}_{sp} &= n f_{sp}(t) + F_{sp,motion}(m,t) = \frac{\hat{D}_n \bullet \hat{t}}{\lambda} \\
&= \frac{nd\sin(\phi_t)\cos(\theta_t)}{\lambda} \\
&\quad + \frac{\hat{D}_{nx}(m)\sin(\phi_t)\cos(\theta_t) + \hat{D}_{ny}(m)\cos(\phi_t)\cos(\theta_t) + \hat{D}_{nz}(m)\sin(\theta_t)}{\lambda},
\end{aligned}
\qquad (3\text{-}42)
$$

where

$$f_{sp}(t) = \frac{d\sin(\phi_t)\cos(\theta_t)}{\lambda} \qquad (3\text{-}43)$$

$$F_{sp,motion}(t) = \frac{\hat{D}_{nx}\sin(\phi_t)\cos(\theta_t) + \hat{D}_{ny}\cos(\phi_t)\cos(\theta_t) + \hat{D}_{nz}\sin(\theta_t)}{\lambda}. \qquad (3\text{-}44)$$

As it is clear from the formulas, the spatial frequency does not depend on the target velocity since the re-calculated locations of the antenna array elements depend only on the aircraft velocity. This is because of the assumption that the target is assumed to be stationary during the CPI time. Therefore, the target orientation to the origin, which is the reference point, does not change.

The NM x 1 dimensional spatial part of space-time steering vector of target can be written as

$$\widetilde{S}_s(t) = S_{motion} \otimes S_s(t) = \begin{bmatrix} e^{j0} e^{j2\pi F_{sp,motion}(1,t)} \\ e^{j2\pi \frac{d}{\lambda}\sin(\phi_t)\cos(\theta_t)} e^{j2\pi F_{sp,motion}(1,t)} \\ \vdots \\ e^{j2\pi \frac{(N-1)d}{\lambda}\sin(\phi_t)\cos(\theta_t)} e^{j2\pi F_{sp,motion}(1,t)} \\ \vdots \\ e^{j0} e^{j2\pi F_{sp,motion}(M,t)} \\ e^{j2\pi \frac{d}{\lambda}\sin(\phi_t)\cos(\theta_t)} e^{j2\pi F_{sp,motion}(M,t)} \\ \vdots \\ e^{j2\pi \frac{(N-1)d}{\lambda}\sin(\phi_t)\cos(\theta_t)} e^{j2\pi F_{sp,motion}(M,t)} \end{bmatrix}, \qquad (3\text{-}45)$$

where

$$S_s(t) = \begin{bmatrix} e^{j0} \\ e^{j2\pi \frac{d}{\lambda}\sin(\phi_t)\cos(\theta_t)} \\ \vdots \\ e^{j2\pi(N-1)\frac{d}{\lambda}\sin(\phi_t)\cos(\theta_t)} \end{bmatrix}, \qquad (3\text{-}46)$$

$$S_{motion}(t) = e^{j2\pi F_{sp,motion}(t)} = \begin{bmatrix} e^{j2\pi F_{sp,motion}(1,t)} \\ e^{j2\pi F_{sp,motion}(2,t)} \\ \vdots \\ e^{j2\pi F_{sp,motion}(M,t)} \end{bmatrix}. \qquad (3\text{-}47)$$

In addition to basic spatial steering vector model, S_{motion} vector models the phase difference due to the change of array element locations in each PRI time due the aircraft motion. In reality, the target velocity makes the target location to change so that there should be some additional phase difference as compared with the initial locations. In simulation, the position change of the target in PRI time is excluded because target velocity assumed to be much slower as compared to the aircraft's. Thus, the spatial steering vector is assumed not to change with velocity of target.

3.2.3.2 Temporal Steering Vector

The velocity of the aircraft and relative velocity is found in a similar way defined in Section 3.2.2.2. However, there is an additional target velocity to be taken into account in relative velocity calculation. Thus, the relative velocity of target differs from the clutter patches so that the difference in Doppler velocity of the target makes the target distinguishable in the angle-Doppler space. It is assumed to have the target moving on the x-y plane that it has no velocity component in the z-axis. The target velocity can be written as a vector given below

$$\hat{V}_t = v_{t_x}\hat{a}_x + v_{t_y}\hat{a}_y,$$ (3-48)

where $\hat{a}_i$ is the unit norm vector in axis i. v_{t_x} and v_{t_y} are the velocities of target along x and y axes, respectively found by

$$v_{t_x} = v_t \sin(\phi_{v_t}),$$ (3-49)

$$v_{t_y} = v_t \cos(\phi_{v_t}),$$ (3-50)

where v_t is the target velocity which is assumed to be constant during the CPI interval.

The target is also assumed to stay in the initial position so that the pointing vector of target to the reference element of the antenna array does not change during the PRI. Otherwise, the target pointing vector should be re-calculated in each PRI instant according to the new orientation. This would affect both the spatial and temporal steering vectors of the target because in each PRI instant, the angles of the target would also change. By using these assumptions, the relative velocity vector between the aircraft and the target is written as

$$\hat{V}_{rel_t} = (\hat{V} - \hat{V}_t) \bullet \hat{t}$$
$$= (V_x - v_{t_x})\sin(\phi_t)\cos(\theta_t) + (V_y - v_{t_y})\cos(\phi_t)\cos(\theta_t) + V_z\sin(\theta_t).$$
(3-51)

If the target relative velocity is compared with the clutter patches, it can easily be seen that the target relative velocity differs in x and y axes. Next, the temporal steering vector of the target is written as;

$$S_t(t) = \begin{bmatrix} 1 \\ e^{j2\pi\frac{2T_p}{\lambda}\hat{V}_{rel_t}(1)} \\ e^{j2\pi\frac{2T_p}{\lambda}\hat{V}_{rel_t}(1)+\hat{V}_{rel_t}(2)} \\ \vdots \\ e^{j2\pi\frac{2T_p}{\lambda}\hat{V}_{rel_t}(1)+\cdots+\hat{V}_{rel_t}(M-1)} \end{bmatrix}.$$
(3-52)

This derived formula is also different than the basic model as it is in the clutter case since the relative velocity is changing in each PRI time due to the velocity irregularities.

3.2.3.3 Power Calculation

The back-scattered power calculation for the target is performed in a similar procedure as stated in Section 3.2.2.5. The back-scattered power depends on the target area and elevation angle of target. Since the target is assumed to stay in it its initial position, the elevation and azimuth angles do not change during the CPI interval. Then, the relative area of target independent from time is calculated as

$$\widetilde{A}_t = A_t \sin(\theta_t),$$
(3-53)

where A_t is the area of target. The area reflectivity of target is taken as $\sigma_0(t)$ so that target has an RCS

$$\sigma_t = \widetilde{A}_t \sigma_0(t).$$
(3-54)

Here again, the reflectivity of target is assumed to be constant in time and angle as it is in the clutter case. The antenna pattern for the target is modeled according to the target elevation and azimuth angles as

$$G_r(\phi_t, \theta_t) = G_{az}(\phi_t)G_{el}(\theta_t), \qquad (3\text{-}55)$$

where G_{az} and G_{el} are the antenna beam pattern models in azimuth and elevation as described in Section 3.2.2.5. Then, signal-to-noise power ratio (SNR) of target is found by the formula given in Section 2.4.2

$$SNR_t = \frac{P_t T_p G_t G_r(\phi_t, \theta_t)\lambda^2 \sigma_t}{(4\pi)^3 N_0 L_s R_t^4}. \qquad (3\text{-}56)$$

Finally, the reflected power from target is found by the formula given in [2]

$$P_t = \sigma^2 SNR_t. \qquad (3\text{-}57)$$

As in the clutter power calculation case, the calculated power is assumed to be same at each element at any time instant in a single CPI. Thus, the calculated power is the power received in each channel at each sampling time. If the target was taken as changing position in time, the power should be re-calculated in each PRI instant according to the new orientation, i.e. angles of target.

3.2.3.4 Generation of Space-Time Snapshot

In the preceding sections for target simulation, the required information to produce the space-time snapshot vector of the target is derived. This information is slightly different from the clutter case in that target parameters are different and target has a velocity changing the relative velocity with the aircraft.

As a final stage of target simulation, the back-scattered received signal vector by the target will be derived by taking into account the back-scattered power, temporal (including additional target velocity) and spatial vectors.

Again, the procedure is analogous to the clutter case. The temporal snapshot is multiplied by the space steering vector and the calculated power to achieve the MN x 1 space-time snapshot vector

$$
\begin{aligned}
X_{t\,MNx1} &= \sigma^2 SNR_t (S_t(t) \otimes \widetilde{S}_s(t)) \\
&= \sigma^2 SNR_t \left[\left(S_t(t) \otimes \begin{bmatrix} 1 \\ \vdots \\ N \end{bmatrix} \right) \circ (S_{motion} \otimes S_s(t)) \right].
\end{aligned}
\tag{3-58}
$$

This vector possesses all of the information of target: azimuth and elevation angle, and target velocity. Clutter and target space-time snapshots are later summed up together with noise to achieve the total received signal.

3.2.4 Simulation of Noise

The receiver channels of airborne radar have different characteristics due to the production. Hence, the receiver noise components of separate channels are supposed to be different. In addition, the receiver noise of a single channel may vary in time. In the simulation, the individual receiver channels behind each of the antenna array elements are assumed to be exactly same having the same receiver noise power. Thus, receiver noise of each channel has equal power over the angle-Doppler space. The noise covariance matrix for each channel is written as defined in Section 2.4.3

$$
R_n = E\{X_n X_n^H\} = \sigma^2 I_{MN} ,
\tag{3-59}
$$

where σ^2 is the noise power which is equal to N_0B. This model implies that the noise is assumed to be uncorrelated both in space and time.

Then, the NM x 1 dimensional noise vector can be written as follows

$$X_n = R_n^{1/2} r_n,$$ (3-60)

where r_n is a complex Gaussian vector with independent entities, zero mean and variance of 1. The receiver noise vector is signal component coming from the nature of the receivers and always present in the signal reaching to the processor.

3.2.5 Total Signal Received

In preceding sections, clutter, target and receiver noise signal simulation models are provided and space-time snapshot vectors are derived in accordance with stated assumptions. In addition to these signal components, there may be some hostile jammers providing some signal components as stated in Section 2.4.4. The jammer signal is not included in the simulator but can be easily incorporated into.

Overall, the total signal received by the radar processor composed of clutter, target and receiver noise vectors is

$$X = X_t + X_c + X_n,$$ (3-61)

where X_t, X_c and X_n are the target, clutter and noise signal vectors, respectively. X is MN x 1 dimensional received signal vector to be fed into the radar processor. It only includes the clutter and target signals related only to the iso-ring of interest.

The final signal receiver signal model achieved is the slice taken from the fast time shown on Figure 2-2. This signal model is equivalent to the N x M dimensional matrix composed of the N spatial samples related to M transmitted pulses.

3.3 Summary

As a conclusion, CHAPTER 3 gives the details of implementation of the receiver signal simulator. In this scope, the details of the clutter, target and receiver signal models are provided. These models are the improved form of the basic models stated in CHAPTER 2. The improvements are proposed in scope of the aircraft motion, velocity irregularity and also the ICM. Furthermore, the velocity vector is modified to be in any direction as opposed to the basic model which is in only x-axis. The target is modeled to have an additional velocity component to aircraft velocity vector so that its Doppler frequency differs from the clutter Doppler frequency. The receiver noise model is constructed to have the samples in space and time uncorrelated.

The reality includes many aspects that affect the received signal but since it is hard to model every aspect, some aspects are assumed to be discarded. These discarded aspects are clearly stated to show the actual receiver signal in reality may include the affects of these aspects.

Finally, at the end of the CHAPTER 3 the total signal model is stated as a sum of the achieved clutter, target and noise signal models. The simulator has been coded in MATLAB environment according to this model. The obtained results during the trials of the simulator and the comments are given in CHAPTER 4.

CHAPTER 4

RESULTS OF SIMULATION

4.1 Introduction

The literature survey on the airborne radar concepts, signal modeling and STAP algorithms is provided in CHAPTER 2. Afterwards, the new signal model is proposed in CHAPTER 3 including some aspects not covered in literature. The received signal simulator has been developed with this information. This chapter will provide the results gathered during the trials of the simulator and finally give the results of optimum STAP and DPCA filter.

Firstly, the simulation parameters including all of the necessary inputs have been carefully selected and stated. Although the parameters used in the simulation are listed, these parameters are left changeable in the simulator to perform the received signal trials. Before starting the trials, results of the simulator with given parameters are presented. These results include the figures of the location of clutter, target and total received signal in the angle-Doppler space.

Afterwards, the simulation parameters are controllably changed to observe the effects on the received signal under different situations. The angle between the spatial and temporal frequency plays an important role to localize the received signal on angle-Doppler space. Thus, it is changed by varying the values of the

aircraft velocity, PRI and also the interelement spacing. Up to this point, the simulation does not include the effects of aircraft motion and change in the direction and magnitude of the aircraft velocity.

Later on, aircraft velocity direction has been changed in accordance with Section 3.2.2.2 to generate the condition that velocity vector of aircraft is misaligned with the antenna array axis. The aircraft or the antenna array is assumed to stay on the x-axis during the CPI interval but the direction of velocity is changed to another direction. This situation was discussed under velocity vector misalignment in the Section 2.4.5.2.2. The theoretical and simulation outputs are analogous that the clutter ridge moves away from the diagonal of the angle-Doppler space.

Another trial has been performed for the velocity irregularities of aircraft which is always available in nature of aircraft. The velocity vector is modified with additional random components in the simulator as the way defined in Section 3.2.2.2. Since the velocity corrupted, the Doppler frequencies of the patches are spread in Doppler space as shown in the output figures of the simulator.

Another aspect to be included in the simulator is the ICM effect of the clutter due to the motion of clutter itself. ICM model is proposed in Section 3.2.2.6. ICM makes the clutter to spread on angle-Doppler output, since the temporal steering vector is affected. .

The last aspect to be considered in the simulator is the aircraft motion. Antenna array is supposed to move to another position in each PRI time. It is clear that the initial positions of the array elements will change generating a phase difference as compared with the reference element at the origin. Section 3.2.2.3 shows the details how the spatial steering vector is modeled.

After the simulator trials with different aspects, a study for investigation of DPCA and optimum STAP response is held. DPCA weight vector has been obtained as defined in [1] and the response of this vector on angle-Doppler has been drawn. As

a final step, the optimum weight vector for STAP is calculated by using the covariance matrix of the clutter and the target steering vector. The response of this weight vector has been obtained and drawn on the angle-Doppler space.

As a summary, this chapter provides the simulation outputs obtained with the simulator developed in accordance with the information derived and makes a comparison over the responses of DPCA and optimum STAP.

4.2 Simulation Parameters

The received signal simulator uses many radar and other system parameters as input for implementation of the signal models. Radar system parameters are described in details in Section 2.2 and summarized in Table 2-1. In the simulation, received signal is modeled in a way that the parameters can be adjusted according to various purposes. Initially, the parameter settings for radar, clutter, target and noise are set to the values given in the following Table 4-1.

Table 4-1 Parameters used in simulation

Parameter Symbol	Definition	Value used
N	Number of antenna array elements	16
M	Number of pulses integrated in a CPI	32
f	Radar operating frequency	$0.5*10^9$ Hz
c	Speed of light	$3*10^8$ m/s
λ*	Radar operating wavelength	0.6 m
d	Spacing between antenna array elements	0.3 m
T_r*	Pulse repetition interval (PRI)	1.25 ms
f_r*	Pulse repetition frequency (PRF)	800 Hz
T_p	Pulse width	10^{-6} ms
P_t	Peak transmitted power	1000 Watt
G_t	Antenna gain on transmit	80 dB

Parameter Symbol	Definition	Value used
G_r	Antenna gain on receive	See Section 3.2.2.5
B	Instantaneous bandwidth	10^6 Hz
L_s	System losses (both receive and transmit)	0 dB
N_0	Receiver noise power spectral density	-100 dB
h	Aircraft altitude	10.000 m
V_{ac}*	Aircraft velocity	120 m/s
V_{dev}*	Aircraft velocity deviation	0 m/s
ϕ_{ac} *	Aircraft velocity angle azimuth	90
θ_{ac} *	Aircraft velocity angle elevation	0
θ_{el} *	Elevation tilt	60
β *	Slope between Doppler and spatial frequencies	1
ρ *	Correlation coefficient	0.98
k	Correlation coefficient exponent	1
l	Clutter patch length	3 m
w	Clutter patch width	200 m
A	Area of clutter patch	600 m^2
$\sigma_0(c)$	Reflection coefficient of clutter	-50dB
-	Azimuth covered	180 degree sidelooking
ϕ_t	Target azimuth angle	60
θ_t	Target elevation angle	60
v_t	Target velocity	30
θ_{vt}	Target velocity angle	45
A_t	Target area	10 m^2
$\sigma_0(c)$	Reflection coefficient of target	-10 dB

* These values are set to the the initial values defined in the table. During the trials, they are changed in accordance with the need of the simulation to obtain the effects of them on the output.

4.3 Simulation Results

According to the modeling and the scenarios described in CHAPTER 3, received signal simulator is implemented on MATLAB. The simulator is built in the following steps; clutter patch generation on ground, clutter signal simulation, target simulation, noise simulation and finally the total received signal simulation. The code includes the cases that cause the change of received signal as described in CHAPTER 3. After the simulator is built, some parameters are varied to see the effects on the signal at the output. The output signal vector is multiplied with all possible signal vectors available on the angle-Doppler space in order to localize the signal in this two dimensional space. The figures present here belong only to a single range sample i.e. fast-time sample. The other slices of the datacube can be obtained by selecting other iso-rings.

4.3.1 Selection of Clutter Patches

The simulator generates the clutter patches to form a grid structure on the ground as defined in Section 3.2.2.1. Each small area on the grid is defined as the clutter patch and its coordinates on the x-y plane is found from the center point of the area. After generation of all possible clutter patches with the coordinate information, these within the iso-ring are selected for signal contribution. Figure 4-1 shows the iso-ring of interested and selected patches.
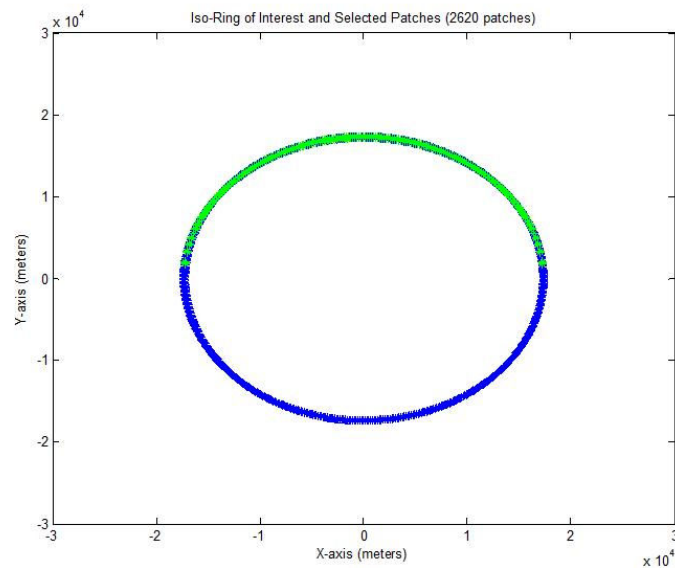
Figure 4-1 Iso-ring of interest and the selected patches. Note that the back-lobe patches are not selected.

First of all, clutter patches belonging to the iso-ring of interest are selected according to the elevation angle of iso-ring and iso-ring width. The other clutter patches on the ground are eliminated from the simulation. Since the back-lobe reception is ignored, the negative side of the y plane is not taken into consideration. That is the green clutter patches seen on the figure enters the simulation and signal contributions are found for them.

4.3.2 Simulator Outputs

This section will give the results of the basic simulator that shows the outputs of the steps in the simulator. Firstly, clutter patch signal or the space-time snapshot is found by superposition of the individual clutter patches which exist in the iso-ring of interest. The clutter ridge is then achieved as seen on the Figure 4-2. Since the parameters are selected as in the normal conditions (like no velocity vector

misalignment etc.) and the effects of the aspects defined in Section 3.2.2 are not included, the clutter patch lies on the diagonal of the angle-Doppler space.

The target behaves like a single clutter patch as defined in Section 3.2.3. Although the calculation of target signal vector is performed in a way similar to the clutter case: the Doppler frequency of the target slightly differs due to the target velocity. The temporal part of the space-time snapshot of the target signal is found in accordance to the relative velocity found with both the aircraft and target velocity vector. The location of the target on the angle-Doppler space is given in Figure 4-3. As it can be easily seen, the spatial and temporal frequencies of the target are not the same as the clutter shown in Figure 4-2. The Doppler frequency shifted from the diagonal because of the additional target velocity on the aircraft velocity.

As a final step of the simulator, the space-time snapshots of clutter and target are summed with the receiver noise and the total received signal vector is achieved. Noise is to be uncorrelated in space and time as described in Section 3.2.4. The total signal is demonstrated in Figure 4-4. This figure indicates the location of the received signal produce by the simulator to be fed into algorithms. Note that the target shown in the figure is slightly shifted away from the diagonal where clutter exists. This shift makes the target distinguishable from the clutter. Nevertheless, as the target velocity gets slower it becomes hard to separate the target from clutter since it will approach the diagonal.
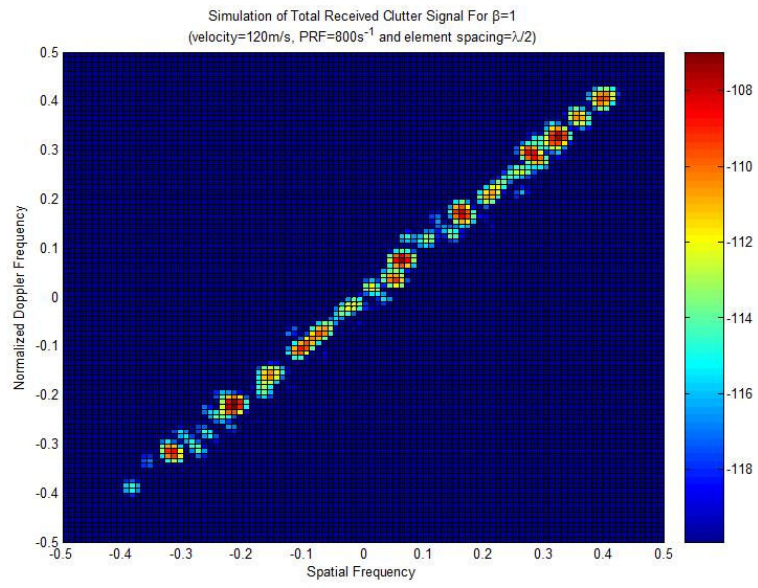
Figure 4-2 Clutter
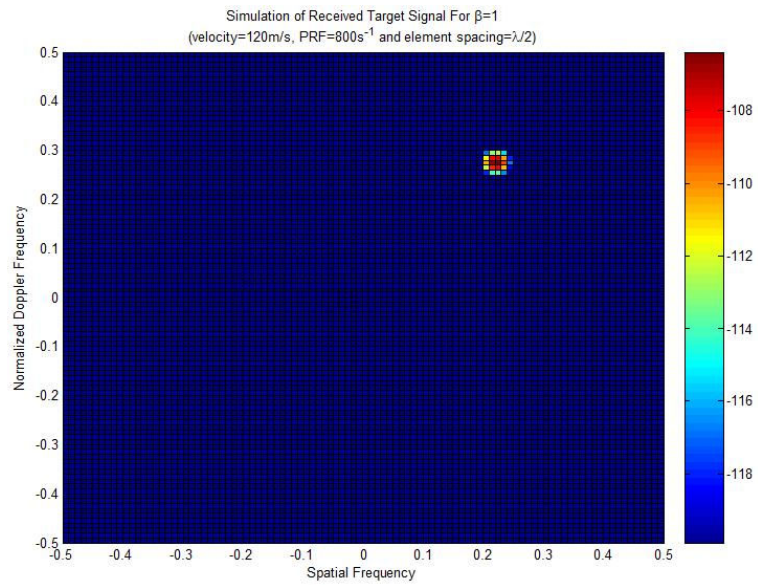
Figure 4-3 Target
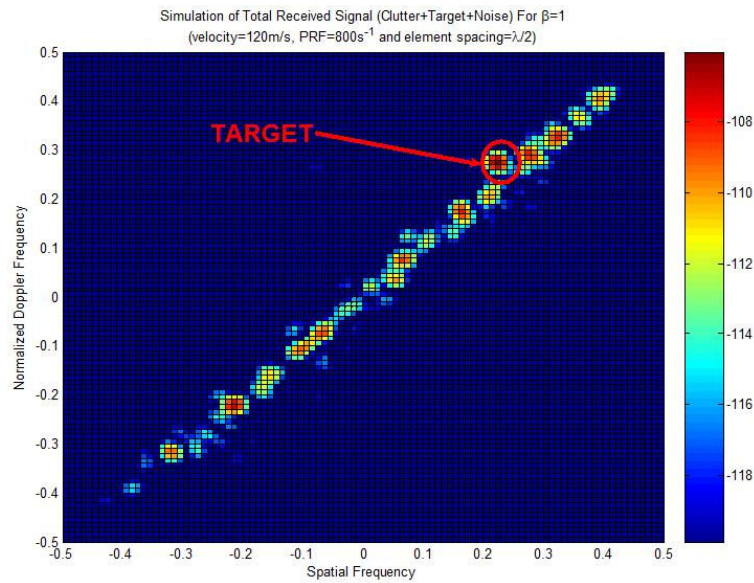
Figure 4-4 Clutter + Target

4.3.3 Simulation With Different β Values

After the demonstration of the output of the received signal simulator, the effect of the selection of the parameters on the received signal is investigated. The β value which is equal to the angle between the spatial and temporal frequencies of a scatterer is taken as 1 in the previous section so that the clutter ridge is found exactly on the diagonal of the angle-Doppler space. In this section, the effect of the β value change is investigated by changing the values of aircraft velocity, PRF and also the interelement spacing. During the adjustment of each of these parameters, the other parameters kept constant to the values written on Table 4-1. In the figures, note also that the location of the target is changing in the angle-Doppler space according to the change of these parameters.

In the figures Figure 4-5, Figure 4-6 and Figure 4-7 the ouput is shown for β value of 0.5. Figure 4-5 shows the output of the simulator when the PRF value is set to double of its initial value to be 1600 s^{-1}. As it can be seen from the figure, there is no clutter or target contribution some region in the Doppler space. Also the target signal shifted a little inside the clutter signal.

Figure 4-6 shows the output of the simulator when the aircraft velocity is set to the half of its initial value to be 60 m/s. If this figure is compared with the Figure 4-5, they seems very similar. But, the target shift into the clutter in Figure 4-5 is more than the shift in Figure 4-6.

Figure 4-7 shows the output of the simulator when the interelement spacing of the antenna array elements are set to double of the initial value to be the same with the wavelength of the signal. Since the spatial sampling rate proportional to the interelement spacing is reduced, the signal produced by the simulator has some alising in the spatial domain.
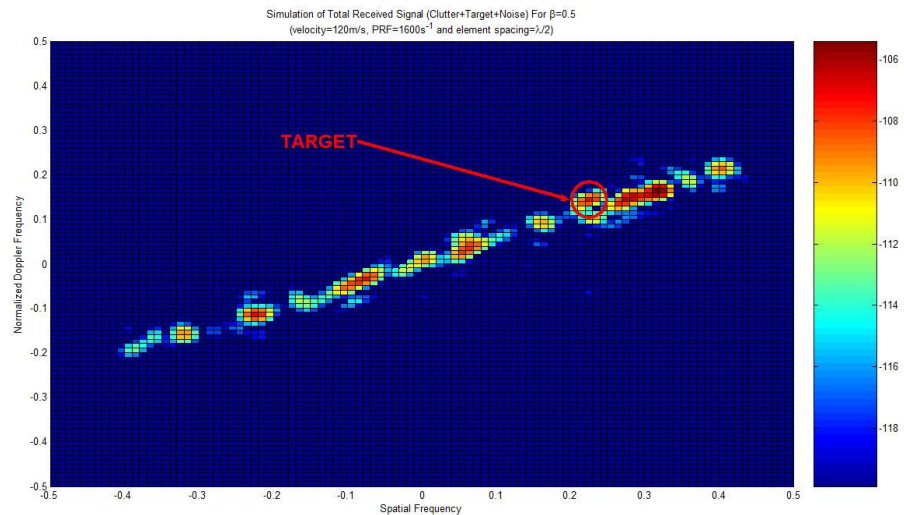
Figure 4-5 PRF is doubled

89
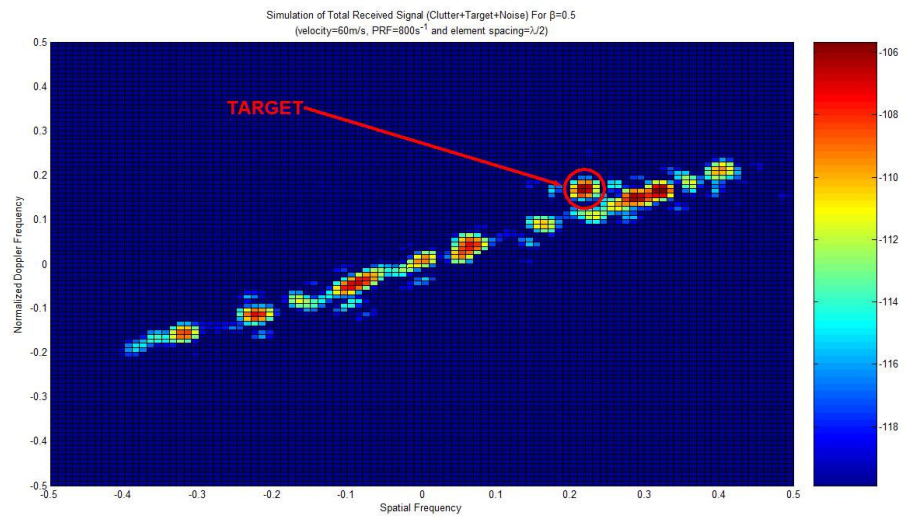
Figure 4-6 Aircraft velocity is half of initial value
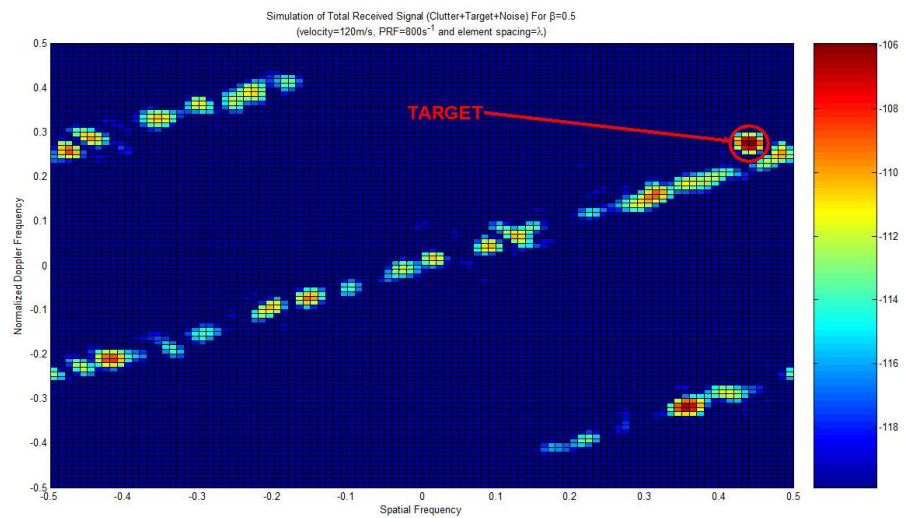
Figure 4-7 Interelement spacing is doubled

Figure 4-8 shows the output of the simulator when the PRF value is set to the half of its initial value to be 400 s^{-1}. As it can be seen from the figure, the signal

produced by the simulator has some alising in the temporal domain since the temporal sampling rate proportional to the PRF is reduced.

Figure 4-9 shows the output of the simulator when the aircraft velocity is set to double of its initial value to be 240 m/s. As in Figure 4-8, the signal produced by the simulator has some alising in the temporal domain since the temporal sampling rate proportional to the velocity is reduced.

Figure 4-10 shows the output of the simulator when the interelement spacing of the antenna array elements are set to half of the initial value to be the quarter of the wavelength of the signal. As it can be seen from the figure, there is no clutter or taget contribution over some region in the angle space. Also the target signal shifted inside the clutter signal.
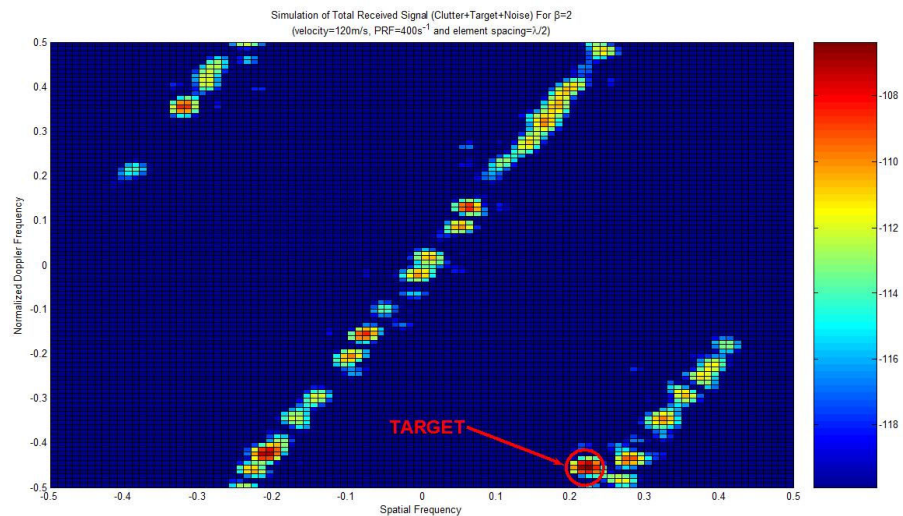
Figure 4-8 PRF is half of initial value
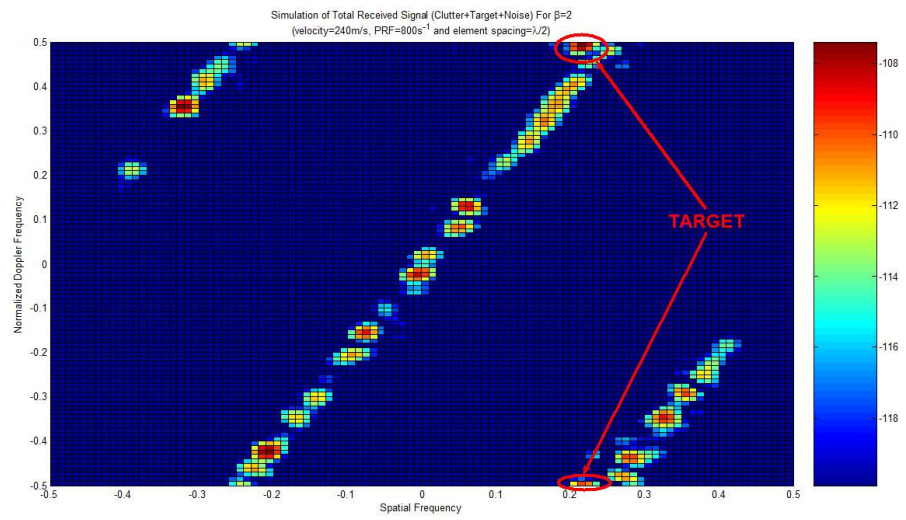
Figure 4-9 Aircraft velocity is doubled
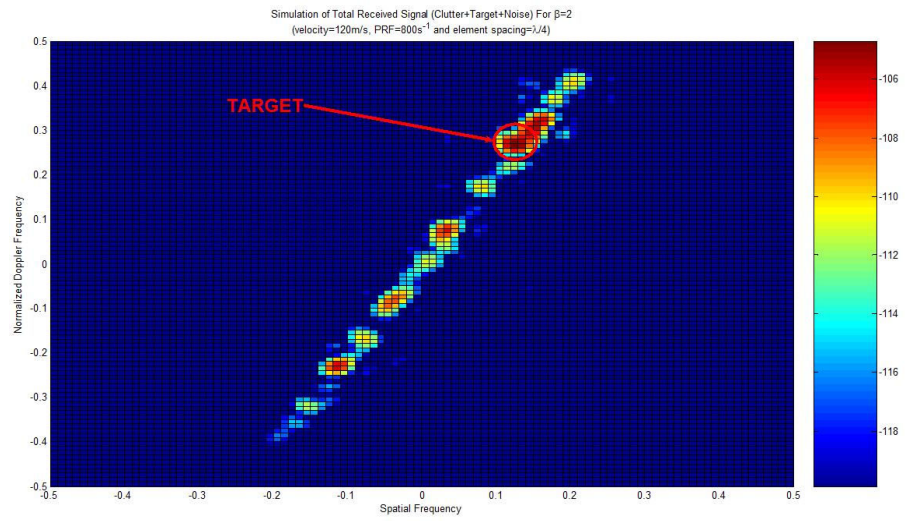
Figure 4-10 Interelement spacing is half of initial value

As it can be seen from the figures, system parameters plays an important role on the received signal. Thus, inappropriate selection of the parameters results in a different localization of the received signal in the angle-Doppler space that the received signal may not be in the expected place. Hence, some detection problems may occur.

4.3.4 Effect of Aircraft Velocity Direction Other Than x-Axis

In the literature, aircraft velocity is assumed to be along the x-axis. In this orientation, the antenna array is said to be aligned with the velocity vector of the aircraft. In Section 2.4.5.2.2, the effect of the crabbing angle of the velocity vector is discussed under the title of velocity vector misalignment. In the received signal simulator the aircraft velocity vector has been coded to move in any direction which is equivalent to the crabbing case. That is the aircraft has some velocity components other than the component on the x-axis. In the following figures, the effect of velocity vector having components in any direction is given.

Firstly, the signal produced in the basic case in which the platform moves in the x direction is given in Figure 4-11. In this case the elevation and azimuth angles of the velocity vector of aircraft are set to 0 and 90 degrees respectively. This is the actual scenario stated in the literature as sidelooking antenna array. The clutter ridge located on the diagonal of the angle-Doppler space as expected.

Figure 4-12 indicates the situation in which the aircraft fly in a direction perpendicular to the antenna array axis (over +y-axis). This is called as the forward-looking antenna array in literature. The elevation and azimuth angles of the motion are both 0 degrees. The clutter ridge and the target locations are changed as compared with the Figure 4-11.

Figure 4-13 and Figure 4-14 also shows how the location of clutter and target change in accordance to have aircraft velocity vectors with elevation and azimuth angles 0, 45 and 0, -45 degrees respectively.
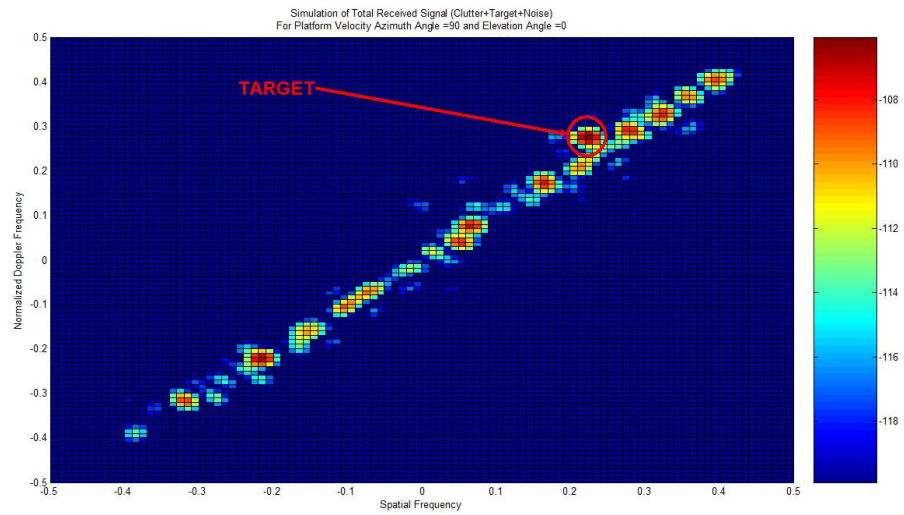

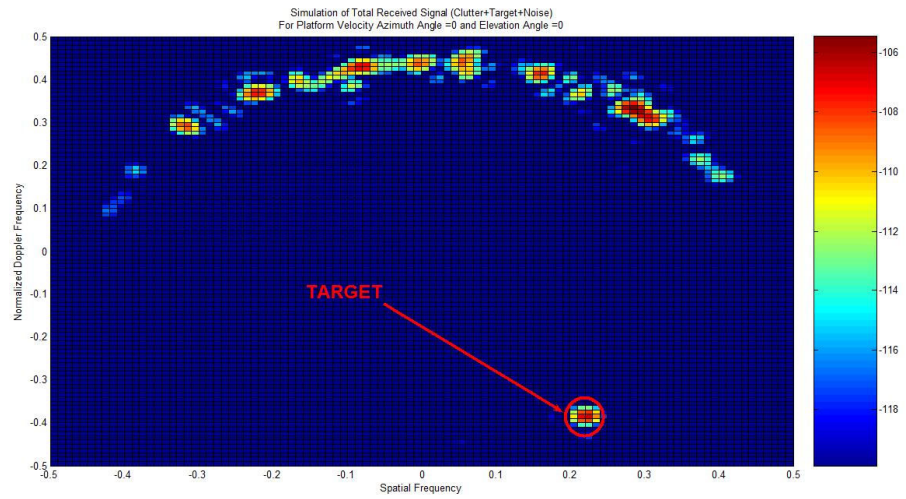Figure 4-11 Azimuth 90 and elevation 0 degrees (sidelooking)

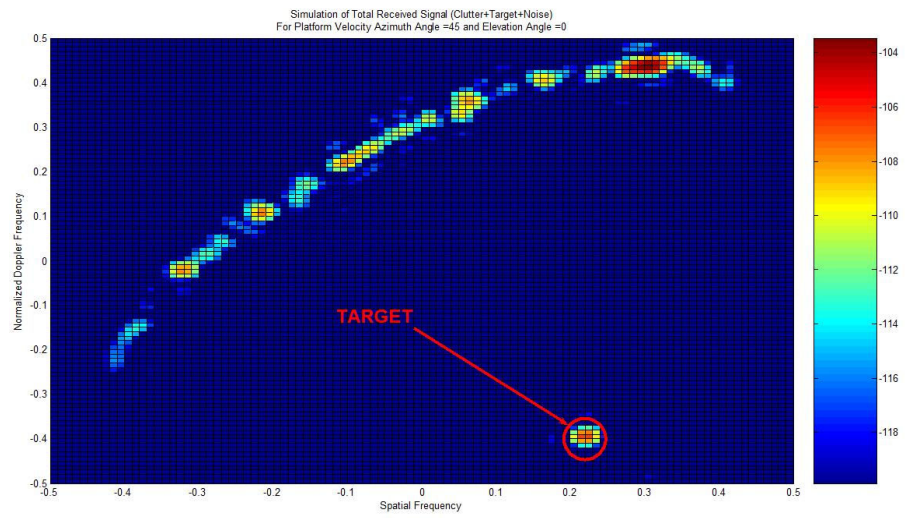Figure 4-12 Azimuth 0 and elevation 0 degrees (forward-looking)
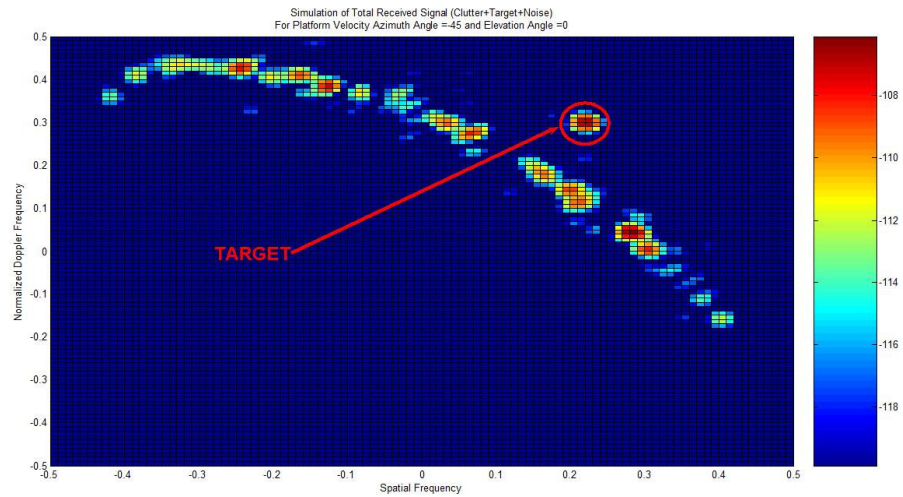

Figure 4-13 Azimuth 45 and elevation 0 degrees

95

Figure 4-14 Azimuth -45 and elevation 0 degrees

Figure 4-15 and Figure 4-16 shows the output of the received signal simulator with azimuth angles 90 degrees as in the sidelooking case. However, the velocity vector of the aircraft is directed in elevation with angles 45 and -45. Thus, these figures demonstrate what happens in the case of ascending and descending while the antenna array is located still on the x-axis.
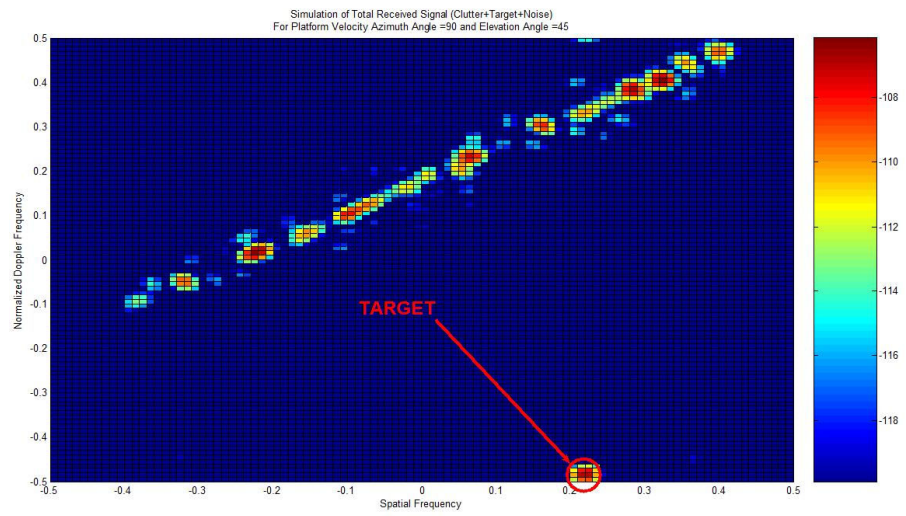
Figure 4-15 Azimuth 90 and elevation 45 degrees
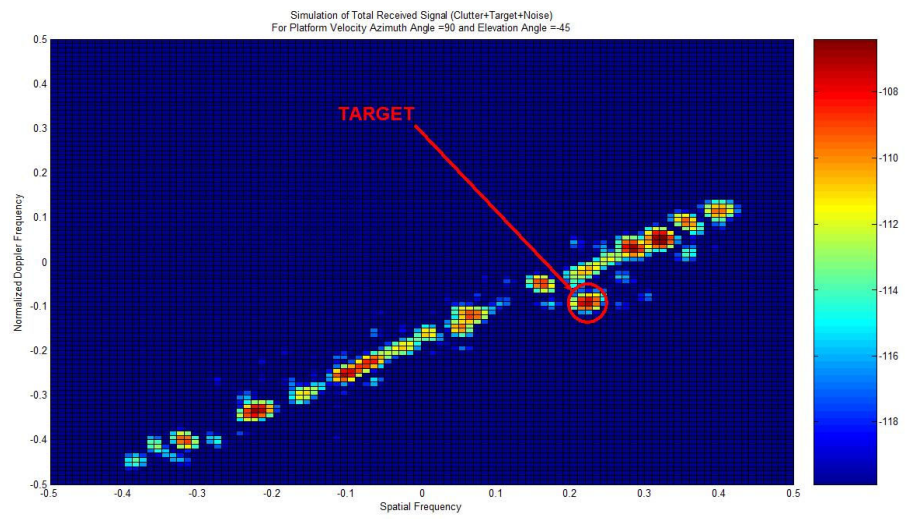
Figure 4-16 Azimuth 90 and elevation -45 degrees

The figures given in this section are the extreme cases of the crabbing angle. In a real flight the velocity vector does not change much as stated here. The crabbing angle may be in any direction with small angles. These figures give insight for the characteristics of the signal to be received in case of such a crabbing angle.

4.3.5 Effect of Aircraft Velocity Irregularities

Another aspect due to the aircraft velocity is the velocity irregularities which may occur in any direction in reality. In CHAPTER 3, the effect of aircraft velocity irregularities is described and modeled. The model is constructed over the basic space-time snapshot vector by changing the velocity randomly in each PRI time. Thus, it can be said that the aircraft velocity is changed slightly in each PRI time. However, the mean of the velocity is the value stated as the initial.

The following figures gives the simulation results with this effect. Firstly, the output without any irregularity is given as reference in Figure 4-17. Later on, the effect of velocity irregularity is stated with different amount of velocity variances.

Figure 4-18 and Figure 4-19 shows how the output of the received signal simulator is affected by the velocity irregularities with variances 10 m/s and 15 m/s respectively. As compared with the Figure 4-17, the clutter ridge and target are spread in the Doppler domain in accordance to the amount of the velocity irregularity variance. The amount of spread is proportional to the variance of velocity irregularity.
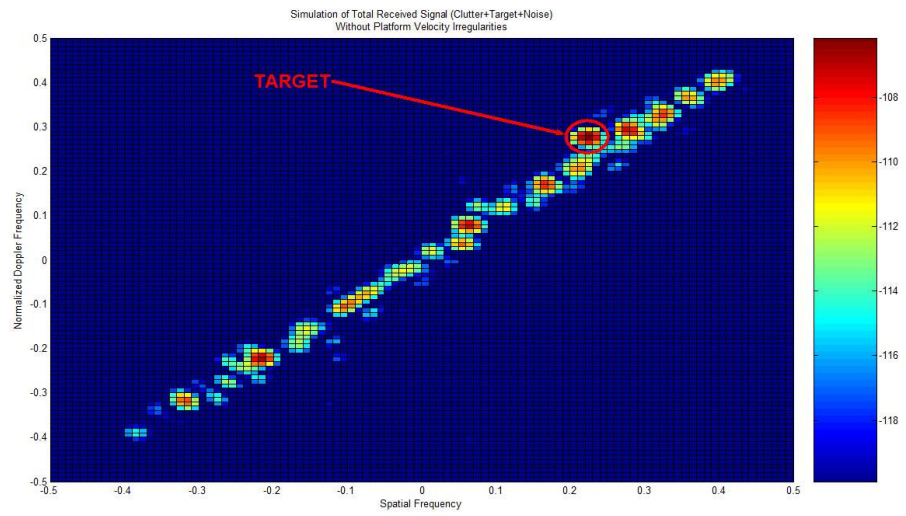
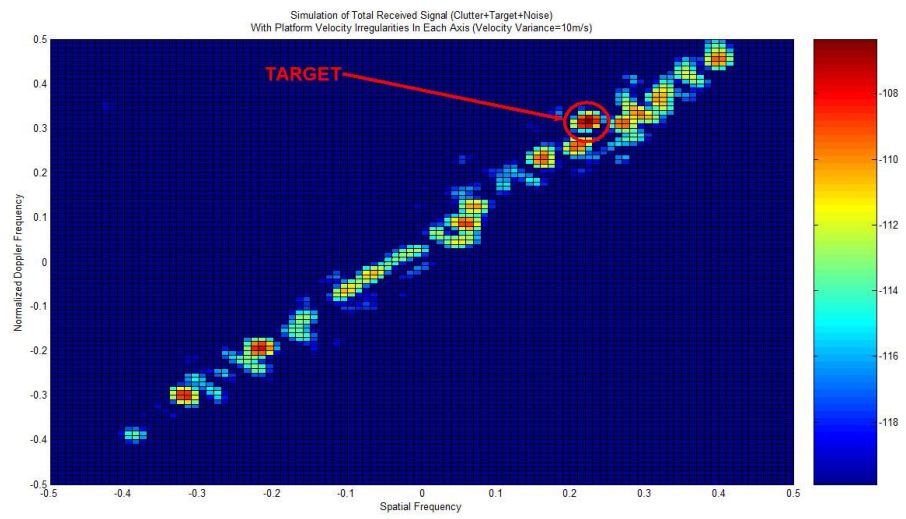Figure 4-17 Without aircraft velocity irregularities

Figure 4-18 With aircraft velocity irregularities in each axis (variance 10 m/s)
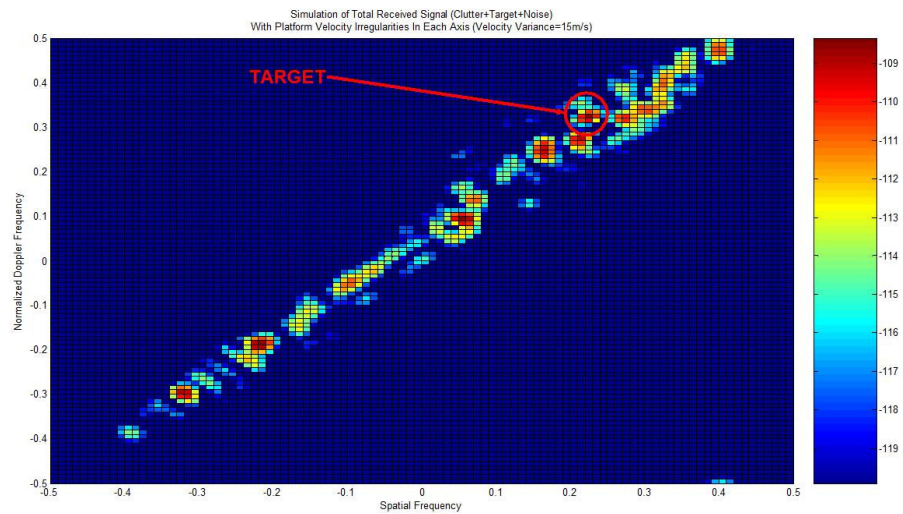
Figure 4-19 With aircraft velocity irregularities in each axis (variance 15 m/s)

4.3.6 Effect of Intrinsic Clutter Motion (ICM)

Intrinsic clutter motion (ICM) is modeled as the correlation diffuses of a clutter patch between the time samples that are taken with a rate equal to the PRI. The simulator has been coded to vary the temporal steering vector to model the reflection behaviour variation of a clutter patch.

Figure 4-20 shows the output of the simulator without ICM effect. This figure is a reference for comparison with the figures with ICM.

Figure 4-21, Figure 4-22 and Figure 4-23 show the effect of the ICM on the simulator output. The correlation coeffient value has been changed to understand how this factor changes the output. The trials are made with the correlation coefficient values 0.95, 0.9 and 0.8 respectively.
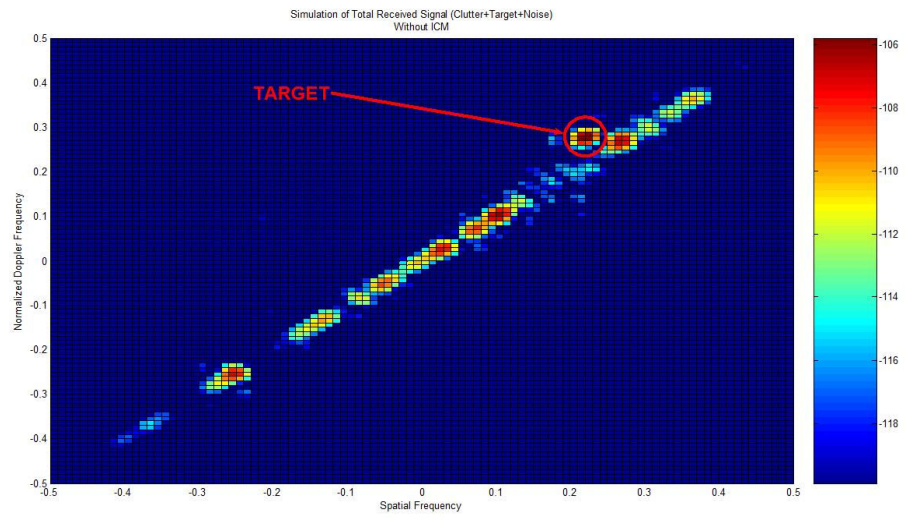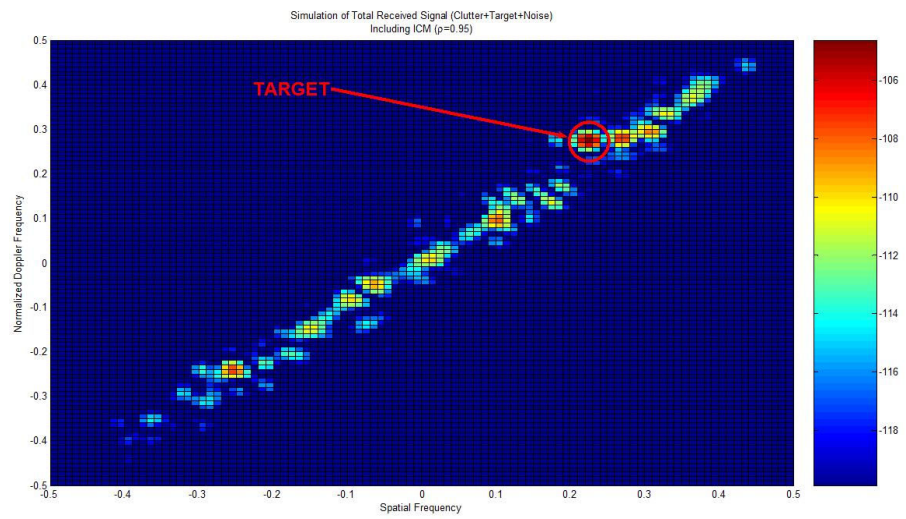
Figure 4-20 Without ICM
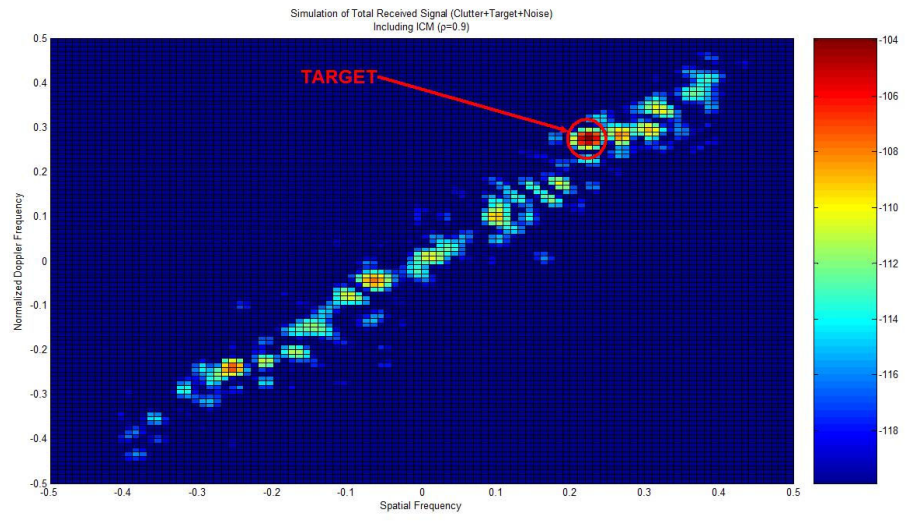

Figure 4-21 With ICM ($\rho = 0.95$)
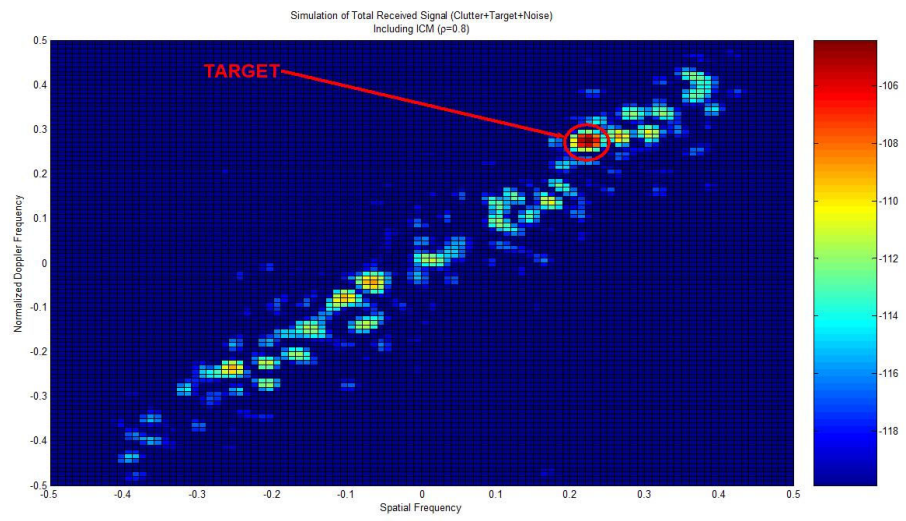
Figure 4-22 With ICM ($\rho = 0.9$)

Figure 4-23 With ICM ($\rho = 0.8$)

Note that as the correlation coefficient decreases from 1, the decorrelation effect of ICM increases so that the clutter is spread on the angle-Doppler space in accordance with the value of correlation coefficient. Thus, the deviation of clutter increases. In addition, the spread may be so much that the target may be buried in the clutter which makes the detection hard. This effect will always available in nature but changing with time and place. Therefore, it is almost impossible to know this effect. So, algorithms utulize the estimation of this correlation from other samples. For example, neighbouring iso-ring samples can be averaged to find the estimate of the clutter auto-covariance in the iso-ring of interest.

4.3.7 Effect of Aircraft Motion

Since in literature the effect of the aircraft motion is discarded due to the short CPI time, the expected signal will be as shown in Figure 4-24. This figure is obtained by using the simulator with the stationary aircraft assumption. According to the stationarity assumption, the spatial frequency does not change for any clutter patch because the positions of the antenna array elements do not change in time. The simulator has the capability of calculating the positions of the array elements at every PRI instant. Therefore, the phase of spatial sampling differs at every PRI instant in accordance with the amount of motion as defined in Section 3.2.2.3.

Figure 4-25 shows the effect of aircraft motion on the received signal produced by the simulator. The clutter ridge and target has changed position on the angle-Doppler space compared with the stationary case in Figure 4-24. Thus, discarding the aircraft or the antenna array motion from the space-time snapshot models during the CPI interval is not totally true. The change of the antenna array elements at each PRI instant due to the motion of the aircraft results in a phase difference which changes the location of the clutter ridge.
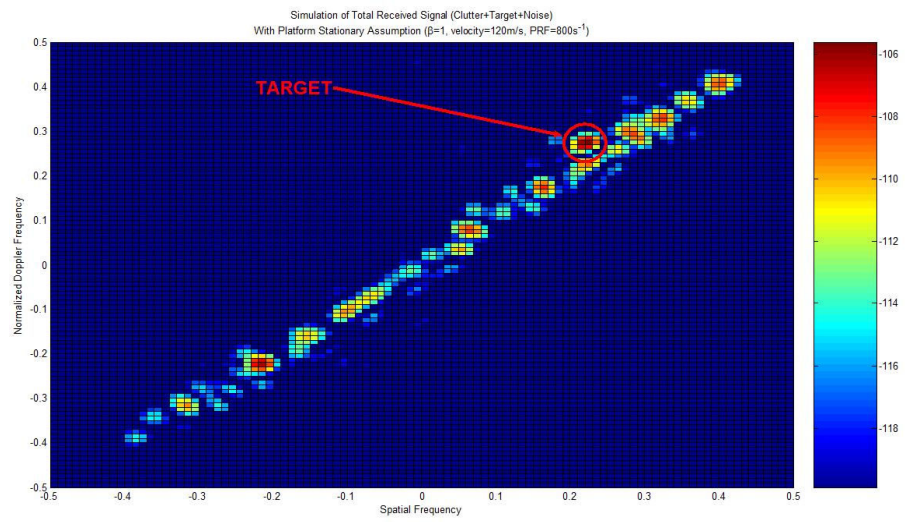
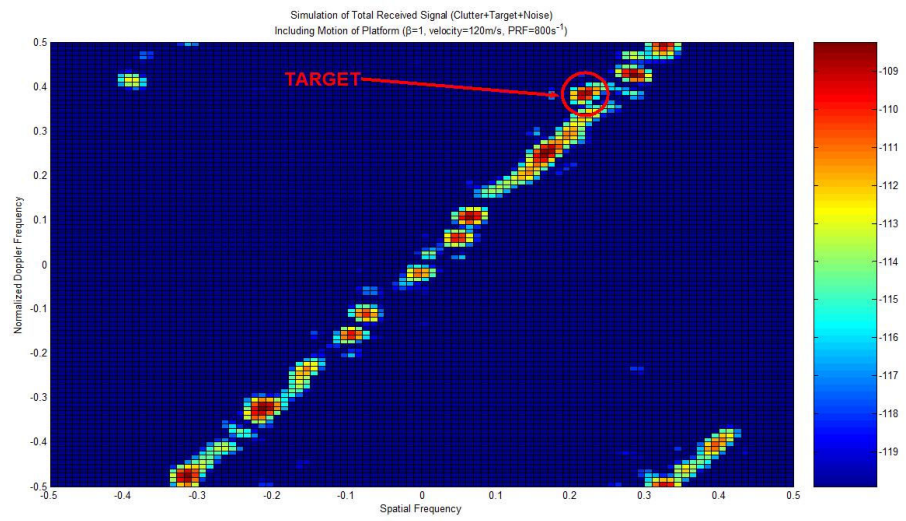Figure 4-24 Aircraft is assumed to be stationary in whole CPI time

Figure 4-25 Aircraft is assumed to move in each PRI interval

4.4 Algorithm Results

This section gives the result of the DPCA and the optimum STAP response. The weight vectors for both of them are calculated and the response of the weight vectors on the angle-Doppler space is obtained.

4.4.1 DPCA

The weight vector of the DPCA approach for N antenna array elements and M pulses is given in Section 2.5.1. This weight vector includes the two pulse cancelling method for platform motion compensation. After the trials of the received signal simulator, DPCA weight vector has been coded in accordance to the formula given in [1]. The target space-time steering vector is used as the desired signal in the formula. In order to see the response of the weight vector, signals with all possible spatial and temporal frequencies are calculated and fed as an input of the DPCA processor. The results are given in figures Figure 4-26, Figure 4-27 and Figure 4-28.
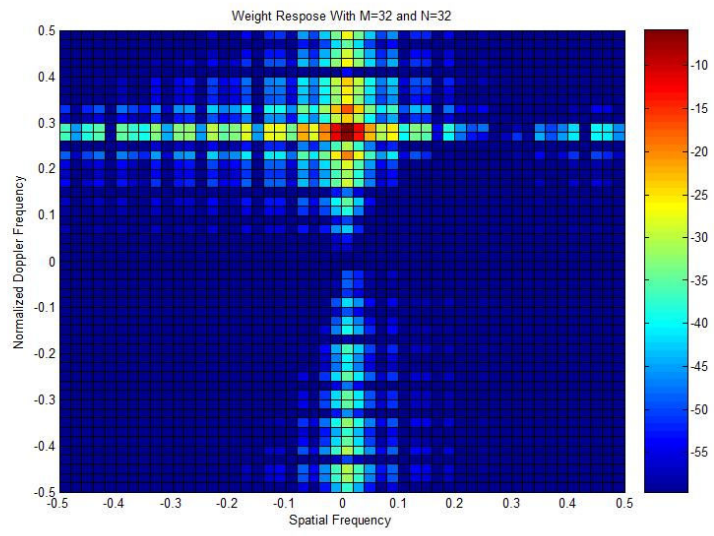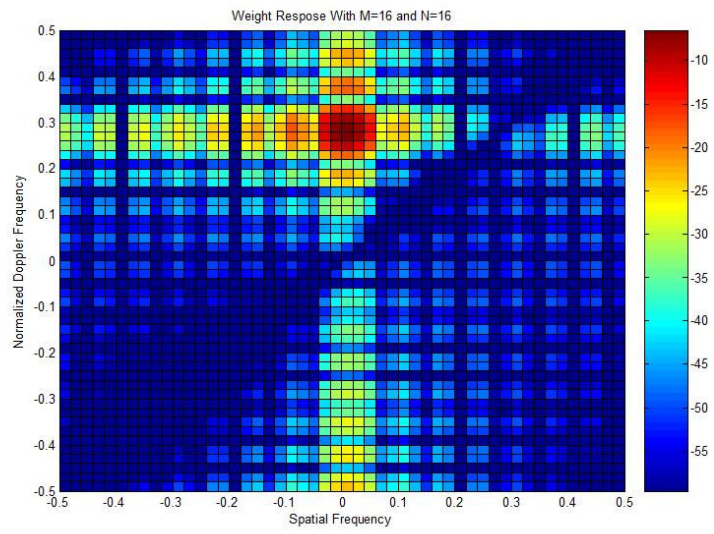
Figure 4-26 DPCA with M=32 and N=32

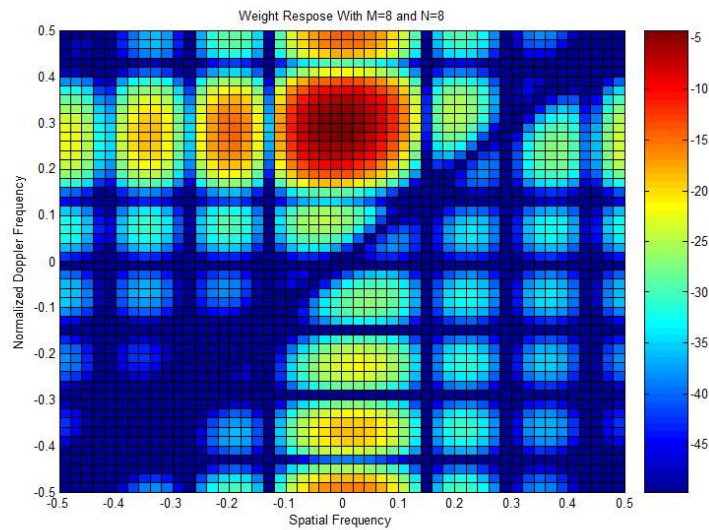Figure 4-27 DPCA with M=16 and N=16

106

Figure 4-28 DPCA with M=8 and N=8

These three figures are produced with different number of antenna array elements and pulses used. It is clear that if the numbers are decreased the resolution in both dimensions worsen. This effect is seen on the figures as a widening in the peak of the output. The peak is the output of the DPCA which tells the location of target.

These figures also tell that the DPCA is succesful to mitigate the effect of the clutter which is located at the diagonal of the angle-Doppler space. However, as shown in the previous figures in this chapter, clutter location may change to another position other than the diagonal due some effects. Consequently, the basic DPCA can not mitigate the clutter sufficiently in those cases.

Another comment on the figures is that DPCA provides a strong information of the target in Doppler domain but the spatial informaiton of target is lost. Hence, it can be conluded that DPCA do not have spatial information capability because the antenna array elements are employed as a phase center at each PRI. Two

consecutive pulses are processed at each process which is similar to the two antenna reception. It is impossible to make a beamforming with two antennas.

Consequently, it can be said that basic DPCA is a succesful method for clutter cancellation. DPCA provides accurate information of the target in the Doppler domain but there is no available spatial information.

4.4.2 Optimum STAP

In Section 2.5.2, the optimum STAP technique has been introduced. STAP tries to reach an optimum solution for the detection of a target at a specific range and angle. The optimum STAP weight vector was derived as the multiplication of the inverse clutter covariance matrix and the target space-time steering vector.

During the simulation, clutter patches are assumed to be independent. Thus, the clutter covariance matrix can be written as the sum of individual clutter covariance matrices found for each clutter patch located in the iso-ring of interest. The formula can be written as [1]

$$R_c = E\{X_c X_c^*\} = E\left\{ (\sum_{k=1}^{K} X_c(k))(\sum_{k=1}^{K} X_c(k)^*) \right\} = E\left\{ \sum_{k=1}^{K} X_c(k) X_c(k)^* \right\}. \quad (4\text{-}1)$$

This formula is revised such that the clutter covariance matrix is found by using the covariance matrix of ICM described in Section 3.2.2.6 and also the spatial and temporal steering vector of the clutter patches described in 3.2.3.1 and 3.2.3.2.

After the calculation of the clutter covariance matrix, the optimum weight vector is obtained by multiplying the inverse of this matrix with the target space-time steering vector as in the formula given in Section 2.5.2.1.

The signal to interference-noise power (SINR) ratio at the output the receiver is the ratio of the power of the signal to the power clutter. This is formulated as

$$SINR = \frac{\left| S^H R_C^{-1} S_{t \arg et} \right|^2}{S^H R_C^{-1} S} . \qquad (4\text{-}2)$$

where $S_{t \arg et}$ is the target space-time steering vector and S is the input signal vector. S is also a space-time steering vector with various spatial and temporal frequencies. The weight response is obtained as in the case of DPCA in Section 4.4.1. All of the possible input space-time steering vectors are found and SINR is calculated for each of them. The output of this process is shown in Figure 4-29, Figure 4-30 and Figure 4-31. These responses are for the case where a priori information of clutter is known.
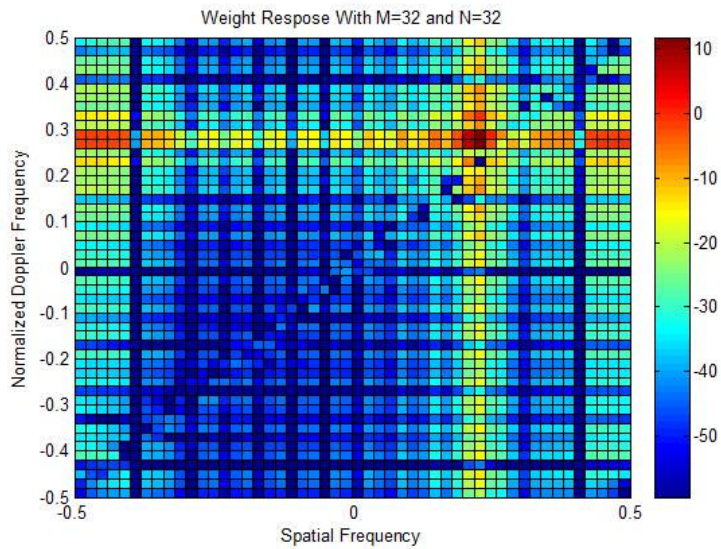

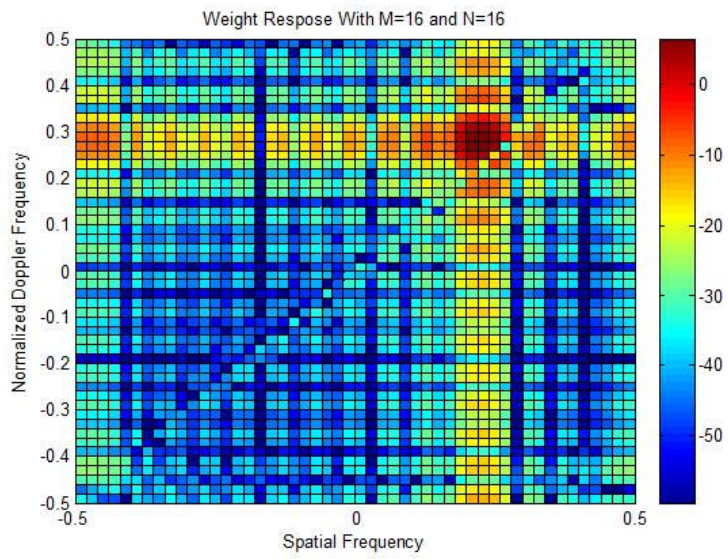Figure 4-29 Optimum STAP weight response with M=32 and N=32

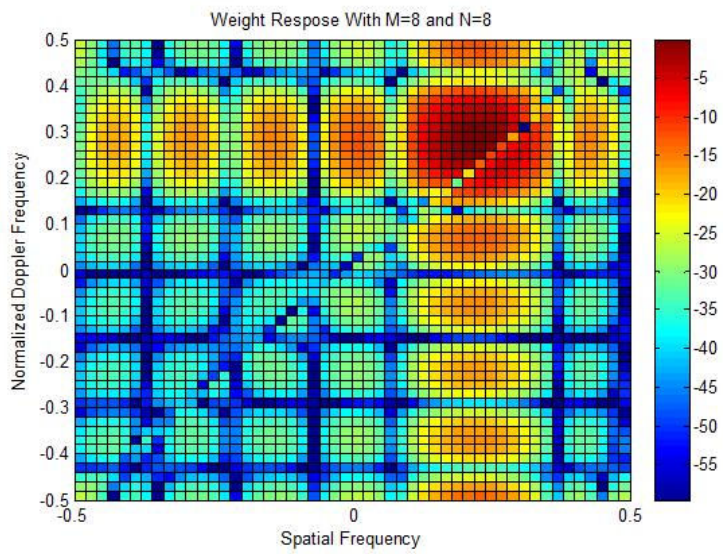Figure 4-30 Optimum STAP weight response with M=16 and N=16

Figure 4-31 Optimum STAP weight response with M=8 and N=8

The figures are obtained with different number of antenna array elements and integrated pulses as in the DPCA case. The effect of the number of antenna array elements and the pulses to be integrated can be easily observed that the peak indicating the location of the target widens or contracts.

The figures show that clutter located on the diagonal of the angle-Doppler space has been cleared successfully. In addition, the output response has a peak at exactly the location of the target. Hence, if the DPCA results are considered, optimum STAP attains additional spatial information that gives the information of at what angle the target is located. This feature of optimum STAP comes from the beamforming capability.

Furthermore, optimum STAP uses the clutter information which is the clutter covariance matrix so that optimum STAP behaves adaptive to the input as oppose to the DPCA case. This means that optimum STAP employs different weight vectors which are specific to the received clutter signal.

To sum-up, optimum STAP succeeds in cancelling the clutter and provides an accurate Doppler and spatial information about the target. The adaptivity to the different kinds of clutter inputs has been achieved with the help of using the clutter information in the weight formation.

CHAPTER 5

CONCLUSIONS

In CHAPTER 1, the thesis study has been introduced to give a basic insight what has been performed throughout the thesis. The study has begun with literature survey on Space-Time Adaptive Processing (STAP). Following the literature survey, it is decided to perform a comparison between the available STAP algorithms in literature. However, due to the lack of the input data, the need of a received signal simulator has been determined. During the development phase of the simulator, it is noticed that implementation of a simulator is a problem on its own because there are many aspects to be considered when simulating the signal received with a real aircraft. Hence, the scope the thesis mostly shifted to the simulator development.

In CHAPTER 2, airborne radar concepts and the signal models of clutter, target, jammer and the noise are presented. Firstly, the system has been stated as the radar flying over ground with an antenna array and there are the scatterers on the ground. One dimensional models are derived for the received signal under the scope of beamforming and Doppler processing. Then, these models are combined to form a two dimensional view of single point scatterer on ground. This is the basic signal structure of the clutter patches and target on ground. The characteristics of the scatterers are used to modify the basic signal structure to gather the individual clutter and target signals. The ground clutter consists of many clutter patches which

are individually back-scattering. Each clutter patch has its own space-time steering vector. This vector is defined with the temporal and spatial frequencies which are based on both the radar parameters and the elevation and azimuth angles of clutter patches. There are some aspects that affect the space-time steering vector of clutter. Velocity vector misalignment, intrinsic clutter motion (ICM) and range walk issues are described on the clutter signal model and their effects on the signal are shown. Target behaves like a single point scatterer moving on ground with a specific area. As opposed to stationary clutter patches, target has an additional velocity which changes the temporal vector. The receiver noise is also modeled to be uncorrelated in time and space.

In the light of the basic signal models described in CHAPTER 2, received signal simulator is developed. CHAPTER 3 explains the details on how the simulator is implemented. Improvements on the basic signal model are introduced in order to approach the reality. The aircraft velocity vector is made adjustable to move in any direction as opposed to the basic model in which the aircraft flies over the x-axis. Additionally, velocity vector of the aircraft is modified to have some irregularities in any direction causing a phase difference as compared with the basic signal model. In the literature, the platform motion effect is discarded such that the aircraft of the antenna array is assumed to be stationary during the CPI interval. The capability of displacements of the antenna array elements is added in accordance with the aircraft velocity. When this aspect is applied, the spatial steering vector is modified not to be constant during the CPI interval. In the other words, this displacement causes a phase difference over the basic signal model. Next, ICM effect is implemented on the signal model so that time samples received from a single clutter patch are slightly uncorrelated. Finally, the power of each clutter patch is calculated according to the location of the clutter patches. The information derived for the clutter signal model is combined for each clutter patch and the signal contributions of these patches are superposed to achieve the space-time snapshot vector of total clutter. Similar method is followed for obtaining the target space-

time snapshot vector. In addition to the clutter case, the target velocity is included in derivation of the relative velocity vector. Noise is generated to be uncorrelated in space and time. As a final step of received signal simulator obtained signals are summed to find the received signal at the input of the receiver.

After the received signal simulator has been developed, some trials have been performed on it. The results of these trials are given in CHAPTER 4. Simulation parameters are changed to observe the effect at the output. The angle between the spatial and temporal frequencies is changed by changing the aircraft velocity, PRF and interelement spacing individually. Figures of the results show that these parameters affect the sampling rate in spatial and temporal domains. Later, the direction of the aircraft velocity is changed and the results in change of the clutter and target locations on the angle-Doppler space are observed. Then, some irregular velocity components are added randomly to the aircraft velocity in any direction at each PRI instant. The clutter ridge is spread over the diagonal of the angle-Doppler space in accordance to the variance of the velocity irregularities. Afterwards, the effect of ICM is observed on the clutter diagonal ridge as spread. The amount of the spread increases with the decrease of the correlation coefficient between the time samples. Final trial on the simulator was performed to see the effect of the aircraft motion. The result due to the motion of the antenna array elements is pictured. These trials depicted that different areas are occupied depending on the system parameters that the target may burden inside the clutter.

After the simulation, the weight vectors of DPCA and optimum STAP are obtained. The resultant figures are drawn on the angle-Doppler space. DPCA method cancels the clutter signal existing on the diagonal of the angle-Doppler space. But it is stated that if the clutter ridge is shifted from the diagonal due to the facts defined in CHAPTER 3, the weight vector does not give a successful result. This happens because the weight vector of DPCA is independent of the clutter signal at the input. Additionally, basic DPCA does not give spatial information of the target since it works with only two phase centers. Optimum STAP proposes an adaptive method

that its weight vector is constructed with the clutter information (clutter covariance matrix). The weight vector response is similar to the DPCA case that the clutter on the diagonal is cancelled successfully. However, additionally the spatial information of the target is available as opposed to the DPCA case. This feature is achieved since beamforming and the Doppler processing are performed at the same time. Thus, the target is observed at exact location on the angle-Doppler space.

As a conclusion, this thesis study has given insight about the received signal characteristics collected by airborne radar. The radar parameters and platform motion have direct influence on the received signal. Inappropriate selection of the system parameters and irregularities of platform motion may dislocate the received signal in both spatial and time dimensions during processing. Additionally, clutter components existing in the received signal may vary during the observation time. Consequently, we improved the basic signal model available in the literature to include these impacts in order to better simulate the reality. According to the output response of optimum STAP and DPCA, DPCA is a non-adaptive solution to suppress the clutter on the diagonal of angle-Doppler space. However, DPCA does not provide spatial information. STAP is a multidimensional solution which employs processing both in space and time jointly. Optimum STAP provides a good cancellation of clutter while raising the power of the target in both space and time domains.

REFERENCES

[1] J.R. Guerci, "Space-Time Adaptive Processing For Radar", Artech House Inc., 2003

[2] J. Ward, "Space-Time Adaptive Processing for Airborne Radar", Technical Report 1015, MIT Lincoln Laboratory, December 1994

[3] William L. Melvin, "A STAP Overview", IEEE A&E Systems Magazine, vol. 19 No.1, pp. 19-35, January 2004

[4] Merrill I. Skolnik, "Introduction to Radar Systems", McGraw-Hill, 3rd Edition, 2001

[5] Brennan L. E., and F. M. Staudaher, "Subclutter Visibility Demonstration", Technical Report RL-TR-92-21, Adaptive Sensors Inc., 1992

[6] Klemm R., "Principles of Space-Time Adaptive Processing", The Institution of Electrical Engineers, 2002

[7] J. Ward, "Space-Time Adaptive Processing for Airborne Radar", MIT Lincoln Laboratory, 1998

[8] S. Burintramart, T.K. Sarkar, Yu Zhang, M. C. Wicks, "Performance Comparison between Statistical Based and Direct-Data Domain STAPs", Department of Electrical Engineering and Computer Science, Link Hall Syracuse University, 2006

[9] J.R. Guerci, J. S. Goldstein, I.S. Reed, "Optimal and Adaptive Reduced-Rank STAP", IEEE Transactions on Aerospace and Electronic Systems, vol. 36 No.2, pp. 647-663, April 2000

[10] Richards M. A., "Fundamentals of Radar Signal Processing", McGraw-Hill, 2005

[11] Strategic Technology Office - Defense Advanced Research Projects Agency, "Knowledge Aided Sensor Signal Processing and Expert Reasoning (KASSPER)", http://www.arpa.mil/sto/space/kassper.html, January 8th 2008, Last date accessed: April 2008

APPENDIX A

HADAMARD & KRONECKER

PRODUCTS

Consider two vectors X and Y with same dimension Nx1. Then the Hadamard product (element by element product) is defined by following equations

$$X \circ Y = \begin{bmatrix} x_1 y_1 \\ x_2 y_2 \\ \vdots \\ x_N y_n \end{bmatrix}_{NxN} . \qquad \text{(A-1)}$$

Consider two vectors X and Y with dimensions Mx1 and Nx1 respectively. Then the Kronecker products are defined by following equations

$$X \otimes Y = \begin{bmatrix} x_1 Y \\ x_2 Y \\ \vdots \\ x_M Y \end{bmatrix} = \begin{bmatrix} x_1 y_1 \\ x_1 y_2 \\ \vdots \\ x_1 y_N \\ \vdots \\ x_M y_N \end{bmatrix}_{MNx1} . \qquad \text{(A-2)}$$